MICROMACHINING OF BOROSILICATE GLASS AND LASER INDUCED BACKSIDE WET ETCHING OF QUARTZ USING AN EXCIMER LASER (248 NM)

By

Ganesh P. Kanbargi
Bachelor of Engineering
Karnataka University,
Dharwar, India
1997

Submitted to the Faculty of the
Graduate College of the
Oklahoma State University
in partial fulfillment of
the requirements for
the Degree of
MASTER of SCIENCE
July, 2005

MICROMACHINING OF BOROSILICATE GLASS AND

LASER INDUCED BACKSIDE WET ETCHING OF

QUARTZ USING AN EXCIMER LASER (248 NM)

Thesis Approved:

Dr. Ranga Komanduri

Thesis Advisor

Dr. L. M. Raff (Co-Advisor)

Dr. H. B. Lu

Dr. A. Gordon Emslie

Dean of the Graduate College

SUMMARY

Borosilicate glass is widely used in optical communications, optoelectronics as well as biomedical technologies and microelectromechanical systems (MEMS). However, it is very difficult to machine this material by conventional machining techniques because of its inherent brittleness. Laser micromachining is an alternative approach for machining of glass. Further, UV transparent materials, such as quartz, and sapphire are materials of importance in optical and optoelectronics because of their outstanding properties, such as transparency in a wide wavelength range and strong damage resistance for laser irradiation. However, laser micromachining of these dielectrics is restricted due to their high transparency. Laser induced backside wet etching (LIBWE) is a novel one step technique for machining transparent materials, such as quartz, fused silica, and sapphire. Excimer lasers possess short pulse lengths, high average as well as peak powers. This lends excimer laser as an appropriate tool for micromachining applications. In this investigation, micromachining of borosilicate glass and quartz is conducted using a short pulse (FWHM = 25 ns) KrF Excimer Laser (248 nm wavelength) that generates laser energy in the range of 100-600 mJ. The machined surfaces were examined using conventional optical and laser interference microscopes. The impact of changing major operating parameters, such as pulse fluence and different media on the resulting micromachining geometries is studied. Simple as well as complex geometries, such as microfluidic channels, inductors, part geometries used in medical applications, and RF circuits were machined.

ACKNOWLEDGEMENTS

I would like to express my sincere thanks to my adviser, Dr. Ranga Komanduri for his constructive guidance, financial support and inspiration throughout the study. I would like to thank him for providing an opportunity to conduct research in the field of micromachining. I would also like to thank Dr. L. M. Raff and Dr. Hong Bing Lu for serving on my committee. I would like to thank Choo, Supradeep, and Kiyoshi Yabata for their useful suggestions and discussions during this study and to Mr. Sony Varghese for his assistance with the use of Excimer Laser.

This project is funded by a grant from the National Science Foundation (EPS-9977830) through a subcontract from the University of Arkansas. The principal investigator at the University of Arkansas is Dr. Ajay Malshe.

I would like to express my gratitude to my parents for their confidence in me. I would like to thank them for their consistent encouragement and love. I would like to extend my gratitude to my brother and sisters for their inspiration, support and love.

Finally, I would like to thank the Department of Mechanical and Aerospace Engineering for providing me with the opportunity to pursue M.S. at Oklahoma State University.

TABLE OF CONTENTS

Chapter **Page**

1. INTRODUCTION……………………………………………………………...…..1

    1.1 Excimer laser………………………...……………………………...…...1

    1.2 Application of Borosilicate glasses…..…………………………………...…..2

    1.3 Excimer Laser Micromachining …..………………………………...……..3

    1.4 Overview………………………………………………………...………..4

2. BRIEF OVERVIEW OF LASERS…...……………………………………..……...6

    2.1 Lasers…………………………………..……………..…………………….6

    2.2 Basic Principles of Lasers……..…………………………………..……….7

    2.3 Types of Lasers………………...…………………………..…………...….9

    2.4 Laser Classifications…..………………………………………………..……12

3. LASER MATERIAL INTERACTION………...……………………………………....14

    3.1 Material Removal Phenomenon………….....………………………………...14

4. LITERATURE REVIEW……..…………………….………..………………...22

    4.1 Laser Induced Backside Etching...……………………………………...…38

5. PROBLEM STATEMENT…………………………….………..………...………44

6. EXPERIMENTAL SETUP AND TEST CONDITIONS…..………………………46

7. METHODOLOGY ……..………..……..…………………………………………...50

8. MICROMACHINING OF BOROSILICATE GLASS USING EXCIMER LASER

8.1 Introduction…………………………………………………………..53

8.2 Experimental setup……………………………………………………..54

8.3 Results and Discussion…………………………………………………55

8.3.1 Effect of low energy…………………………………………...59

9. LASER INDUCED BACKSIDE ETCHING OF QUARTZ USING EXCIMER LASER

9.1 Introduction……………………………………………………………73

9.2 Experiment Set up for LIBWE……...…………..…………………………73

9.3 Results and Discussions…………………………………………………76

10. CONCLUSIONS and FUTURE WORK…………..…………………………….....101

11. REFERENCES...…..104

LIST OF FIGURES

Figure **Page**

2.1. Gas Laser Layout. 9

2.2. Solid state laser layout...12

3.1. Schematic representation of impact of laser pulse on polymer surface 15

3.2 Variation of the Etch rate Versus Fluence 17

3.3 Schematic showing laser hole drilling..18

3.4 Ablation depth per pulse on number laser pulses for different laser fluences at 50Hz and 100μm...19

3.5 Ablation depth per laser pulse on the number of laser pulses for different laser at 500 Hz repetition rate and 100 μm.......................................20

3.6 SEM images of 50 μm thick Pyrex glass drilled with different laser fluences and repetition rates..21

4.1 Representation of various schemes of laser etching in water.......................23

4.2 Comparison of hole profiles (a) silicon laser-etched in air and (b) laser etched in water...23

4.3 Comparison of the dependencies of the ablation rate on the laser fluence of laser etching of Si in water and in air...25

4.4 Schematic representation of laser breaking of silicon wafers……………………26

4.5 Effects of repetition rate on surface morphology of glass holes ablated at 2.4J/cm2 with 2000 shots (a) 2Hz, (b) 5Hz, (c) 10Hz……..……………………….31

4.6 SEM images of surface morphology of ablated glass holes after 10% HF etching ablating at 5 Hz, (b) ablating at 10 Hz…………………………..............32

4.7 Direct ablation on the rear surface of Corning microslide 2947 by 532nm and 3-ns laser pulses at a threshold fluence of 22.6 J/cm^2 and 200 laser shots……...33

4.8 Pit with a diameter of 15 µm and a central depth of 3.2 µm on a Corning…………………………………………………………………..34

4.9 SEM images of crater rims generated by overlapping laser pulses……………...34

4.10 Depth of ablated features in soda lime plate glass at an intensity of $5J/cm^2$ with 266nm (squares) and 157nm (diamonds)……………………………………..35

4.11 Comparison of ns and fs laser ablation of bariumalumoborosilicate glass in air………………………………………………………………… 36

4.12 Schematic diagram of the setup for LIBWE method……………………………39

4.13 Plausible mechanism for LIBWE by cyclic multiphotonic absorption…………40

4.14 Etch rate of fused silica versus laser fluence using a 0.4 pyrene/acetone Solution…………………………………………………………………………41

4.15 Array of micro-sized blind holes etched in fused silica by LIBWE…………….42

4.16 Etch rates of quartz versus laser fluence………………………………………...43

6.1 Schematic of the optical delivery system for laser micromachining…………….48

6.2 Schematic and (b) photograph of experimental the setup used in laser machining49

8.1 Schematic of setup for micromachining underwater…………………………….54

8.2 Optical micrographs of the top view of borosilicate glass ablated at fluence of 2.43J/cm^2……………………………………………………………...56

8.3 Solid surface map of borosilicate glass dry machining………………………….57

8.4 Optical micrographs of glass with (a) and (c) wax on top and (b) and (d) oil layer on top of glass surface at a fluence of 2.43 J/cm^2…………………..58

8.5 (a) Top view and (b) 3D surface map of borosilicate glass under 50 %methanol + 50 % distilled water at E = 0.535 mJ…………………............60

8.6 (a) Top view and (b) 3D surface map of borosilicate glass under water at E = 0.535 mJ………………………………………………………………….61

8.7 (a) Top view and (b) 3D surface map of borosilicate glass with wax on top at E = 0.535 mJ….………………………………………………………62

8.8. (a) Top view and (b) 3D surface map of borosilicate glass with salt water at E = 0.535 mJ...……………………………………………………..63

8.9 (a) Top view and (b) 3D surface map of borosilicate glass underwater at E = 37.6 μJ…………………………………………………………...……….64

8.10 3D surface map of borosilicate glass (a) dry and (b) under 50 %methanol + 50 % water at E= 37.6μJ………………………………………65

8.11 (a) Top view and (b) 3D surface map of borosilicate glass first dry and then underwater at E = 37.6 μJ…………………………………...………66

8.12 a) Top view and (b) 3D surface map of borosilicate glass first dry and then under 50 % methanol + 50 % water at E = 37.6 μJ……………………………...67

8.13 (a) Top view and (b) 3D surface map of borosilicate glass underwater at E = 37.6 μJ…………………………………………………………………69

8.14 a) Top view and (b) 3D surface map of borosilicate glass first dry and then under 50 % methanol+ 50 % water at E = 37.6 μJ……………………………….......70

8.15 (a) Photographs of circuit similar to the one used in flat panel display and (b)Microfluidic channel micromachined on laser machined on borosilicate glass ……………………………………………………………........71

(c) Spider circuit micromachined on borosilicate glass and (d) An inductor micromachined by excimer laser………………………………72

9.1 Experimental setup for backside etching of Quartz……………………………..74

9.2 Quartz transmission spectrum…………………………………………………....75

9.3 (a) Top view of quartz (100% Toluene)…………………………...…………..77

9.3 (b) 3D solid surface map of quartz (100% Toluene)……………………………77

9.3 (c) 3D wire map of quartz (100% Toluene)……..……………………….………78

9.4 (a) Top view of quartz (Toluene: Acetone :: 90:10)…………………....……..79

9.4 (b) 3-D solid surface map of quartz (Toluene: Acetone :: 90:10)………...…...79

9.4 (c) 3D wire map of quartz (Toluene: Acetone :: 90:10)…………………………80

9.5 (a) Top view of quartz (Toluene: Acetone :: 70:30)...…………………….…......81

9.5 (b) 3D solid surface map of quartz (Toluene: Acetone :: 70:30)...……….……...81

9.5 (c) 3D wire Map of quartz (Toluene: Acetone :: 70:30)……………………..........82

9.6 (a) Top view of etched surface of quartz (Toluene: Acetone :: 85:15)..………...83

9.6 (b) 3D solid surface map of quartz (Toluene: Acetone :: 85:15)……………......83

9.6 (c) 3 D wire Map of quartz (Toluene: Acetone :: 85:15)……………….………84

9.7 (a) Top view of the etched surface of quartz (E = 0.826 mJ)…………….……..….85

9.7 (b) 3D wire Map of the etched surface of quartz (E = 0.826 mJ)……………......85

9.7 (c) 3D solid surface map of quartz (E = 0.826 mJ)…...…………………………86

9.8 (a) Top view of the etched surface of quartz (E = 0.789 mJ)……………….…...87

9.8 (b) 3DWire Map of the etched surface of quartz (E = 0.789 mJ).………………87

9.8 (c) 3D solid surface map of quartz (E = 0.789 mJ)………………………………88

9.8 (d) X-Y Profile of the etched surface of quartz (E = 0.789 mJ)……….……..88

9.9 (a) Top view of the etched surface of quartz (E = 0.757 mJ)……….…………..89

9.9 (b) 3D wire map of the etched surface of quartz (E = 0.757 mJ)…...……………89

9.9 (c) 3D solid surface map of quartz (E = 0.757 mJ) ……………………………..90

9.9 (d) X-Y Profile of the etched surface of quartz (E = 0.757 mJ)……...…………90

9.10 (a) Top view of the etched surface of quartz (E = 0.704 mJ)..…………….……...91

9.10 (b) 3D wire map of the etched surface of quartz (E = 0.704 mJ).………………91

9.10 (c) 3D solid surface map of quartz (E = 0.704 mJ) ……...………………………92

9.10 (d) X-Y Profile of the etched surface of quartz (E = 0.704 mJ)………………..92

9.11 (a) Top view of the etched surface of quartz (E = 0.652 mJ)……………………93

9.11 (b) 3D wire map of the etched surface of quartz (E = 0.652 mJ)………………93

9.11 (c) 3D solid surface map of quartz (E = 0.652 mJ) ……………………………94

9.12 (a) Top view of the etched surface of quartz (E = 0.596 mJ) …………………95

9.12 (b) 3D wire map of the etched surface of quartz E = 0.596 mJ………...……95

9.12 (c) 3D solid surface map of quartz (E = 0.596 mJ)...…………………………...96

9.12 d) X-Y Profile of the etched surface of quartz (E = 0.596 mJ)………………..96

9.13 (a) Top view etched surface of quartz (E = 0.522 mJ)……..……………………97

9.13 (b) 3D wire map of the etched surface of quartz (E = 0.522 mJ)…..……………97

9.13 (c) 3D solid surface map of quartz (E = 0.522 mJ)……………………………...98

9.13 (d) X-Y Profile of the etched surface of quartz (E = 0.522 mJ)…………………98

9.14 The variation of ablation depth with fluence or quartz………………………...99

LIST OF TABLES

Table. **Page**

6.1 Specification of Gases used in laser ablation..47

8.1. Properties for borosilicate glass (Corning 0211 glass)..................................55

8.2 Different media used in laser ablation of borosilicate glass................................59

9.1 Threshold fluence of quartz by light induced backside wet etching (LIBWE) and thermodynamic properties..75

9.2 Fluids used in laser ablation of quartz at (E = 0.522 mJ) 76

CHAPTER 1

INTRODUCTION

1.1 Excimer Lasers

Excimer lasers are gas lasers that emit pulses of light with duration of 10 ns to several 10 ns in the ultraviolet spectral range. They are the most powerful lasers in the UV range. They posses the ultraviolet wavelength with shorter pulse duration to ensure high fluence and high pulse energies which allow the radiation to be absorbed by the material surfaces. There is a growing demand from industry for microprocessing of materials particularly for the applications in the field of microsystems technology. It is necessary to produce structures with dimensions down to the micrometer scale especially in materials that could not be processed or processed well by conventional technologies. Excimer laser is a common popular tool for micromachining of various geometries for all types of materials, including ceramics, polymers, and metals. The shorter wavelength permits fine imaging of excimer lasers. Hence, excimer laser ablation allows fine

resolution and high machining quality that makes the technique of choice for many applications.

1.2. Applications to Borosilicate glass

Borosilicate glass is made from silica and boric oxide. This glass is highly resistant to chemical corrosion and temperature changes (thermal shock) and is particularly suitable for laboratory ware (test tubes, etc.). Borosilicate glasses, because of their optical transparency, electrical insulation, and thermal stability find wide variety of applications in the microelectronic industries. Microdevices composed of glass are in great demand in many fields including optical communication and opto-electronics, biomedical technology, microelectormechanical system (MEMS) industry, environmental technology, photovoltaic, wafer substrates, measurement and sensor technologies. Microchannels fabricated on glass have a growing importance in miniaturization of microfluidic devices for chemical and biological analysis systems (Yaker *et al*., 2003). Also, glass is an excellent material for laser ablation of single and arrayed microstructures which are in great demand in fabricating a variety of microdevices for photonics and communications industries. It is an extremely brittle material and difficult to process by conventional machining process. It is amorphous and has no crystal structure. Therefore, slip or plastic deformation cannot take place. As a result of strong bonding between atoms, glass exhibits very high compressive strength and a theoretical tensile strength of about 10^7 kN/m^2. The presence of impurities or imperfections in glass induce stress concentrations to localize and exceed the bond strength between the atoms and eventually the glass will crack.

1.3. Excimer laser Micromachining

Srinivasan and Mayne-Branton (1982) first demonstrated excimer laser ablation technique in the early 1980's. They named this process, "ablative photo-decomposition" (APD), a key part of LASIK (Laser *in situ* Keratomileusis) and PRK (Photorefractive Keratectomy), both of which permanently re-shape the cornea using an ultraviolet excimer laser. The hallmark of this heatless, pulsed laser etching of tissue resulted in the absence of thermal damage, which meant that living tissue can heal with virtually no scarring. Until 1981, lasers used in eye surgery created regions of damage, resulting in the formation of scar tissue that had therapeutic value.

Considerable efforts have been made towards an understanding of the basic physical and chemical processes involved in laser ablation. Numerous models have been proposed to explain the observed etching behavior of various materials.

Ihlemann (1992), based on a comparative study of different wavelengths, pulse durations, and surface qualities concluded that different ablation mechanisms are involved. They are based on the volume absorption, bond breaking, and material expansion. Experimental work by Garrison and Srinivasan (1984) showed that photochemistry played a less important role for wavelengths higher than 193 nm and that main ablation mechanism seems to be thermal in nature with photochemical bond breaking.

An important requirement in micromachining of semiconductor materials is production of high quality surfaces. In the case of laser ablation, the surface of the ablated material is usually surrounded by redeposition of molten material or debris that has to be subsequently removed by other methods. One of the methods would be to

remove it during the laser ablation process itself. This can be accomplished by either machining underwater, methanol, or by applying a layer of wax.

1.4. Overview

This study concentrates on micromachining of borosilicate glass and quartz using a short pulse (FWHM = 25 ns) (KrF 248 nm wavelength) laser that generates laser energy in the range of 100-550 mJ. Simple microstructures as well as complex geometries, such micro fluidic channels, inductors, medical part geometry, and RF circuits were machined successfully. The changes in morphology and debris formation during ablation are studied. The possibility of removing this debris is also explored and demonstrated. The impact of changing the major operating parameters, such as pulse fluence and different media on the resulting microstructural shapes is also studied.

In Chapter 2, a brief history of lasers, types of lasers, and basic principles of lasers are presented. This in followed by Chapter 3, a discussion of the laser-material interactions, and various mechanisms involved in laser ablation. Typical ablation curve is discussed and results regarding various factors affecting the laser ablation are presented.

In Chapter 4, earlier experimental studies, results and analyses reported in the literature are presented. Literature on micromachining of various materials, such as glass, silicon, quartz, and fused silica as well as laser induced backside wet etching (LIBWE) are reviewed and discussed. The effect of various operating parameters, including wavelength, pulse duration, and repetition rate on laser micromachining are reviewed. Work reported in the literature addressing these issues is presented. Chapter 5 presents the problem statement. Chapters 6 and 7, deal with experimental setup and sample preparation. Chapter 8 and Chapter 9 cover micromachining of borosilicate glass and

quartz along with the results and discussion. Finally Conclusions and Future Work are covered in Chapter 10.

CHAPTER 2

BRIEF OVERVIEW OF LASERS

2.1 Lasers

LASER is an acronym for **L**ight **A**mplification by **S**timulated **E**mission of **R**adiation. It is essentially a coherent, convergent, and monochromatic beam of electromagnetic radiation with wavelength ranging from UV to infrared. There are different types of lasers, but they share a crucial element, namely, material capable of amplifying radiation. The physical principle responsible for amplification is known as stimulated emission. Einstein conceived the idea that if an electron were in an excited state when a photon previously emitted and having the proper energy collided the electron would drop to a lower energy state and emit another photon of the same energy that would move in the same direction, resulting in two identical photons traveling in the same direction and same phase. Albert Einstein first proposed this phenomenon in a 1916 paper proving Plank's law of radiation.

Schawlow and Townes (1958) invented MASER (**M**icrowave **A**mplification by **S**timulated **E**mission of **R**adiation) in 1954, using ammonia gas and microwave radiation. Maser was invented before laser. In 1958, Schawlow and Townes theorized a visible laser, an invention that would use infrared and/or visible spectrum light. Javan. *et.al* (1960) invented the first gas laser using helium and neon in 1960. This is used in such applications as reading bar codes, surveying equipment, etc.

The major features of He-Ne laser are the following

1. It was the first laser to emit a continuous beam.
2. The lasing action can be initiated by an electric discharge rather than intense discharge of photons from a flash lamp in the case of other lasers.

2.2 Basic Principles of Lasers

To explain how a laser light is generated, we need first to investigate the energy transition phenomena in atoms or molecules. These phenomena include: spontaneous emission, stimulated emission/absorption and nonradiative decay. According to quantum mechanics, the electrons of atoms can take different energy states, say E_1, E_2, E_3, etc., where $E_1 < E_2 < E_3 <$.... The lower energy level is more stable than higher energy levels. So, electrons at high energy levels tend to decay to low energy levels. The energy difference between two levels can be given out as electromagnetic radiation. This process is called spontaneous radiation. The energy difference between two levels is given by:

$$E_2 - E_1 = h \nu_0 \tag{2.1}$$

where E_2 is the upper energy level, E_1 is the lower energy level, h is the Plank's constant, and ν_0 is frequency of the radiated EM wave.

The energy difference between two levels can decay in forms other than radioactive decay or, spontaneous radiation, which is called nonradiative decay. The energy difference can change into kinetic energy or internal energy through collisions with surrounding atoms, molecules, or walls.

When external EM waves of frequency ν_0 are incident on the material whose atoms initially are at energy level E_2 and ν_0 is very near to the transition frequency between E_2 and E_1, there is a finite probability that the incident waves will force the atoms to undergo transition from $E_2 \longrightarrow E_1$. Each such transition gives rise to an EM wave (a photon), while the incident wave (incident photon) still exists. Thus, we have two photons. The above transition process is caused by external excitation, hence is called the *stimulated radiation*. In spontaneous emission, the radiation is in all directions and in random phases. In stimulated radiation, the emitted waves of any atoms are in the same direction and in the same phase with the incident wave.

If the atom is initially at level E_1, and this is at the ground level, the atom will remain in this level unless excited. When an EM wave of frequency ν_0 is incident on the material, there is a finite probability that the atom will absorb the incident energy and jump to energy level E_2. This process is called *stimulated absorption*.

Normally the number of atoms at lower energy levels is larger than those at higher levels. Stimulated radiation/absorption, spontaneous emission and nonradiative decay take place at the same time. Even if we ignore the decay factors, stimulated absorption still dominates over stimulated radiation, the incident EM wave cannot be amplified in this case. Amplification of incident wave is possible only when the number of upper level atoms is greater than that of lower level atoms. This case is called *population inversion*.

To get more atoms in to the upper level than in to the lower level, we have to raise the atoms from the lower level to the upper level. This process is called *pumping*.

2.3. Types of Lasers:

The three major types of lasers are classified by their state of the lasing media, namely, gas, liquid, and solid. All of them can be operated either as a continuous wave or pulsed mode.

2.3.1 Gas lasers

Gas lasers are lasers with a gaseous lasing medium. This can be subdivided into three categories, based on the compilation of the gas: neutral atom, ion, or molecular. Both neutral atom and ion lasers are important in many applications but not for laser machining. Molecular gas lasers, such as CO_2 laser on the other hand are one of the most widely used lasers for machining applications. Figure 2.1 shows an example of a gas laser showing the lasing medium layout.

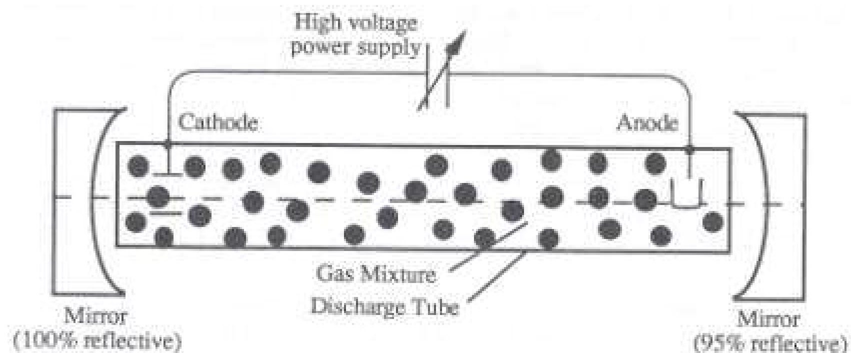

Fig. 2.1 Gas Laser Layout

In a molecular gas laser, the molecules in the lasing medium are excited and the vibrational mode of the molecules change, thus producing photons. The lasing medium of a CO_2 laser is actually made up of a number of different gases, such as nitrogen, helium, and carbon dioxide. While the lasing medium does require some energy input to become excited, most of the excitation of the CO_2 actually comes from the collisions of the molecules, as opposed to the actual input. As for their energy outputs, CO_2 lasers have a theoretical maximum energy output of 15 mW at 10% energy efficiency, all depending on the type of gas flow used in the lasing medium (sealed discharge, axial, traverse, or cross flow). Considering power output, traverse flow lasers are by far the best; all lasers but for the inefficient sealed discharge, have reasonable uses in industry.

The other type of gas laser used for laser machining is the excimer laser. The name Excimer is a contraction of "Excited dimer", a description of diatomic molecule in which the component atoms are bound in the excited state but not in the ground state. The excimer lasing medium is usually made of a compound of noble gases and halogens. Excimer lasers are excited by passing a short, intense electrical pulse through a mixture of rare gas and halogen. The mixture contains 90% of buffer rare gas (helium or neon) and small percentage of rare gas (argon, krypton, or xenon). The halogen atoms come from the halogen molecules, such as F_2, Cl_2.

Electrons in the discharge transfer energy to the laser gas, breaking up halogen molecules and causing formation of electronically excited molecules such as xenon fluoride. The reactions are complex and depend on the type of the gases used. The molecules remain excited for about 10 ns, then drop to the ground state and dissociate. The energies involved are large, and the output is at ultraviolet wavelengths.

Excimer lasers produce high-powered, pulsed beams, with average power over 100 W and average pulse repetition rate of 1000 pulses per second. These lasers are commonly used to machine solid polymer workpieces, micromachine ceramics and semiconductors, along with many other various uses. The material removal process of an excimer laser is different from that of the other commonly used lasers. Instead of removing material through melting and or vaporization, an excimer laser removes material through ablation, breaking down the chemical bonds of the target material until it dissociates into its chemical components. The main difference between an excimer laser and other lasers is that excimers do not focus a beam at a particular point and traverse the material; instead, they produce a large area beam which is masked to achieve the desired beam size.

2.3.2 Liquid lasers

Liquid lasers typically use large organic dye molecules as the lasing media. These lasers are designed so that the frequency at which they emit a beam can be varied, and are considered tunable. These lasers are typically not used for laser machining applications.

2.3.3 Solid state lasers

Solid state lasers use ions suspended in a crystalline matrix to produce laser light. The ions, or "dopants," provide the electrons for excitation, while the crystalline matrix propagates the energy between ions. The major type of solid laser used in laser machining is the Nd: YAG laser, which stands for a neodinium-yttirium-aluminum-

garnet laser. The YAG crystal has relatively high thermal conductivity. Therefore, high continuous operating power outputs of a few hundred watts are available, and when pulsed, up to 1 kW is possible. In machining applications, Nd: YAG lasers are typically used for cutting and hole drilling operations. Fig. 2.2 shows the solid state laser layout. The ends of the lasing rod are polished flat and parallel, then coated with reflecting material. Light form external source flash lamp enters the laser rod and excites the light emitting atoms. The beam is propagated by reflection of photons generated by stimulated emission traveling normal to the mirrors.

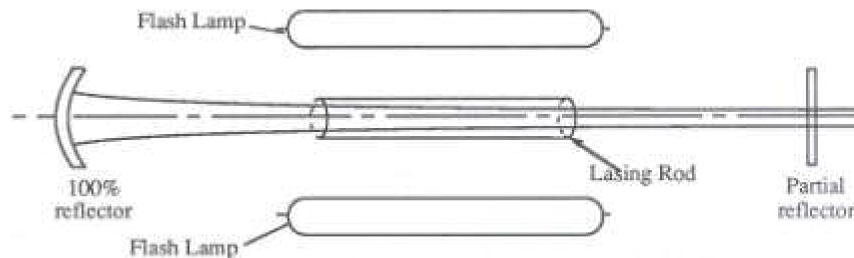

Fig. 2.2 Solid state laser layout

2.4. Laser Classifications

Lasers are classified into four broad types depending on the potential for causing biological damage.

Class I: These lasers cannot emit laser radiation at known hazard levels

Class I. a: This is a special designation that applies only to lasers that are "not intended for viewing," such as a supermarket laser scanner. The upper power limit of Class I. a. is 4.0 mW.

Class II: These are low-power visible lasers that emit above Class I levels but at a radiant power not above 1 mW. The concept is that the human aversion reaction to bright light will protect a person

Class III.a: These are intermediate-power lasers (cw: 1-5 mW), which are hazardous only for intrabeam viewing. Most pen-like pointing lasers are in this class.

Class III.b: These are moderate-power lasers

Class IV: These are high-power lasers (cw: 500 mW, pulsed: 10 J/cm^2 or the diffuse reflection limit), which are hazardous to view under any condition (directly or diffusely scattered), and are a potential fire hazard and a skin hazard. Significant controls are required of Class IV laser facilities.

CHAPTER 3

LASER MATERIAL INTERACTIONS

3.1 Material Removal Phenomenon

The phenomenon of the material removal process for excimer lasers is different from that for CO_2 or ND: YAG lasers. Excimer lasers remove material from the substrate by either photothermal (vaporization) or photochemical or by a combination of both of these phenomena. The excimer laser removes material through ablation, by breaking the chemical bonds of the material until it dissociates into its chemical components instead of removing material through melting, and or vaporization, where the material is heated from solid to liquid and/or gaseous states as in CO_2 or ND: YAG lasers. In ablation, no liquid or gaseous phases of the material are present. Shorter wavelengths in the UV range have higher photon energy leading to photochemical reactions. Longer wavelengths in the infrared range have lower photon energy leading to thermal reactions.

3.1.1 Laser Ablation Mechanisms:

Most of the material removal is by ablation where the absorbed UV photons directly break the chemical bonds. Hence, if sufficient photons are incident on a thin layer of material in a short time interval, a pressure increase is generated due to rapid formation of lower molecular weight components. The process is essentially photochemical in nature leading to little or no thermal heating.

When a laser pulse from an excimer laser impinges on a surface as shown in

$$I_t = I_0 \cdot 10^{-\alpha l} \qquad (3.1)$$

Fig 3.1, the penetration of the radiation through the solid follows a simple relation, which is known as the Beer's law. Where I_0 and I_t are the intensities of the beam before and after transmission through a slice of material of thickness *l*, and *a*,

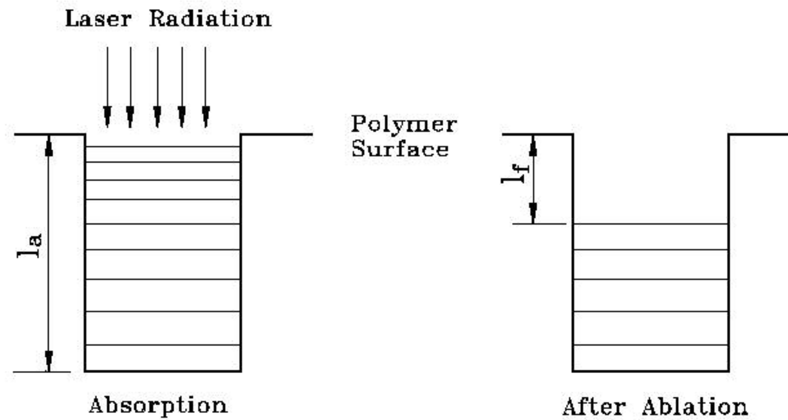

Fig. 3.1 Schematic representation of impact of laser pulse on a polymer surface before and after ablation

the absorption coefficient is a characteristic property of the material. If the fluence F of the laser beam at the workpiece exceeds a certain threshold value, F_0, then a depth, l_f of the material is ablated by the pulse. The next pulse will go through the virgin material underlying it till the depth of the hole is reached. Above the ablation threshold, the etch depth per pulse or so-called etch rate, l_f, can be approximated by

$$l_f = \frac{1}{\alpha} \ln\left(\frac{F}{F_0}\right) \qquad (3.2)$$

Etch rate increases with increasing fluence. The etch rate is calculated by taking the average of a few hundred pulses at the given energy fluence. Individual pulses may cause slightly different amounts of material removal due to energy fluctuations. The effect of these fluctuations is insignificant for the multi-pulse drilling process. It has been observed that clean and smooth edges are obtained with energy densities below 2.7 J/cm^2 while higher energies lead to the formation of some structures or debris at the top surfaces of the edges. One possible reason is, at high fluence, the process no longer remains purely photochemical in nature and significant thermal degradation can occur.

3.1.2 Typical Ablation Curve:

From Fig 3.2, it may be noted that at low target density (fluence) there is no material removal. But as the fluence is increased a point will be reached known as ablation threshold where the material removal begins. As the fluence is increased there is more amount of material removed per volume of the photons till a point where the curve plateaus. Once the curve reaches this plateau there is no more material removal with increasing fluence. Hence it is not beneficial to run lasers beyond this point, which may

only result in thermal damage. The energy of additional photons (as this energy is not used to eject material) transforms to heat and causes secondary thermal effects which may not be beneficial. Factors affecting ablation mechanisms include laser wavelength, energy on the target, pulse length, repetition rate, and most important the nature of the target material.

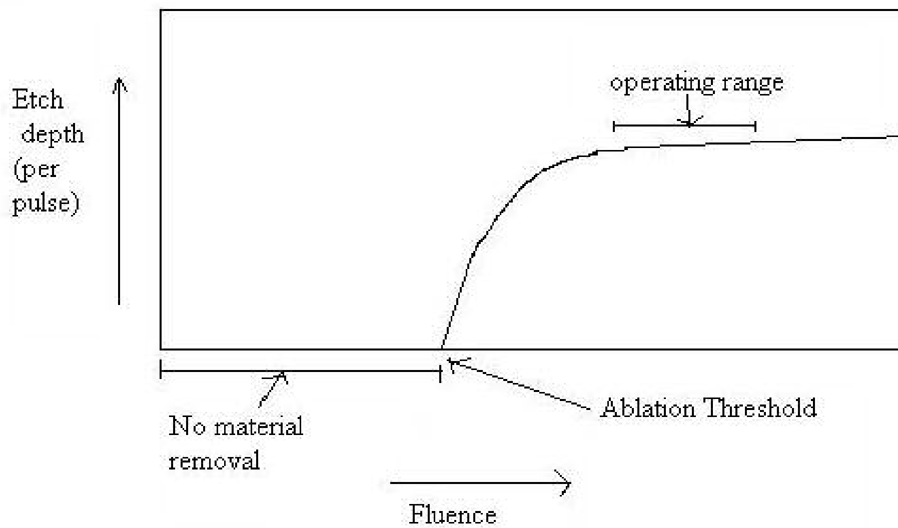

Fig.3.2 Variation of the Etch rate Versus the Fluence

.

3.1.3. Laser Hole Ablation:

When drilling holes with a laser, it is always necessary to take into account the inherent taper of the laser process, which limits the thickness of material that can be processed with respect to the diameter of the holes being drilled. For glasses, this process has even more limitations as deeper the hole drilled, the less likely the heat generated can

escape, thereby causing problems such as glazing and microcracking. In addition, the exit usually is a problem as the glass shows breakdown induced from the thermal stresses and the acoustic shock of the material being ejected through the entrance side as it is drilled.

3.1.4 Various Factors affecting drilling:

The exit and entrance hole sizes, hole taper, recast and heat affected zone (HAZ) are important output parameters. The input parameters have to be so chosen that to obtain desired output parameters.

The depth of focus affects the depth of penetration and the shape of the cavity ablated. The depth of focus for a diffraction limited beam is given by the equation

$$d_f = 2.56\, F^2 \lambda / \pi \tag{3.3}$$

where 'F' is the ratio of focal length to the beam diameter and λ is the wavelength.

Holes deeper than the depth of focus can be drilled but requires sufficient fluence, but will result in significant taper.

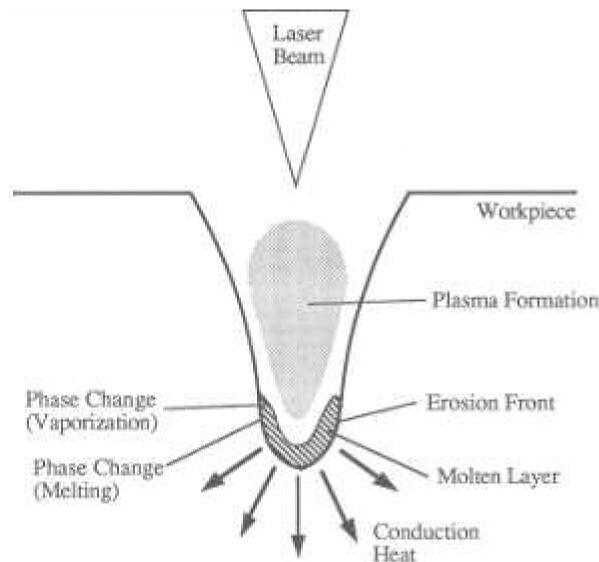

Fig. 3.3 Schematic showing drilling of laser hole

There are several ways to minimize the thermal effects. By reducing the energy and/or the repetition rate when nearing the end point so that the minimum fluence is used for final material removal. The second method is to use a sacrificial layer on the bottom to induce artificial mechanical rigidity into the part. Because of the hole taper, the exit before lapping must be slightly smaller than the desired exit after lapping as the hole diameter gets somewhat bigger as material is removed from the bottom up. The repetition rate has a minor influence on the quality of the holes at the rear side of the wafer, whereas increasing laser fluence leads to an increasing crack formation and break-off of material but also a decreasing hole diameter at the rear side of the wafer. This behavior is due to high pressure of the expanding laser plasma. The ablation depth per laser pulse depends both on the number pulses as well as the fluence.

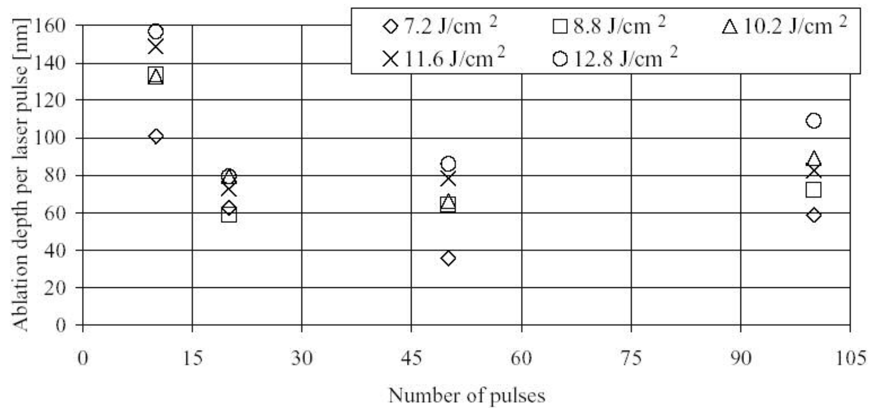

Fig 3.4 Ablation depth per pulse on number laser pulses for different laser fluences at 50 Hz and 100 μm (Keiper *et al.*, 1999).

It can be seen from Fig 3.4 that for the first laser pulse no ablation depth could be measured, since it led only to a laser induced change of the sample surface, like the ablation of impurities or water as well as increasing roughness and absorption. After ten

laser pulses relatively high ablation depths between 100 and 160 nm per pulse were observed. The following ten laser pulses show only half the ablation depth per pulse.

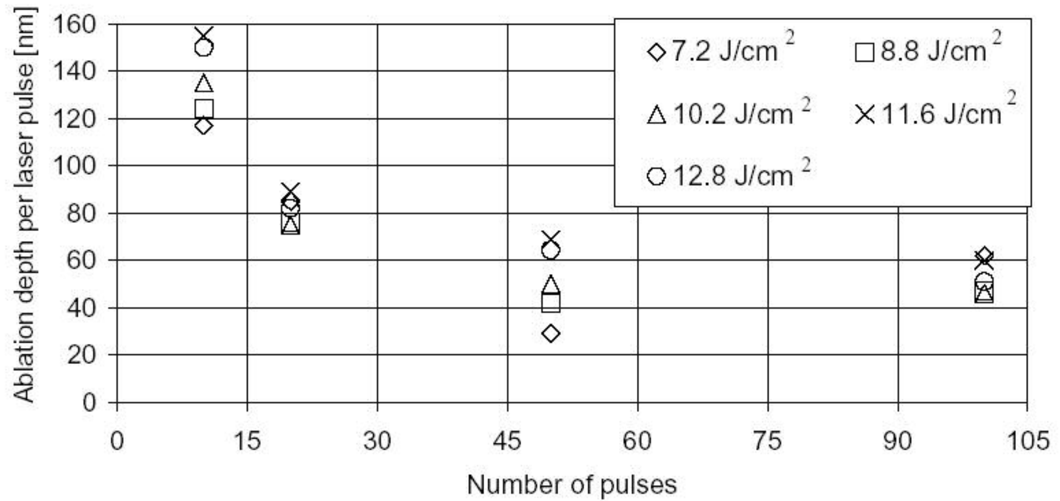

Fig. 3.5 Ablation depth per laser pulse on the number of laser pulses for different laser at 500 Hz repetition rate and 100 μm (Keiper *et al*., 1999).

From Figs 3.4 and 3.5 it may be noted that the repetition rate has only a minor influence on the quality of the holes at the rear side of the wafer. But increasing the laser fluence leads to an increasing crack formation and break-off of the material at the bottom of the wafer. Lower laser fluences have lead to crack-free holes and little break-off material, but results in holes of smaller diameter. As the number of pulses increase with increase in fluence, the ablation depth is found to decrease. Hence, the number of pulses and the change in fluence have considerable influence on the ablation rate. Consequently, an optimum fluence should be determined (Keiper *et al*., 1999).

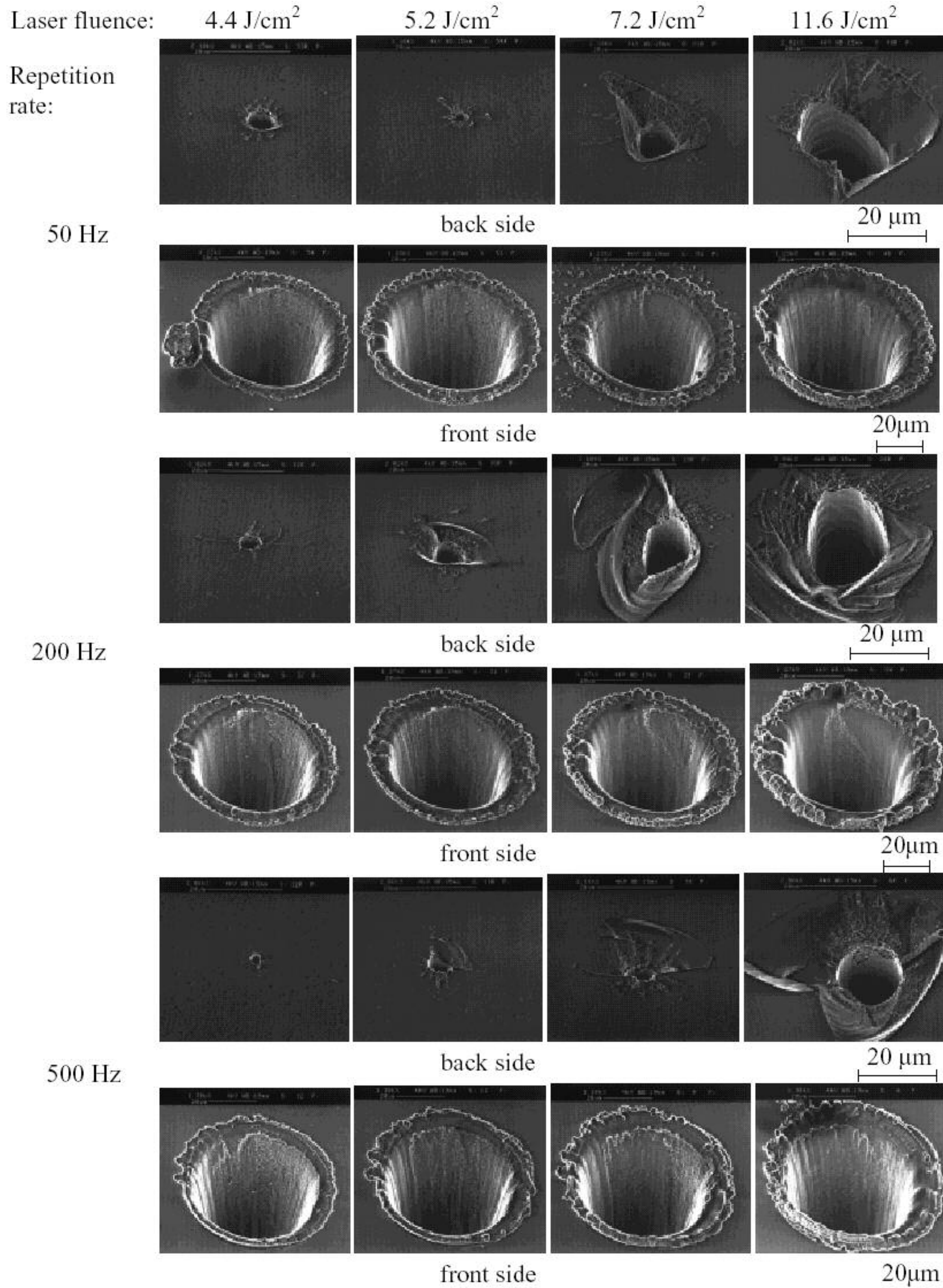

Fig. 3.6 SEM micrographs of 50 µm thick Pyrex glass drilled at different laser fluences and repetition rates (Keiper *et al*., 1999).

CHAPTER 4

LITERATURE REVIEW

Borosilicate glasses because of their enormous potential have widespread applications in micromachining and microtechnologies, such as microoptics and biomedical devices. Apart from their outstanding chemical, optical, and mechanical properties, borosilicate glasses also have good thermo-mechanical stability. But due to their brittle nature, they are very difficult to machine by most conventional machining techniques. Laser micromachining is an attractive alternate approach for the machining of glass. The linear absorption for glasses, however, is very low in the visible range. As a result, high power UV and CO_2 lasers have to be used for processing glass that are thermally sensitive, because of high photon energy per pulse. Short-wavelength excimer laser radiation is used for the ablation of materials. Hence, in almost all cases it is desirable that the ablated surfaces have minimal damage. In the case of laser ablation, the surface of the ablated material is usually surrounded by redeposition of molten material or debris that has to be removed subsequently by other methods. An alternative would be to remove it during the laser ablation process itself. This can be accomplished by laser

machining under water. Laser etching in water is similar to the laser shock processing with regard to laser pulse parameters, with the exception that shock is not desired, while ablation is desired. This is achieved by lowering the fluence and increasing the pulse number. The fluence is taken at the level where the material at least melts, but usually vaporizes and ionizes (plasma forms). Fig. 4.1 shows various schemes of laser etching in water. In other neutral liquids, backside laser etching of transparent materials is also used.

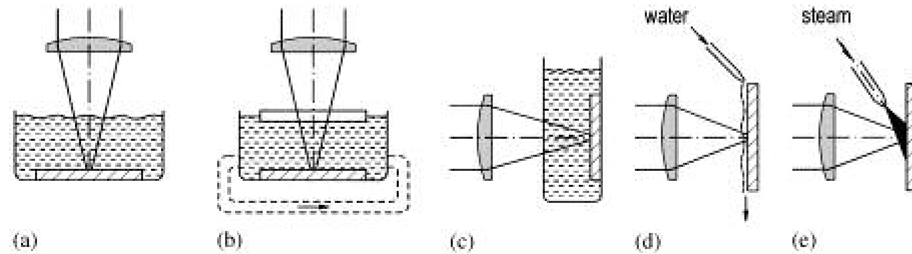

Fig. 4.1. Representation of various schemes of laser etching in water (Kruusing 2004 a, b).

The main reason for water-assisted laser etching is the elimination of debris redeposition in the machined area. This results in cleaner and more precise surface profiles and avoids any need for after-cleaning of the work-piece, which is usually done in an ultrasonic bath. The effect of liquid on laser etching depends on the material and processing parameters. When laser etching is done in liquid, the debris is carried away due to the thermal convection of liquid or by bubble-induced liquid motion,

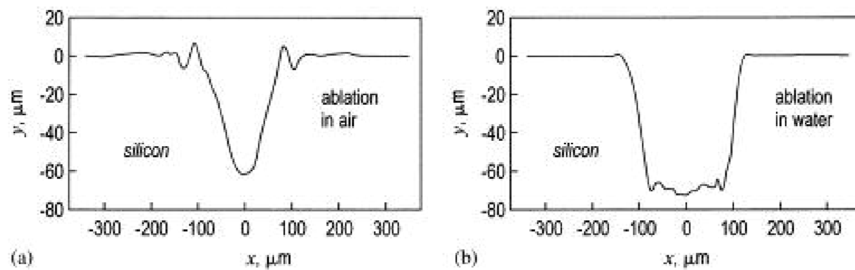

Fig.4.2. Comparison of the hole profiles of silicon laser-etched in air (a) and (b) in water (Kruusing 2004 a, b).

2.1 Reasons for laser machining under water (film) are the following:

- To cool heat-sensitive materials.
- To avoid cracks in the machining of ceramics.
- To avoid a graphitized layer on diamond; this layer is electrically conducting and decreases the catalytic activity of diamond for metal deposition
- To avoid silicon layer formation on a SiC surface, leading to catalytic activity of metal deposition
- It is easier to capture and fix micro-particles by laser tweezers in liquid than in gas (Kruusing 2004 a, b).

The decrease in the etching rate in water at a high number of pulses (low scanning speed) in liquids is probably due to an accumulation of debris suspension, reduction in the transparency of the liquid, and an increase in the etching rate at a low pulse number. Kruusing (2004) reported a similar difference between etching in gases (air, argon) and etching in water. In water, the etching rate for the initial laser pulse was considerably larger than the subsequent pulses later. Dupont *et. al* (1995) offered a possible explanation for this phenomenon in the case of 304 AISI stainless steel material is hardening due to laser shocks. Laser etching of diamond involves no qualitative differences between the results obtained in air and in liquid.

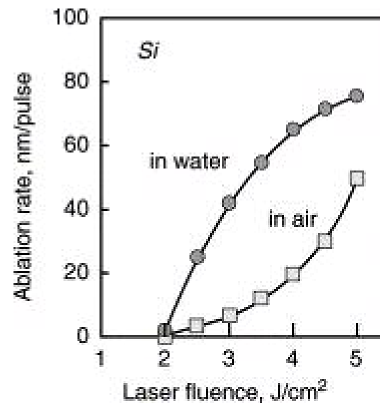

Fig. 4.3. Comparison of the dependencies of the ablation rate on the laser fluence of laser etching of Si in water and in air (Kruusing 2004 a, b).

There are materials (or experimental conditions) where the laser ablation rate in water is lower than in air and others where the opposite is true. The etch grooves were deeper in water than in air for polyimide, the etching rate was nearly the same in air and in water, when the laser fluence is below 20 J/cm^2. The etching rate of Si was 2-fold in water compared to air at a fluence of 0–5 J/cm^2. The etching rate of the materials (steel, $A1_2O_3$, SiO_2) investigated was many times greater in water than in air at 0.1–30 J/cm^2 and vertically flowing water. The etching rate in water was about half that in air; pulse length 140 μs, 10^6-10^{10} W/cm^2 power; for $A1_2O_3$ and porous MgO the etching rate was greater in water, for ZrO_2, SiC, Si_3N_4, glass, stainless steel, and polyamide the etching rate was lower in water for a fluence in the range of 0–35 J/cm^2 . The surface of $A1_2O_3$ remained rough and porous. For laser ablation in liquid, mechanical processes play a considerably greater role than ablation in gas (Kruusing 2004 a, b).

Dupont *et al*. (1995) assumed the ablation rate to be higher in water due to higher pressure of the confined plasma and shock waves. They observed an increase in the surface hardness of AISI 304 stainless steel after every irradiation pulse.

Geiger *et al*. (1998) reported that both brightness of the plasma and the emitted sound were significantly lower at laser ablation under water than in air at a laser fluence up to 30 J/cm^2. Water was sprayed on the workpiece surface.

Laser induced breaking of a single-crystal silicon wafers, with the backside in contact with water is shown in Fig. 4.4. An Nd: YAG laser was used at powers up to 80 W and feed rates of 0.4–20 mm/s. The use of water was reported to result in nearly two times lower crack deviation, damage depth, and branching crack length. The authors explain this by the cooling effect, but the chemical phenomena at crack promotion, such as in the case of glass cutting under water (formation of Si–OH and Si–O$^-$ at crack edges) may also play a role, because water absorbs dissociatively on silicon surface.

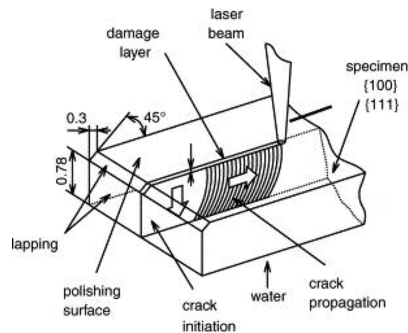

Fig.4.4. Schematic representation of laser breaking of silicon wafers (Kruusing 2004 a, b)

Geiger *et al*. (1998) devised a method of avoiding the redeposition of ablated material by applying thin liquid (water) film to substrate surface, which resulted in better quality of machining. In this type of machining, water film is continuously sprayed onto the vertical workpiece. Their experiments showed that redeposition of ablated workpiece

particles were avoided completely and that there were neither melt particles nor warps surrounding the structure. The ablation rate plays a very important role in excimer laser micromachining. As the energy density increases, the ablation rate also increases but once the saturation point is reached, the ablation rate increases negligibly. Results of these experiments showed that the ablation rate of the ceramic materials was greatly reduced.

Kawaguchi *et al.* (2002) investigated the onset of surface optical breakdown on silica glass using KrF Excimer laser. They observed a transient localized luminescence as the laser fluence increases. Also, as the fluence was further increased, the luminescence reappeared and grew more intensely with continued exposure. Surface optical breakdown is accompanied by localized luminescence due to excited neutral Si atoms region. The craters reflect localized heating and vaporization that give rise to Si luminescence. The morphology of the surfaces damaged by cumulative exposure at fluences below the damage threshold and by single pulses at fluences above the threshold is similar, suggesting that damage under cumulative exposure involves the damage centers responsible for single pulse damage.

Ihlemann (1992) investigated ablation of fused silica using nanosecond excimer laser at 193, 248 and 308 nm wavelengths and 500 fs pulses at 248 nm wavelength. He observed rear side ablation of fused silica with an ablation rate of 0.4 µm/pulse at a fluence of 3 J/cm^2 . But at high fluence front side ablation reached only 0.3 µm/pulse. Thus, based on a comparative study, he concluded that different ablation mechanisms are involved. The first is based on volume absorption, bond breaking, and material

expansion, and the second appears to be controlled mainly by damage in relation to the singularity conditions at the surface.

Allcock *et al.* (1995) investigated microcracking of soda-lime and borosilicate glass by laser irradiation using a transversely excited atmospheric pressure (TEA) CO_2. They concluded that residual stresses caused by thermal cycling of glass resulted in microcracking. They observed relatively large fragments in glass with a characteristic thickness that is dependent on the laser pulse duration. They found that marks are formed by combination of surface crazing and material removal. They also evaluated the gas phase products evolved during the interaction using spectroscopy and high-speed photographic techniques.

Omori and Inoue (1992) conducted excimer laser ablation of inorganic materials to study thermal effects associated with ablation. They observed two different absorption mechanisms. The first occurs during the initial laser pulses with fluences above the ablation threshold and this determines the incubation range. There, multi-photon absorption results in moderate energy volume densities. The second mechanism is determined by a much higher absorption at defects created irreversibly during each additional pulse. They concluded that there are additional thermal effects, such as melting- coagulation, preferential vaporization of the high vapor pressure element and changes in the stiochiometry due to the ablation process in spite of shorter pulse duration.

Dyer *et al*. (1996) found the ablation threshold fluence for soda lime glass to be 1.0 J/cm^2 for 248 nm. Fluence above this value produced microcracking on the surface. Also, the fracture extended well beyond the margin of the irradiated zone. No significant incubation effect was observed below the ablation threshold even after 103 pulses.

Buerhop *et al.* (1990) investigated laser ablation and surface modification of glasses using a CO_2 laser and a XeCl excimer laser (308 nm). They reported that float glass fractures when irradiated for 40 s at 60 W/cm^2 with a CO_2 laser and, vitreous silica withstands higher intensities and material removal occurs by evaporation. For XeCl laser, tests were conducted between 9 and 20 J/cm^2. They observed that glasses with higher absorption coefficient have lower ablation rates. When the threshold fluence was exceeded, noise emission, plasma generation and ablation of front surface were observed. They reported that glass with 8% iron gave a constant ablation rate (0.7 µm/pulse) regardless of the energy density. Float glass gave an ablation rate of 2 µm/pulse with a slight increase in ablation rate with increasing fluence. However, in contrast to this, they found that borosilicate and vitreous glass showed a decrease in ablation rate with increase in fluence.

Jackson *et al.* (1995) performed excimer laser ablation of neodium (Nd) doped glass and Nd doped yttrium aluminum garnet (YAG) using ArF (193 nm) and KrF (248 nm). They found the threshold fluence to be in the range of 0.5-1.6 J/cm^2.

Konovalov *et al*. (2000) reported that 157 nm laser ablation of fused silica generated localized tensile stresses in a thin surface layer (~275 nm) that is independent of fluence (1.9-4.7 J/cm^2) and ablation depth (150-1000 nm).

Buerhop *et al*. (1992) used a 1.5 kW CO_2 laser (10.6 µm), pulsed Nd: YAG laser (1064 nm) and 2 J/ 20 Hz pulsed XeCl excimer laser (308 nm) to investigate melting, softening and ablation effects of fused silica and soda-lime silicate glass using power densities of 10^6 W/cm^2. They observed that fused silica reacted differently because of its optical properties when irradiated at various wavelengths. At 10.6 µm, the glass heats up

due to its strong absorption. Holes of 0.3 mm diameter were drilled in fused silica due to evaporation of material. At 10.6 μm wavelength, fused silica transmits most of the energy. Hence no obvious surface reaction takes place; XeCl gave high ablation rate of 10 μm/pulse but rough surface finish. They reported tangential cracks around the hole during the cooling process for CO_2 and Nd: YAG laser heat treatment of soda-lime-glass. For XeCl excimer laser, cracks were observed only in the solidified thin molten layer with a threshold fluence of 3 J/cm^2.

Keiper *et al.* (1999) investigated drilling on borosilicate glass (Pyrex®) with 248 nm and 193 nm excimer laser. Wall angle of 3.5° and 1.6° were reported with respect to 100 and 30 μm beam diameter. Break-off of material were reduced by applying a thin layer of alcohol between a second wafer underneath the drilling wafer. They reported formation of cracks and a break-off of material at the rear side of the wafer depends upon the processing parameters. They observed the ablation depth to be nearly independent of the repetition rate and only decreases at 500 Hz. Drilling from both sides of the wafer can make holes with the best quality. This method allowed producing holes without break-off of material on the rear side.

According to Zhang *et al.* (2002), when a workpiece is irradiated by an intense (>1 GW/cm^2) laser pulse, the surface layer instantaneously vaporizes at a high temperature and pressures (1~10 GPa) by plasma. This plasma induces shock waves during expansion from the irradiated surface, and mechanical impulses are transferred to the target. If the plasma is not confined (in open air), the pressure can only reach several tenth of a GPa. If the plasma is confined by water or other media, the shock pressure can be magnified by a factor of 5 or more compared to the open air condition (Fox, 1974).

The shock pressure lasts 2 to 3 times longer than the laser pulse duration. When a shock wave is acting on the substrate, material beneath the shock undergoes both plastic and elastic deformations. Shock pressure is attenuated as it propagates downwards and outwards. When the shock wave reaches the bottom, it is bounced back.

Jackson *et al.* (1994) investigated laser ablation of neodymium (Nd) doped glass and Nd doped yttrium aluminium garnet (YAG) crystals using 193 nm and 248 nm excimer lasers. They have reported that the ablation of Nd: YAG and Nd: glass at 193 nm produced etch pits of superior quality to those pits produced using 248 nm laser.

Chen *et al.* (2004) studied ablation of single and arrayed microstructures using an excimer laser. The single feature microstructure was fabricated for evaluating ablation mechanism, threshold fluence and material removal rate. They also investigated changes in the morphologys during ablation with focus on the formation of ablation defects, debris, and recast.

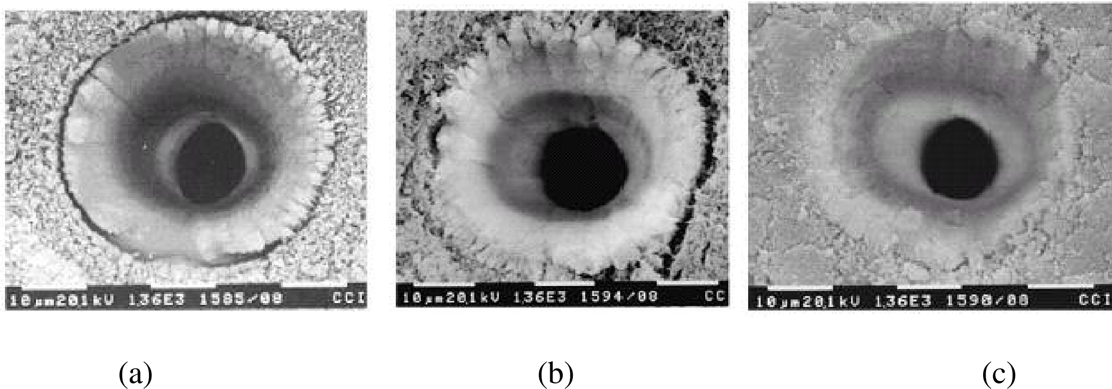

(a) (b) (c)

Fig.4.5 Effects of repetition rate on surface morphology of glass holes ablated at 2.4 J/cm^2 with 2000 shots (a) 2Hz, (b) 5Hz, (c) 10Hz (Chen *et al.,*2004)

Fig. 4.5 shows the SEM micrographs of the ablated holes at three different pulse repetition rates while the fluence and pulse number are kept constant at 2.4 J/cm^2 and 2000 shots respectively. Chen *et al.* (2004) observed that at lower pulse repetition rates

the machined surface is rough, while the higher repetition rates results in more compact material residues and smoother surface. At low repetition rates the debris or recast from laser ablation have sufficient time to cool down to accumulate into larger debris resulting in rougher surface. At high repetition rates, the debris is bombarded by subsequent laser pulses and is ionized into much finer sizes resulting in smoother surface.

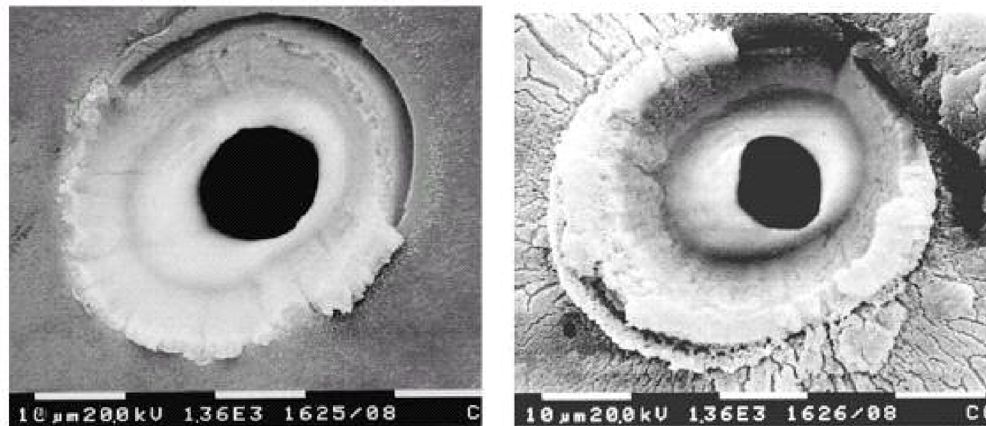

(a) (b)

Fig. 4.6 SEM images of surface morphology of ablated glass holes after 10% HF etching ablating at 5 Hz, (b) ablating at 10 Hz (Chen *et al*., 2004)

Chen *et al.* (2004) reported that debris is mainly an oxide layer accumulated on the ablated surface. Fig.4.6 shows SEM micrographs after 10% HF etching. They show that debris is removed almost 90% for 5 Hz, while the debris for 10 Hz is discharged near 10%. This indicates that the debris produced at higher repetition rates are denser and more cohesive and cannot be easily eliminated even by HF etching.

Li *et al.* (2002) have reported that laser produced metal plasma etching of glass in the atmosphere provides high quality machining. They attribute the mechanism responsible for this high quality machining to the bombardment of high speed, high

temperature electrons and low energy ions from the corona region of the plasma. A solid state, grazing-incidence, diode pump Nd: YVO_4 with 532 nm wavelength was used in this investigation. Corning microslide 2947 with 1mm thickness was used as glass substrate and carbon steel was used as plasma source metal target.

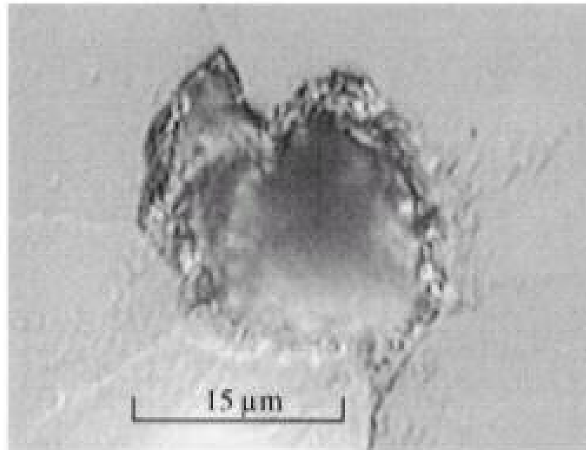

Fig.4.7. Direct ablation on the rear surface of Corning microslide 2947 by 532 nm and 3- ns laser pulses at a threshold fluence of 22.6 J/cm^2 and 200 laser shots. (Li *et al*., 2002)

The surface morphology in Fig. 4.7 presents typical characteristics of an undefined pattern with significant cracks formed during direct laser ablation process because of the optical breakdown mechanism. Plasma etching of the same microslide etched by use of carbon steel plasma at fluence of 3.8 J/cm^2 and 4000 shots glass substrate resulted in a highly defined, clean, mirror-like smooth pit with a diameter of 15 μm.

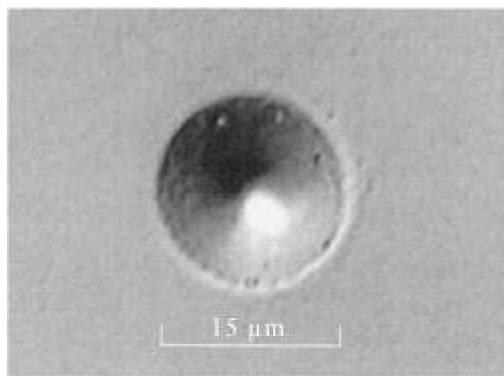

Fig.4.8. Pit with a diameter of 15 µm and a central depth of 3.2 µm on a Corning (Li *et al.*, 2002)

Yakar *et al.* (2003) studied the morphology of borosilicate glass surface machined by a femtosecond laser. They observed the formation of a thin rim around the ablated craters after a single laser pulse. The glass samples were irradiated with 740-800 nm femtosecond (100- 200 fs)

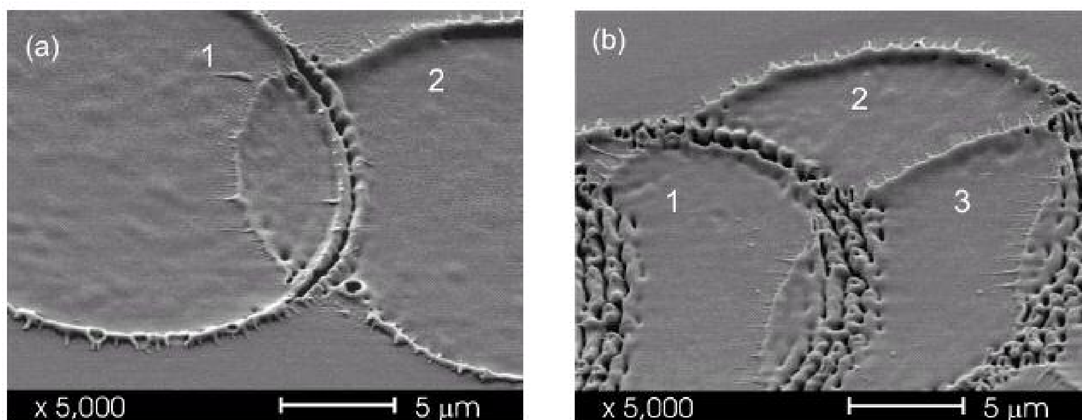

Fig.4.9. SEM images of crater rims generated by overlapping laser pulses (a) 2 pulses, (b) 3 pulses of 800 nm and 100 fs. Fluence, F=0.34 J/mm^2 (Yakar *et al.*, 2003)

laser pulses from a Ti: sapphire laser. Fig. 4.9 shows that the second rim follows the first one on the ablated side of the first crater. The second laser beam diffracts through the

edges of a previously formed crater and hence creates a modulated light intensity at the bottom of the crater due to interference of diffracted light in the near field. They reported that when multiple laser pulses overlap, the crater rim also overlaps and produces rough surface. The rim is resolidified splash of a molten layer generated during ablation process. They have suggested that a very thin melt zone exists during the ablation process and that during the melt lifetime the molten fluid moves from the center of the crater to the edge depositing a thin rim around the ablated area.

Argument *et al*. (1999) conducted ablation rate studies of drilling of glasses using a fourth harmonic Nd: YAG laser and the F2 laser. The 266 nm laser resulted in a higher ablation rate leading to more efficient drilling. However, the edge quality of the hole was not perfect with several microcracks around the perimeter of the hole. In contrast, they found that F2 laser provided a greater control over the ablated depths and surface finish quality.

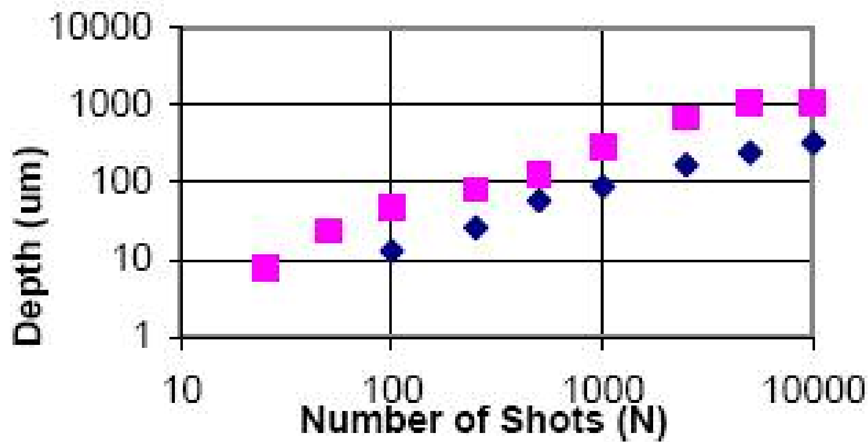

Fig.4.10. Depth of ablation versus number of shots in soda lime plate glass at intensity of 5 J/cm^2 with 266 nm (squares) and 157 nm (diamonds) (Argument *et al*., 1999).

Fig. 4.10 shows that 266 nm pulse laser drill faster compared to 157 nm pulse laser for similar fluence conditions. 157 nm laser offers more precise depth control and smoother finish, while 266 nm lasers drive more rapid excisions. Argument *et al*. (1999) have reported high aspect ratios of more than 20:1 can be achieved in drilling 25 to 50 micrometer diameter holes with depths up to 1mm.

Rudolph *et al.* (1999) studied the machining precision of 130-fs pulse laser ablation (λ = 800 nm) of barium aluminium borosilicate glass and compared the results with those obtained with results using a 10-ns pulse laser (λ =266 nm). Different ablation thresholds and heat-affected zones (HAZ) were observed.

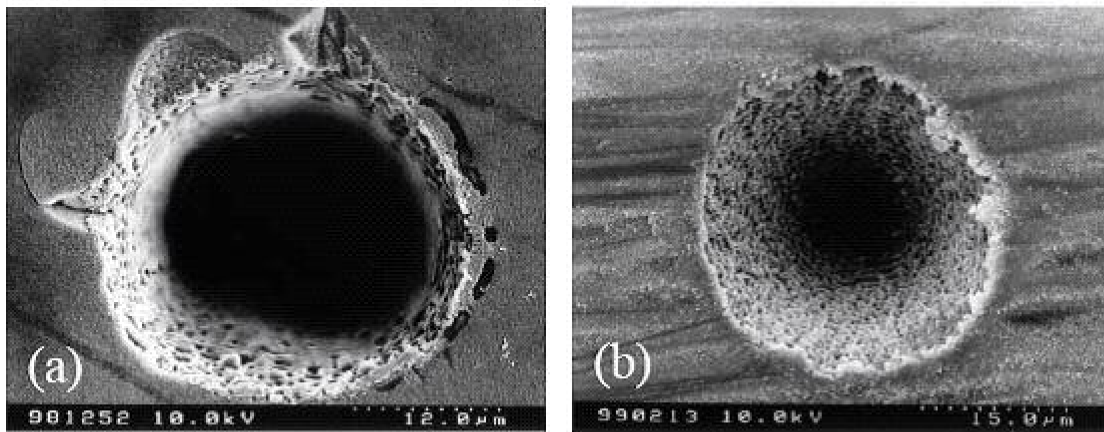

Fig.4.11. Comparison of ns and fs laser ablation of barium aluminium borosilicate glass in air. (a) λ = 266 nm*;* τ = 10 ns*;* N = 100; F = 2.7 J/cm^2 (b) λ = 800 nm*;* τ = 130 fs*;* N = 100*;* F = 3.6 J/cm^2 (Rudolph *et al.,*1999).

Fig. 4.11 (a) shows the hole wall was covered with a smooth melt layer, which occluded the rough bulk morphology. Slightly above the ablation threshold, the outer edge exhibited extended splintering and cracking. While it can be seen in Fig. 4.11 (b) that the application of 100 laser pulses of 130 fs at 800 nm, resulted in a completely different machining quality. Practically no melting has occurred. The lateral precision

was much higher than in the nanosecond case. They report that laser ablation with a single nanosecond pulse leads to the formation of singular resolidified melt bubbles at the center of the illuminated area in the range of $3.4 < F < 5.4$ J/cm^2. Glass was extruded from the bulk volume. The appearance of these melt bubbles can only be rationalized by the creation of an expanding vapor phase. At laser fluences above 5.4 J/cm^2, bubbles disappear and leave behind circular holes of at least 200 nm diameter, depending on the applied fluence. In the case of fs-pulse laser ablation, the application of 5 shots at a fluence (F = 6.7 J/cm^2) slightly above the ablation threshold leads to the formation of a very thin melt layer. When the glass material has been modified by repetitive pulse illumination, generally called, incubation, ablation takes place.

Nikumb *et al.* (2004) used short pulse solid-state lasers with pulse duration in the ns to fs range to process different types of glass materials. The effect of the pulse duration and other process parameters on the machined features were analyzed to reveal the underlying thermal effects and nonlinear processes. Edge quality, circularity, aspect ratio, formation of redeposited material, and machining rate were investigated with respect to the process variables, such as focusing optics, laser power, wavelength, and repetition rate. They also machined complex features on a number of glasses. In order to obtain a burr-free machining, a solvent based masking material MAC-STOP 9554 from MACERMID in the form of a thin film was applied to the material surface. The film was then stripped off manually after the cutting operation. They observed that the maskant film reduced the material deposits at the edges significantly and resulted in smooth, clean cuts even at sharp turning points and curvatures. They also reported that in comparison to nanosecond lasers, the femtosecond laser offers distinct advantages during the processing

of glass material, which includes significant reduction in heat dissipation, thermal damage, and possible utilization of multiphoton processes for machining transparent materials.

Navarrete *et al.* (2003) reported results of an experimental investigation on the induced damage by cumulative pulses generated by an Nd: YAG laser beam focused into the bulk of the BK7 glass. They reported that optical detonation generates a shock wave emission and microcrack formation. The induced photo-acoustic wave emerging from the sample was monitored using a piezoelectric sensor. These signals provide a simple, reliable and highly sensitive indication of the damage, the processes involved, and the most appropriate laser parameters for two and three-dimensional engraving.

Yen *et al.* (2003) developed a direct writing microfabrication system for glass machining by photo assisted chemical etching (PACE). They report that this process produces smooth and debris-free surface. Very low average power is needed. In this method the substrate is in contact with the etchant (pyrene solution in acetone or xylene). When the etchant is excited by the laser energy, the substrate surface is smoothly etched by the transiently activated etchant. High aspect ratios can be achieved by this method and since no photomask is needed for the direct writing process, the substrate size is not limited by the mask and that substrates larger than 12 inches can be used.

4.1. Laser induced backside wet etching (LIBWE)

UV transparent materials, such as silica glass, quartz, and sapphire are materials of importance in optics and optoelectronics because of their outstanding properties such as transparency over wide wavelength range, strong damage resistance for laser

irradiation and high thermal and chemical stability. However, micromachining of these dielectrics is restricted due to high transparency and great mechanical stability. Conventional methods of machining these materials are optical and electron beam lithographies, which are complicated processes involving techniques of patterning a multilayer mask and transferring the pattern to the substrate surface by reactive ion etching. This technique requires high vacuum conditions, an excellent control of the exposure dose, the resist characteristics, and the proportional etching process. Wang *et al* (2000) have investigated a one step method of micro-fabricating silica glass using laser-induced backside wet etching (LIBWE) upon irradiation with a ns-pulsed UV excimer laser.

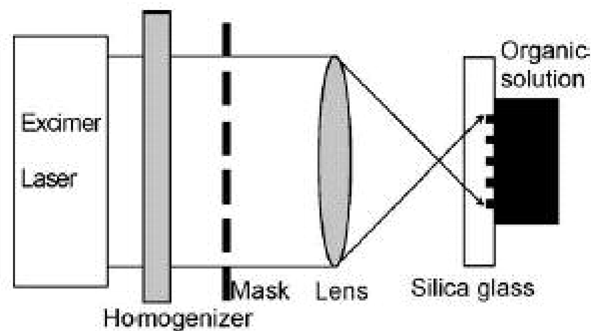

Fig.4.12. Schematic of the setup used for LIBWE method (Ding *et al*., 2004)

Fig.4.12 shows that one side of the silica glass plate is in contact with an organic solution whereas laser beam is introduced from the opposite end. Wang *et al.* (2000) have reported that LIBWE originates from laser ablation of the solution rather than laser ablation of the fused silica. Efficient etching is due to the deposition of laser energy in the solution near the rear. The solution absorbs the laser energy and reaches high

temperatures by a cyclic multiphotonic absorption mechanism. The superheated liquid heats the surface of the silica plate. The vapor with high temperature and pressure attacks the softened surface. After the laser pulse, the irradiated area cools immediately.

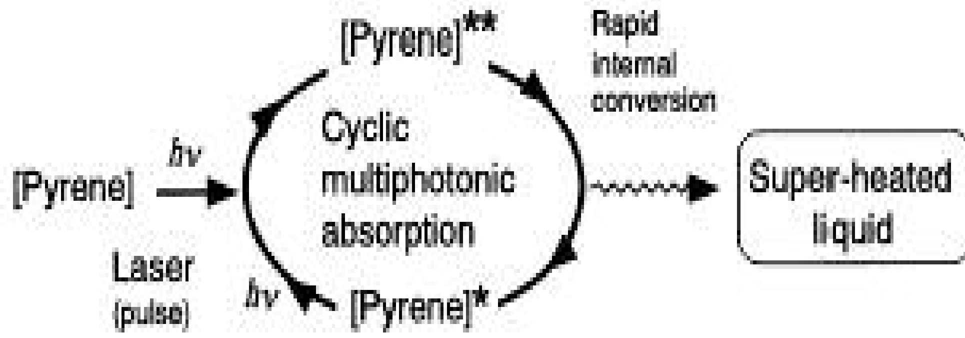

Fig. 4.13 Plausible mechanism for LIBWE by cyclic multiphotonic absorption (Wang *et al.*, 2000)

This rapid cooling behavior prevents bulk plate from thermally damage. Wang *et al.* (2000) reported that LIBWE has several advantages, such as low laser fluence and high etch rate, a constant etch rate, sharp edges for micro-pattern, and crack-free and debris -free surface.

Bohme *et al.* (2002) studied the KrF-excimer laser etching at the interface to liquids for the fabrication of well defined microstructures in UV transparent materials. They found the etch rates and surface morphologies of the materials depend upon the laser parameters, the solution used, and the material itself. The most important effect on the etch rate and the etched surface quality is the laser fluence. They reported that threshold fluence for fused silica to be at 460 mJ/cm^2 which is less than an order of magnitude or more than for laser ablation of fused silica in air (>10 J/cm^2).

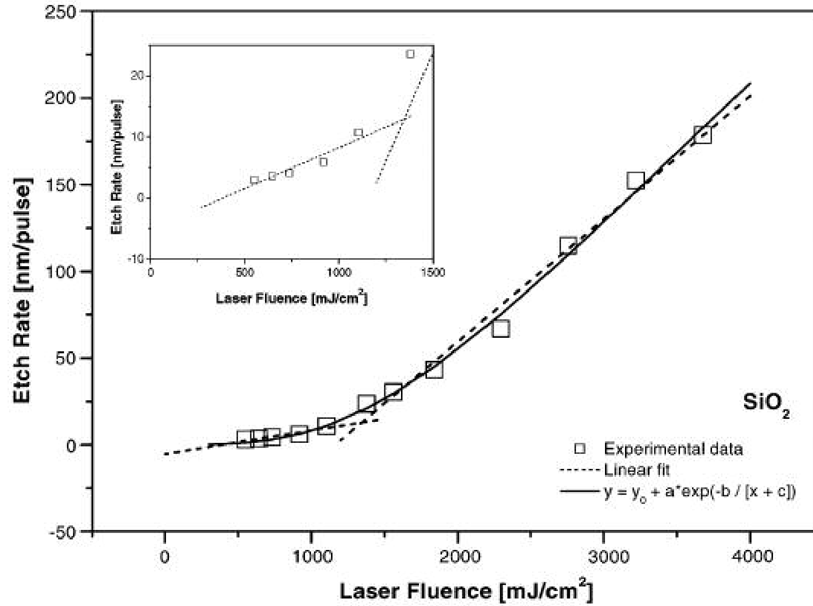

Fig.4.14 Etch rate of fused silica versus laser fluence using a 0.4 pyrene/acetone solution (Bohme *et al.,* 2002)

Bohme *et al.* (2002 reported that in the low fluence range (up to 1.5 J/cm^2), the etch rate per pulse increases linearly. At high fluences, the etch rate increases to 200 nm/pulse. They observed soft etch behavior in the low fluence range to be replaced in higher fluence range by a more ablation dominated mechanism similar to the ablation at a solid gaseous interface. They also used the LIBWE for the fabrication of microstructures such as the one shown in Fig.4.15. The holes with a size of 40 µm x 40 µm and depth of 25 µm were etched by a mask projection at a laser fluence of 0.6 J/cm^2. In all experiments, no debris was observed around the etched structures.

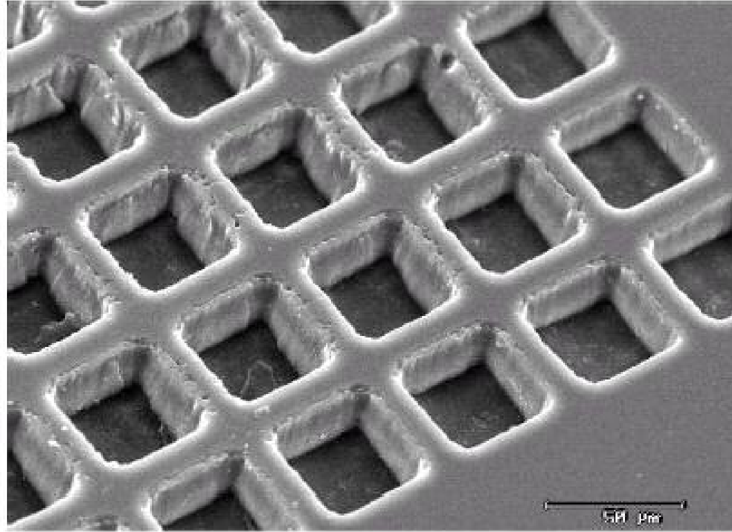

Fig.4.15 Array of micro-sized blind holes etched in fused silica by LIBWE (Bohme *et al.*, 2002)

Kopitkovas *et al.* (2003) have used LIBWE for the fabrication of complex patterns with continuous profiles, Fresnel lenses in quartz. A KrF laser (248 nm, FWHM 30 ns) was used. A solution of pyrene in acetone with a concentration of 0.4 M/1 was used as the etchant. Laser fluence in the range of 0.7 to 1.1 J/cm^2 was used with a variable number of pulses. They reported that etching of quartz by LIBWE showed a behavior similar to the ablation of polymer where a threshold fluence of ablation exists. The threshold fluence of 0.3 J/cm^2 was observed for 248 nm and 0.5 J/cm^2 for 308 nm laser irradiation. These threshold values are well below the damage threshold of quartz, which ranges from 10 to 20 J/cm^2 for 248 nm and 308 nm lasers. From Fig. 4.16, it can be seen that at low fluences the etch rate increases slowly with fluence while above these values the slopes of the curves are 2.5 times higher. The efficient etching of quartz is due to the deposition of the laser energy in a thin pyrene-acetone layer above the quartz surface. The laser induced temperature of the quartz surface in contact with the liquid is

1900 K. This temperature corresponds to the melting point of quartz (1880 K). When the laser induced temperature in the pyrene-acetone solution exceeds the critical temperature, the solution vaporizes and forms bubbles.

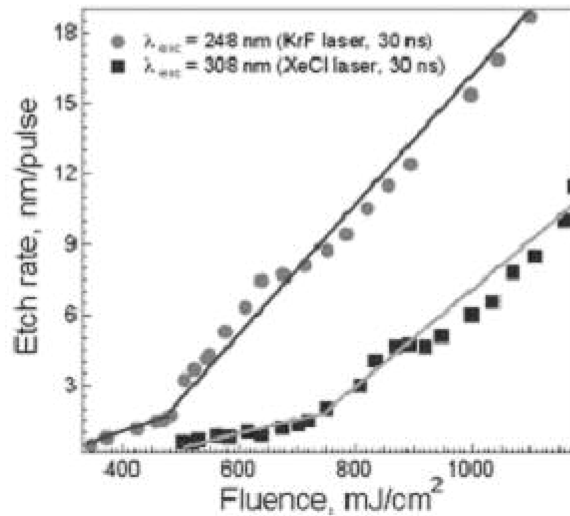

Fig. 4.16 Etch rates versus laser fluence for quartz (Kopitkovas *et al.*, 2003))

The fast expanding or collapsing bubbles create a high pressure, which interacts with the surface of the melted quartz and removes the quartz by mechanical forces. They suggested that this mechanism explains the experimental etching results in a low fluence range, while for high fluence range another mechanism may be dominant.

CHAPTER 5

PROBLEM STATEMENT

Borosilicate glasses are widely used in micromachining applications, but due to their brittle nature, they are very difficult to machine by most conventional machining techniques. Laser micromachining is an attractive alternate for the machining of glass materials. Excimer lasers possess short pulse lengths, and high average and peak power. This makes excimer laser a choice tool for micromachining applications. One of important aspect of laser ablation is to have high quality finished surface.

The objectives of this investigation are as follows:

1. Focus this study to conduct experiments on borosilicate glass so as to investigate the laser-material interactions under different operating conditions, such as changing the pulse energy and machining under different media, such as underwater, methanol, and acetone. The surface morphology of the ablated glass is analyzed using an optical microscope and MicroXam laser interference microscope.

2. To optimize the process parameters so as to produce a machined surface with minimal thermal damage.

3. Analyze the effect of the liquid layer and low energy on the borosilicate glass workmaterial.

4. To conduct micromachining of quartz. As quartz is transparent, a new setup was developed to conduct experiments by changing the concentration of fluids used and changing the pulse energy.

5. To analyze the results after quartz micromachining, using MicroXam laser interference microscope.

CHAPTER 6

EXPERIMENTAL SETUP AND TEST CONDITIONS

6.1. Introduction

Micromachining of Borosilicate glass, and quartz was conducted using a short pulse (FWHM= 25 ns) KrF (λ = 248 nm) excimer laser that generates laser energy in the range of 100-600 mJ. The Excimer laser system can be divided into three main components: Excimer laser generator, stage and motion controller, and Optical or laser beam delivery system. A computer is used to interface excimer laser generator with the stage and motion controller. In the following, the main components of the excimer laser system are briefly described.

6.1.1. Excimer laser generator system:

This system consists of a short pulse (FWHM= 25 ns) KrF (λ = 248 nm) Lambda Physik COMPex205i excimer laser. The laser system uses a KrF gas as the lasing medium at λ = 248 nm. The COMPex205i excimer laser is equipped with Lambda Physik's NovaTube technology. Typical lifetime of gas of COMPex205i is on order of 10^6 laser pulses.

Specifications of COMPex205i excimer laser are the following:

Wavelength (λ) : 248 nm

Energy : 650 mJ

Maximum average power : 30 W

Maximum pulse repetition rate: 10 Hz

Nominal pulse duration : 25 ns

Orientation of the laser beam : horizontal

Type of the homogenizer : dual axis.

COMPex 205i is connected to an 115V (10%), 25A power supply. Table 6.1 gives the specifications of the gas system.

Table.6.1 Specification of the gases used in laser ablation

	Buffer	Rare	Halogen	Inert
Type of Gas	Ne	Kr	5% Fluorine/ 95% He	He
Purity	99.995%	99.99%	99.995%	99.995%

All the gas cylinders have a ¼" Gyrolock pressure regulator and the gases are injected and stored in the lasing tube. When the laser energy drops significantly the gases must be purged and replaced with a new fill. The valves and gas inlets are opened only during the refill process and are closed during all other times.

The laser generator system is controlled by internal and external triggers. The control panel is used to purge gases, change the voltage, repetition rate, and pulse energy.

6.1.2 Stage and Motion control:

An Aerotech's ATS100-150 (X-axis), ATS100-100 (Y-axis) and AVS105 (Z-axis) stages are used. The X and Y-axes stages are linear positioning devices that use a ball screw to drive the stage back and forth along a single axis of motion. The motion control card used is UNIDEX 500 system. This system is a combination of the U500 PC bus based motion control card and the windows based MMI interface software. It integrates with amplifiers and positioning stages to form a complete, programmable, customized control system suitable for a wide range of motion control applications.

6.1.3. Optical or laser beam delivery system:

The optical or laser beam delivery system comprises of five elements: attenuator module, homogenizer, field lens, mask, and doublet. The attenuator module controls the intensity of the laser. Homogenizer cuts the raw excimer laser beam into segments and overlay the segments at the object plane to create a homogeneous beam. The field lens gathers the laser light and converges it into a doublet. Mask controls the shape of the structures produced. Imaging doublet demagnifies the object or the mask. Figure 6.1 shows the setup of the optical delivery system. The laser beam from the laser generator passes through a beam homogenizer. A mask is imaged on the workpiece located on an

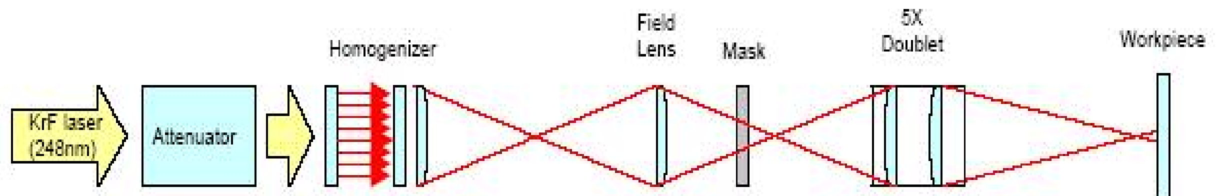

Fig.6.1.Schematic of the optical delivery system for laser micromachining (Choo *et al*. 2004).

X-Y-Z table.

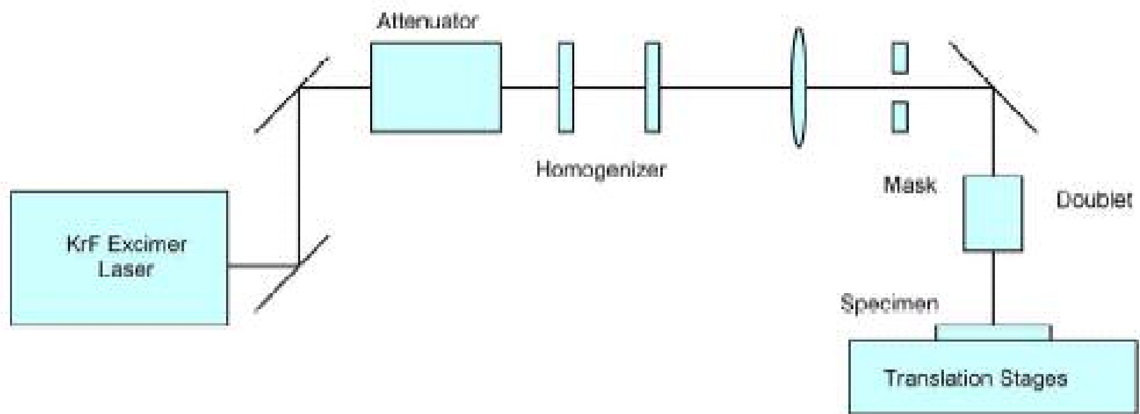

Fig.6.2 (a) Schematic of experimental setup used in laser machining (Choo *et al*. 2004).

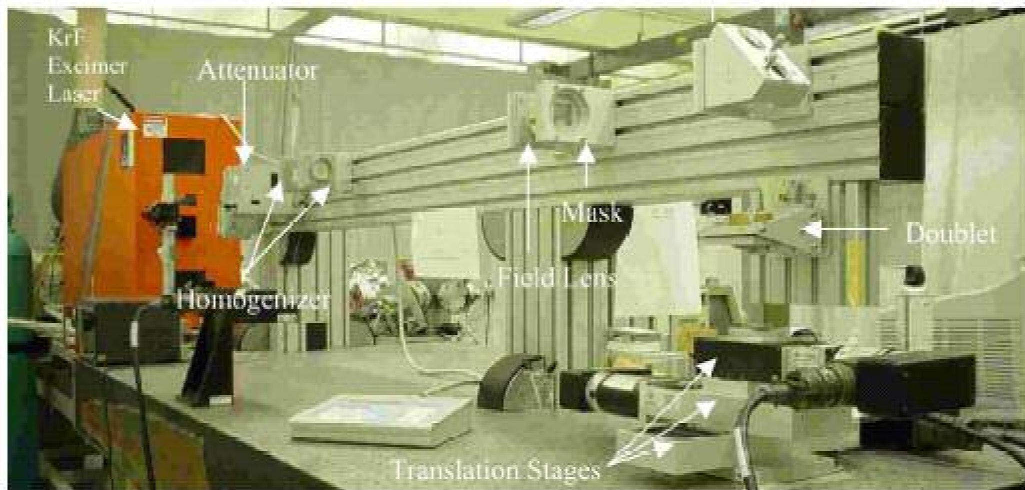

(b)

Fig.6.2 (b) Photograph of experimental the setup used in laser machining (Choo *et al.*,2004).

Figs. 6.2 (a) and (b) show a schematic and a photograph of the experimental set up used in this investigation.

CHAPTER 7

METHODOLOGY

7.1. Introduction

The standard test procedures for laser micromachining are as follows.

1. Sample preparation, 2. Determination of laser fluence, 3. Laser Micromachining, 4. Laser micromachining in different media, 5. Optical microscopy, 6. MicroXam laser interference microscopy.

7.1.1 Sample Preparation

Steps to clean the sample before micromachining

1. Place the sample in a beaker with a detergent solution and subject to an ultrasonic treatment for 2 minutes.
2. Rinse with distilled water.
3. Place the sample in a beaker containing distilled water and subject to an ultrasonic treatment for 2 minutes.
4. Rinse with methanol.

5. Place sample in a beaker containing methanol and subject to an ultrasonic treatment for 2 minutes.
6. Use compressed air to dry up the sample

7.1.2 Determination of Laser Fluence

Pulse energy decreases with the usage of laser energy. Hence, it is important to determine the fluence or energy per unit area each time prior to carrying out the experiments. A Molectron M400 energy detector is used to measure the laser energy. The fluence is calculated using the following equation:

$$f = \frac{E_{avg}}{\pi \,.(D/4)^2} \tag{5.1}$$

where, E_{avg} is the average of the single pulse energy and D is diameter of the mask

7.1.3. Laser Micromachining

Excimer laser with 25 ns FWHM is used to machine glass substrate. The experimental results are presented in Chapters 8 and 9.

7.1.4. Micromachining in different media

A liquid medium is used to reduce thermal damage of the laser irradiated area and different liquids, such as methanol, acetone, and saltwater are also used.

7.1.5. Optical Microscopy

The surface profiles of the machined surfaces are observed using an optical microscope. The thermal damage caused under different laser micromachining areas are observed and compared.

7.1.6 MicroXam Laser Interference Microscopy

A MicroXam laser interference microscope is used for examining the machined samples. It uses different wavelengths of light to scan through the irradiated area and provides a three dimensional profile of the machined surface. The height and depth of the machined areas are obtained using this microscope.

CHAPTER 8

MICROMACHINING OF BOROSILICATE GLASS USING AN EXCIMER LASER

8.1 Introduction

Borosilicate glasses have been widely used in microelectronics and optoelectronics industries. Because of short wavelength, excimer lasers are used for the ablation of semiconductor materials and especially thermally sensitive materials. One of the most important aspects of micromachining is the production of high quality machined surfaces. In the case of laser ablation, the surface of the ablated material is surrounded by redeposition of molten material or debris that has to be removed by other methods. One alternative would be to remove it during the ablation process itself. In this study, micromachining is conducted using different fluids, such as methanol, acetone by varying the concentrations with distilled water. A thin layer of oil and wax are applied on top of the borosilicate glass surface in order to investigate the surface morphology after laser ablation.

8.2. Experimental set up:

The excimer laser micromachining system used in this investigation is described in Chapter 6. The surface of borosilicate glass is irradiated with an excimer laser at different fluences and under different media. In the case of underwater machining, the borosilicate glass is immersed in water with water level ht. of 2 mm above the borosilicate glass surface. Fig.8.1 is a schematic showing the setup used. The borosilicate glass subjected to laser ablation is subsequently examined using conventional optical microscope and MicroXam laser interference microscope for surface mapping and to determine the ablation depth.

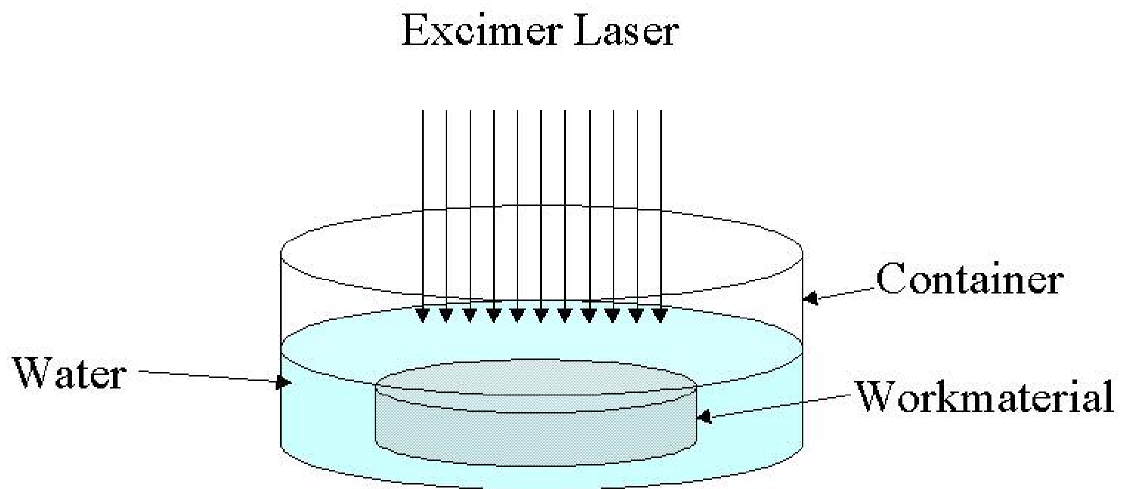

Fig.8.1 Schematic of the setup for micromachining underwater (Choo *et al*., 2004)

A borosilicate glass (Corning 0211) was used as the workmateial in this investigation. Table 8.1 lists the properties of the glass used. Micromachining was conducted with different fluids, such as acetone, methanol and by varying the concentration with distilled water.

Table 8.1. Properties for borosilicate glass (Corning 0211 glass)

General Properties :	
Thickness	0.20 mm
Density	2.53 gm/cm^3
Coefficient of expansion 0-300ºC	$74x10^{-7}$ ºC
Annealing temperature	550 ºC
Softening temperature	720 ºC
Working temperature	978 ºC
Chemical composition :	
Silicon dioxide	64%
Boron	9%
Zinc	7%
Potassium oxide	7%
Sodium oxide	7%
Titanium oxide	3%
Aluminum oxide	3%

8.3. Results and Discussion:

Figs 8.2 (a) to (d) show optical micrographs of borosilicate glass ablated at a fluence of 2.43 J/cm^2 in air, under water, and under 50% methanol and acetone. It can be seen that there is absence of thermal damage in the case of underwater, methanol, and acetone. But the number of cracks is considerably more in the case of machining under these fluids as compared to dry machining. As reported by Park *et al.* (1996) when a

short pulse (ns) KrF excimer irradiates water on a solid surface it induces rapid thermal expansion and explosive vaporization. It is also reported that high pressures and high temperatures associated with laser driven shock waves result in cracking. Water facilitates the propagation of cracks due to thermal expansion leading to more number of cracks. It can be seen that cracks do not propagate beyond the laser-irradiated region Which is due to localized heating of the surface.

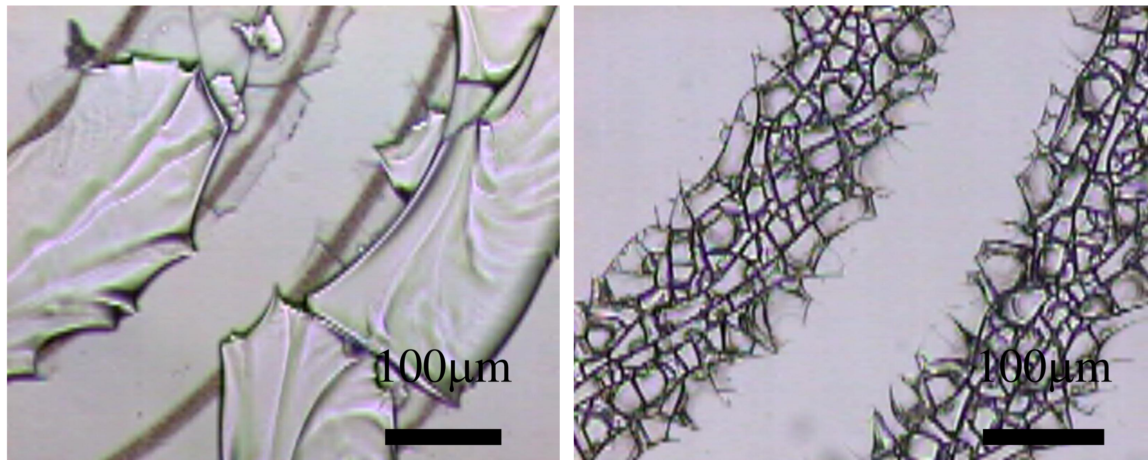

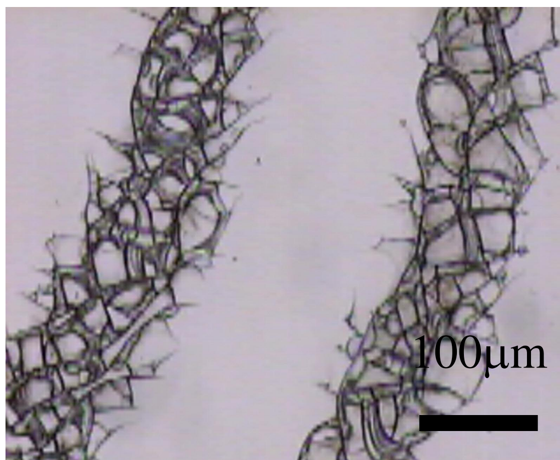

(c) 50 % methanol

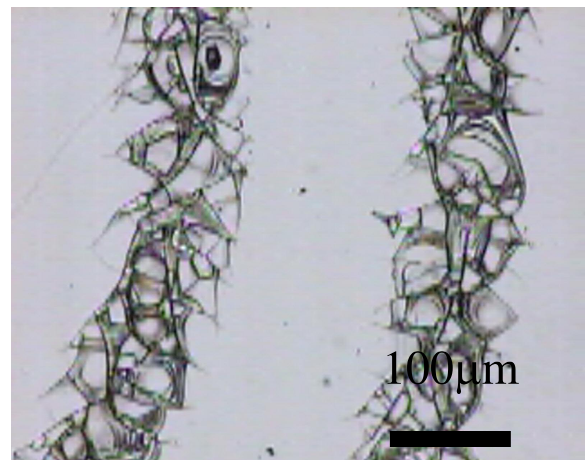

(d) Acetone

Fig. 8.2 Optical micrographs of the top view of borosilicate glass ablated at a fluence of 2.43 J/cm^2

Fig. 8.3 shows the solid surface map of borosilicate glass in dry machining. It shows a thin rim around the ablated region. As reported by Yaker *et al.* (2003), this rim is a resolidified splash of the molten layer generated during the laser ablation process.

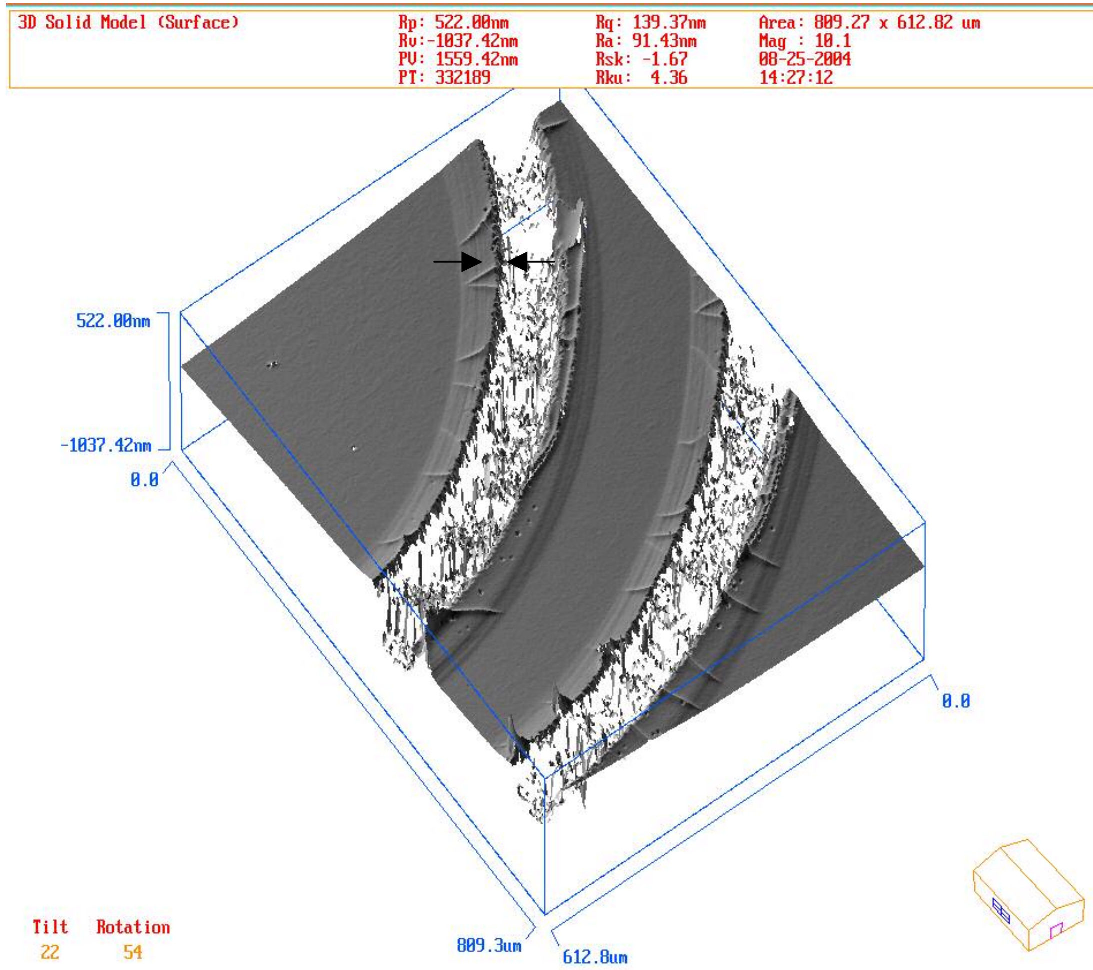

Fig.8.3 Solid surface map of borosilicate glass in dry machining

The molten material moves from the center to the edge depositing a thin rim around the ablated area. Yaker *et al.* (2003) reported that two forces affect the surface of the molten layer, namely, thermocapillary forces and hydrodynamic forces. The hydrodynamic forces are due to pressure gradients caused by the plasma. The pressure

gradients are large at the edges of the ablated area because of plasma-air interface thereby driving the material from the hot center of the melt to the cold periphery.

Micromachining of borosilicate glass was also conducted with a layer of wax and thin layer of oil on top the workpiece so as to study the surface morphology. Figs.8.3 shows the optical micrographs of borosilicate glass with wax and oil on top of the glass surface.

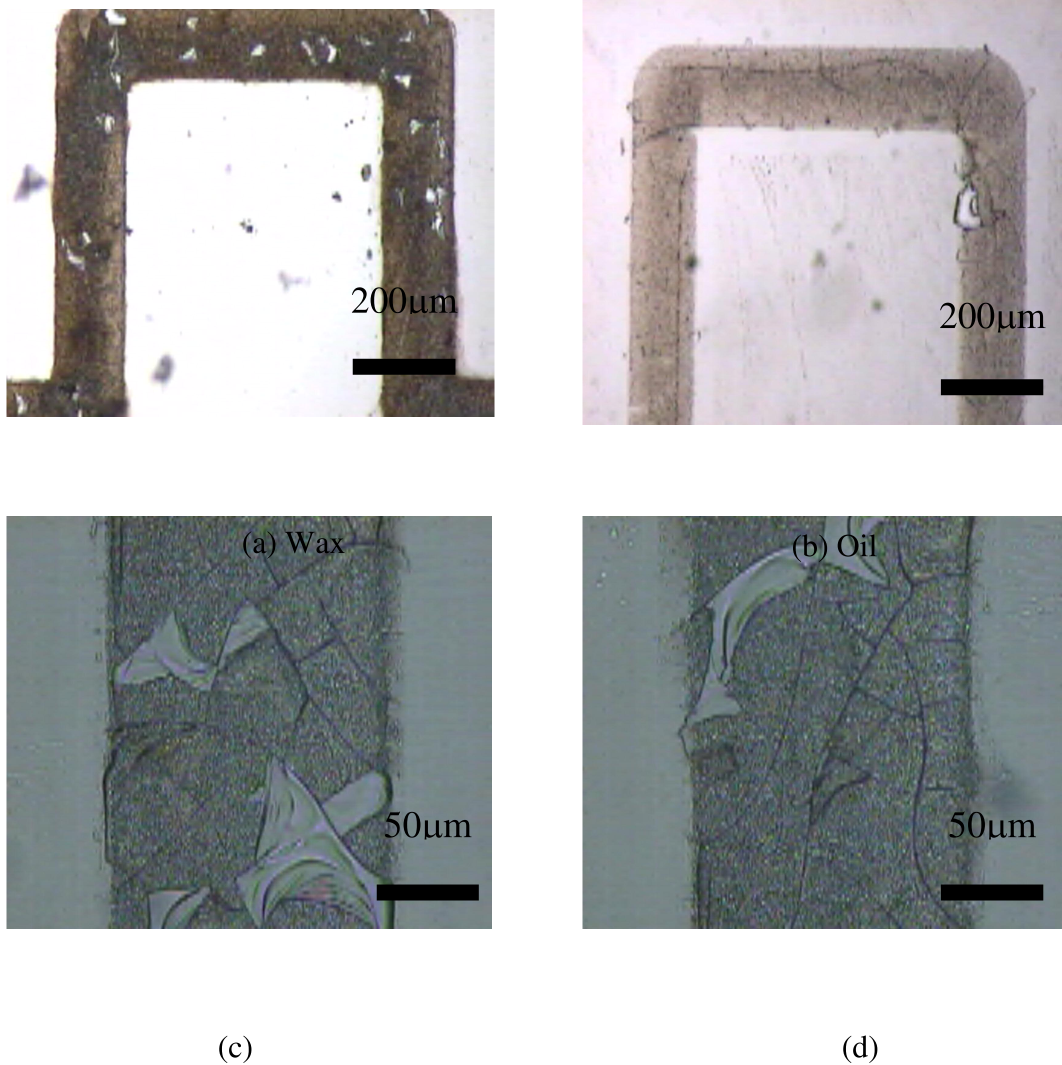

Fig.8.4 Optical micrographs of glass with (a) and (c) wax on top and (b) and (d) oil layer on top of the glass surface at a fluence of 2.43 J/cm^2

It can be seen from Figs.8.4 (a) to (d) that with a layer of wax on top of the glass surface, the number of cracks is considerably fewer as compared to underwater machining. The cracks are larger which are similar to those seen in dry machining in Fig. 8.2. With a thin layer of oil similar results can be seen. The ablation depth is found to be less in the case of wax and a layer of oil because these absorb most of the laser energy during the ablation process.

8.3.1 Effect of low energy:

Laser ablation of borosilicate glass was performed using a low fluence and under different conditions, such as under methanol, with wax on top, and underwater. A mask of 1000 μm was used. Laser ablation was performed at low energy of (0.14 - 0.596 mJ). Table 8.2 shows different medium used for laser ablation at E = 0.535 mJ with a 1000 μm mask

Table 8.2 Different media used in laser ablation of borosilicate glass

Substrate	Type of medium	Ablation depth
Borosilicate glass	50% methanol + 50% distilled water	Built up of 12 nm
Borosilicate glass	Underwater	350 nm
Borosilicate glass	With wax on top	425 nm
Borosilicate glass	Under salt water	Built up of 4-6 nm

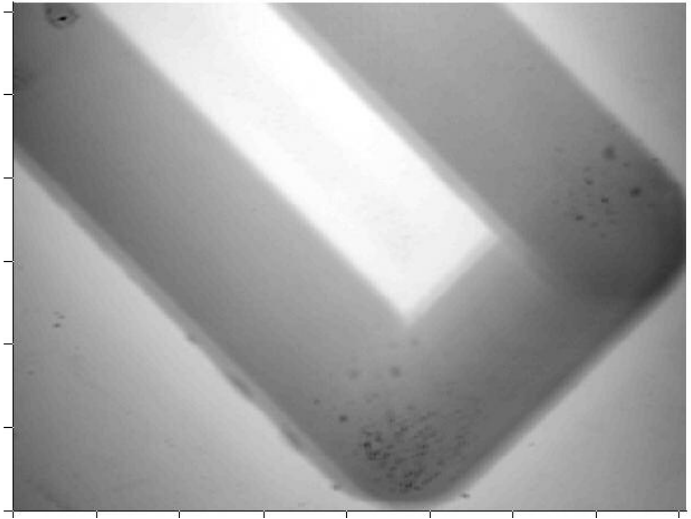

(a)

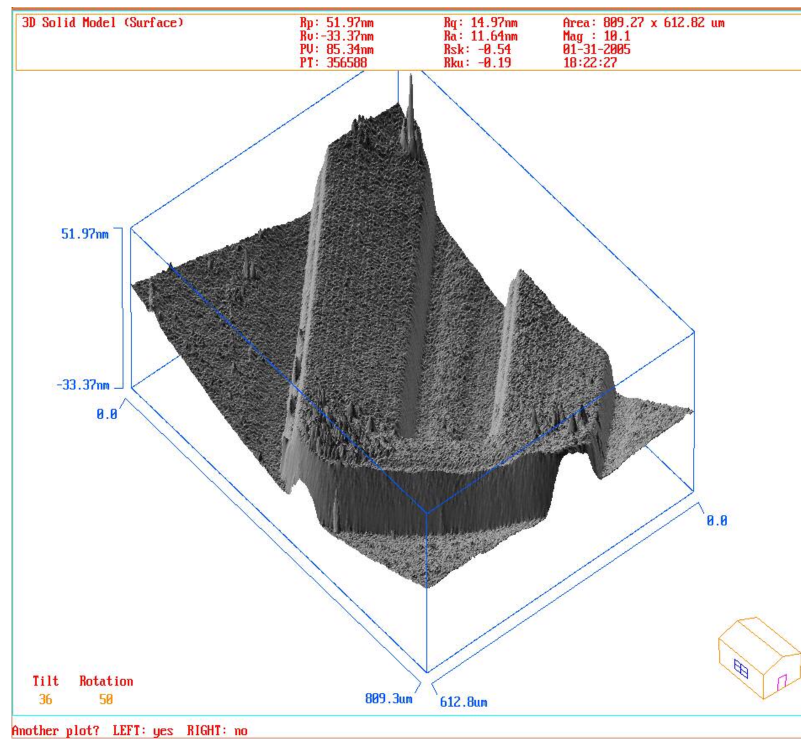

(b)

Figs.8.5 (a) Top view and (b) 3D surface map of borosilicate glass under 50 %methanol + 50 % distilled water at E = 0.535 mJ (height ~ 12 nm).

From Figs. 8.5 (a) and (b) it can be seen that instead of ablation there is built up with a height of ~ 12 nm. The fluid absorbs laser energy and as there is not enough energy to break the bonds a built up is seen.

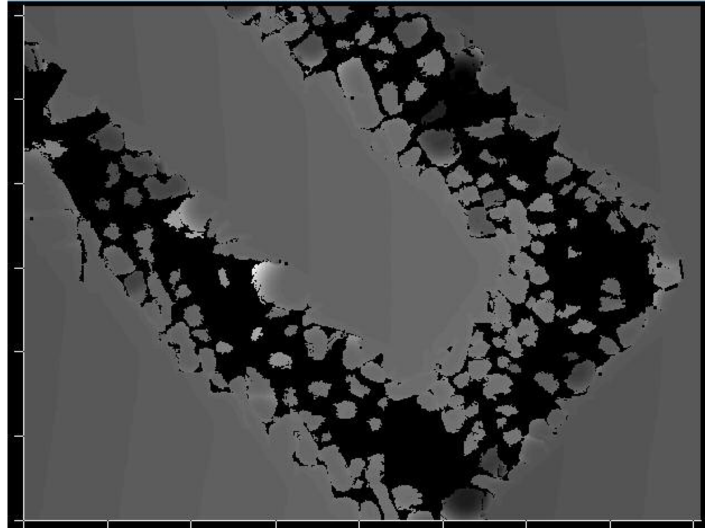

(a)

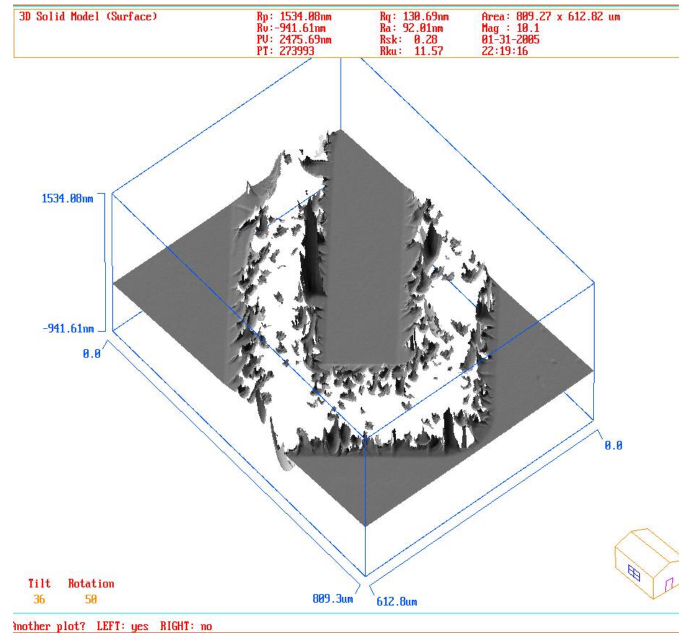

(b)

Figs.8.6 (a) Top view and (b) 3D surface map of borosilicate glass under water at E = 0.535 mJ (ablation depth = 350 nm)

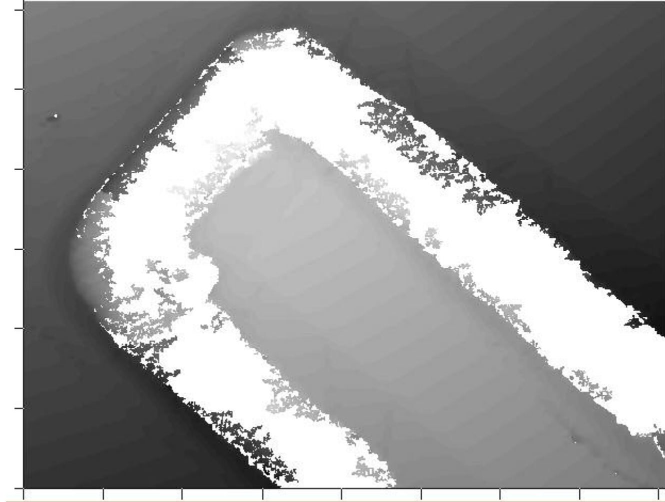

(a)

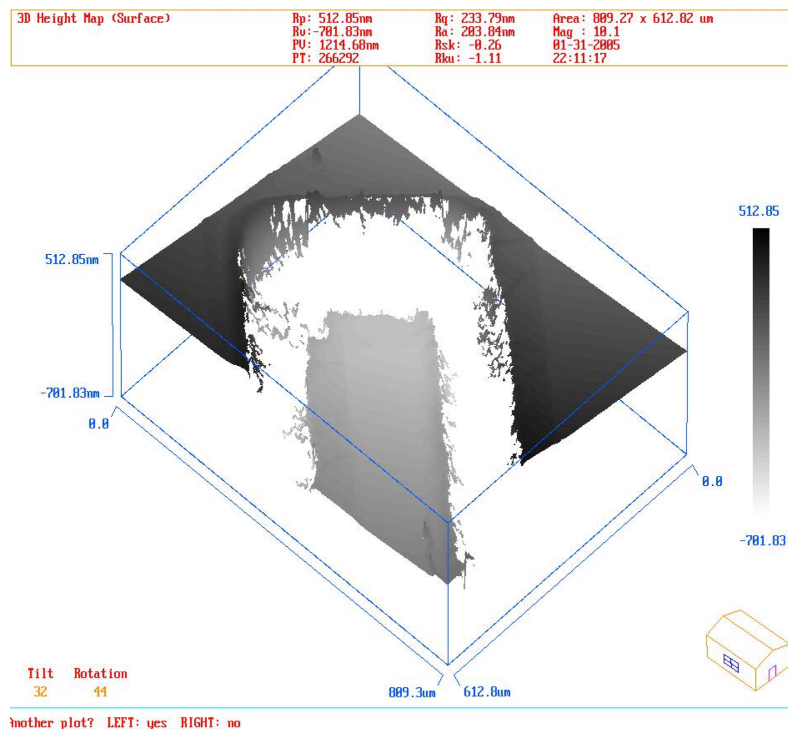

Figs.8.7 (a) Top view and (b) 3D surface map of borosilicate glass with wax on top at E = 0.535 mJ (ablation depth = 425 nm)

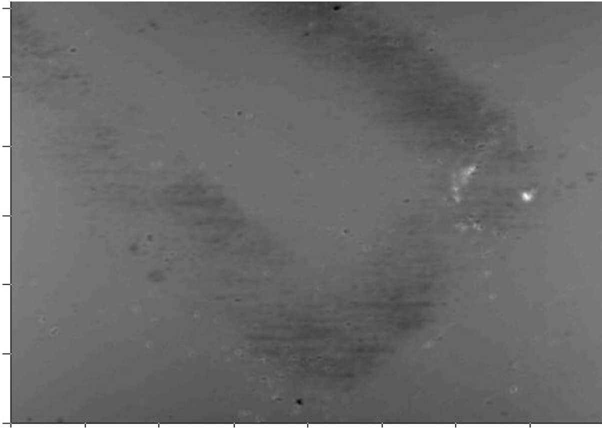

(a)

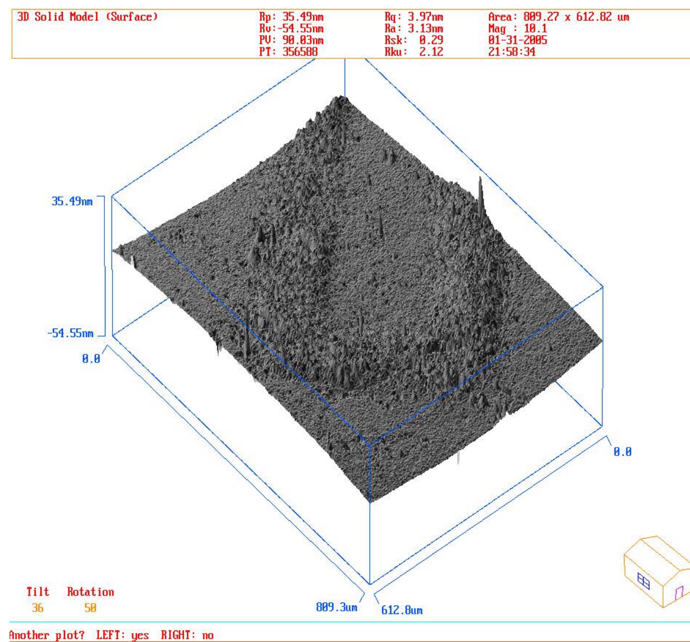

Figs. 8.8 (a) Top view and (b) 3D surface map of borosilicate glass with salt water at E = 0.535 mJ

A similar phenomenon was observed when salt water (NaCl) is used. Salt water absorbs more energy and as a result of laser energy, crystals of salt are formed on the

surface. The surface is very rough and built-up height is approximately 4 to 6 nm. But for underwater and with wax on top, there is ablation and the ablation depth is more than 300 nm in both cases. Additional experiments were performed using a 300 µm mask and under different media. Using a 300 µm mask, the final size of the geometry is 60 µm. Figs 8.9 to 8.12 show the laser ablation of borosilicate glass at low energy under different media.

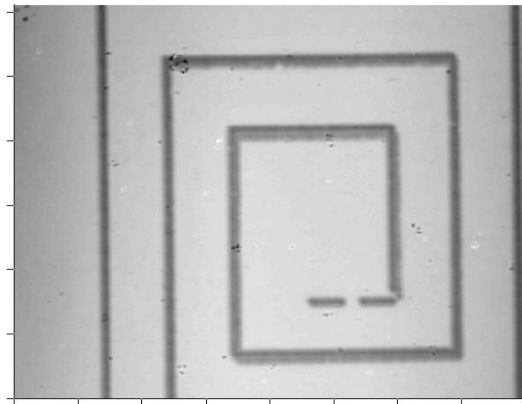

(a)

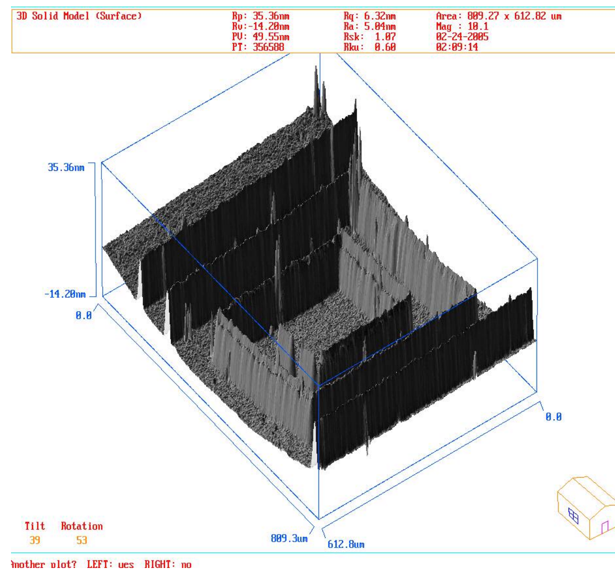

(b)

Figs.8.9 (a) Top view and (b) 3D surface map of borosilicate glass underwater at E = 37.6 µJ

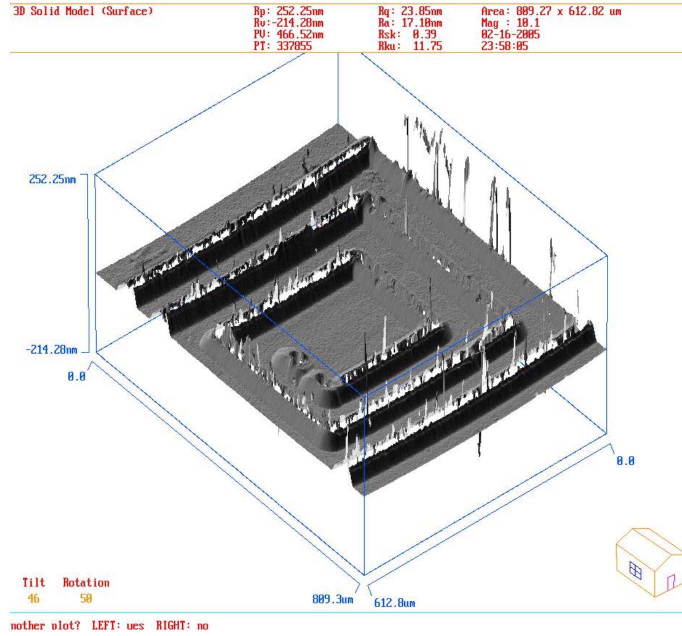

(a)

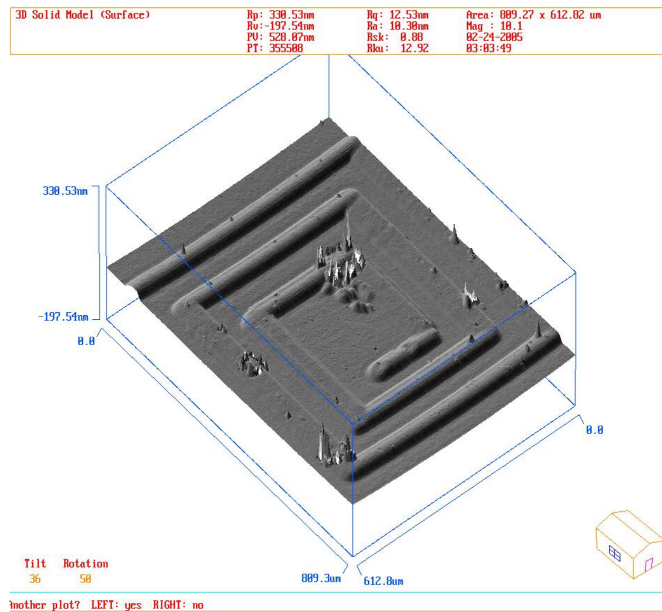

(b)

Figs.8.10 3D surface map of borosilicate glass (a) dry and (b) under 50 % methanol + 50 % distilled water at E = 37.6 μJ

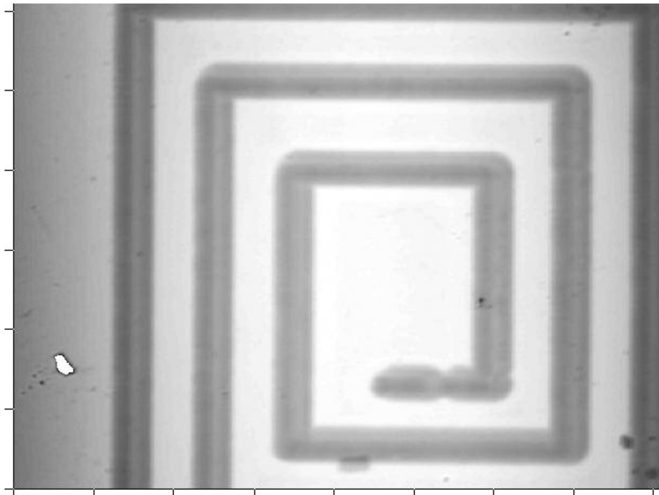

(a)

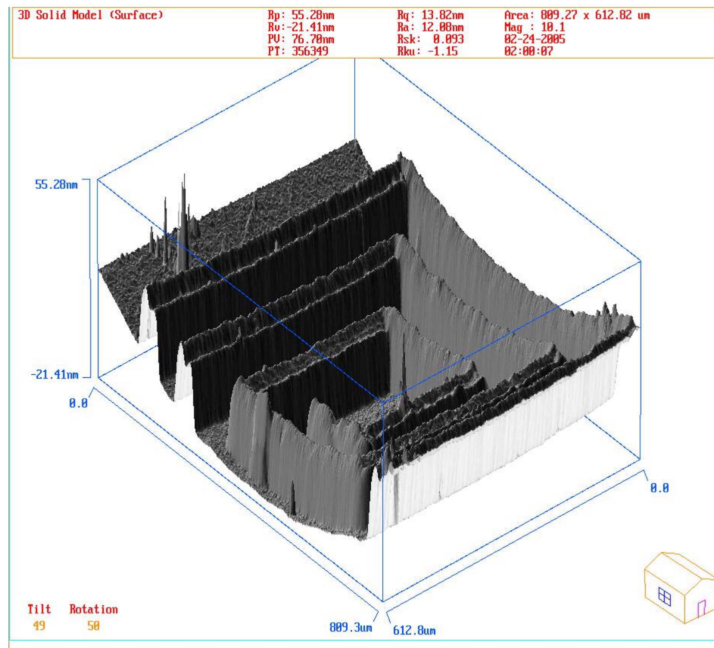

(b)

Figs.8.11 (a) Top view and (b) 3D surface map of micromachined borosilicate glass first dry and then underwater at E = 37.6 μJ

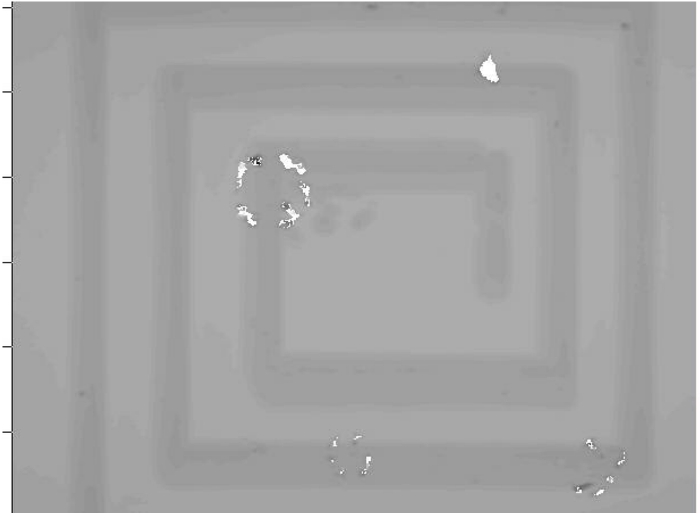

(a)

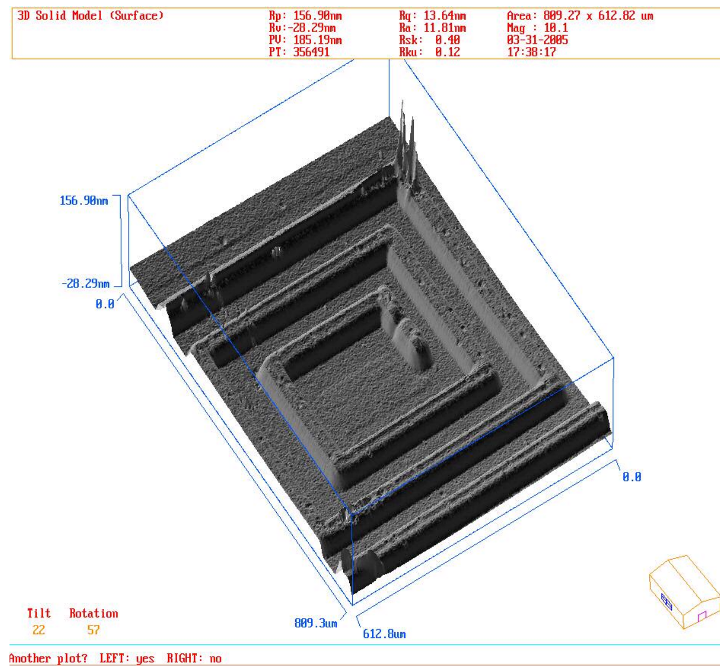

(b)

Figs.8.12 (a) Top view and (b) 3D surface map of micromachined borosilicate glass first dry and then under 50 % methanol + 50 % distilled water at E = 37.6 μJ

From Figs 8.9 (a) to (b) it can be seen that there is a built up (with height ~ 18 nm) and the profile has a very sharp inverted V shaped structure at a laser fluence of 1.33 J/cm^2. In the range of this fluence**,** energy is not adequate to break the bond energy between the atoms and molecules. However, energy is enough to cause thermal boiling and thermal explosion and evaporation of the borosilicate glass. As reported by Chen *et al*. (2004), a low fluence (0.6 and 1.4 J/cm^2) photothermal ablation is more dominant and the thermal energy gradually transfers to the neighborhood. But, when machining is performed using 50% methanol + 50% distilled water, the built-up has a inverted U-shape as compared to underwater at this particular energy with a mask of 60 µm. Energy is sufficient to create plasma with the evaporated material that is caused by thermal ablation. This plasma cloud absorbs most of the laser energy, thereby reducing the final energy reaching borosilicate glass surface (Choo, 2004). The presence of sharp built-up may not be ideal for micromachining as it may lead to stress concentration. So, in order to avoid the sharp built-up, machining was performed first under dry condition and then underwater/methanol. Figs 8.11(a) and (b) and 8.12 (a) and (b) show the results of experiments. It can be seen that there is no longer a sharp built-up. The built-up as seen in Fig 8.12 (a) and (b) has a height of 8 to10 nm.

Additional experiments were conducted to check for repeatability. Figs 8.13 and 8.14 show the results for a different geometry. It can be seen that the results are reproducible with a built up height of 14 to15 nm for underwater. Hence, absence of a sharp built-up by machining first dry and then under 50% methanol + 50% distilled water can also be seen.

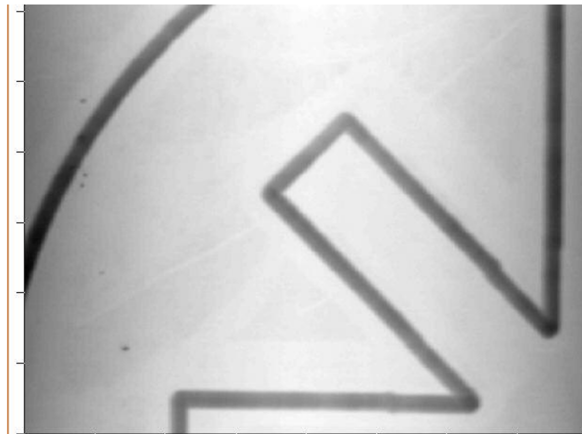

(a)

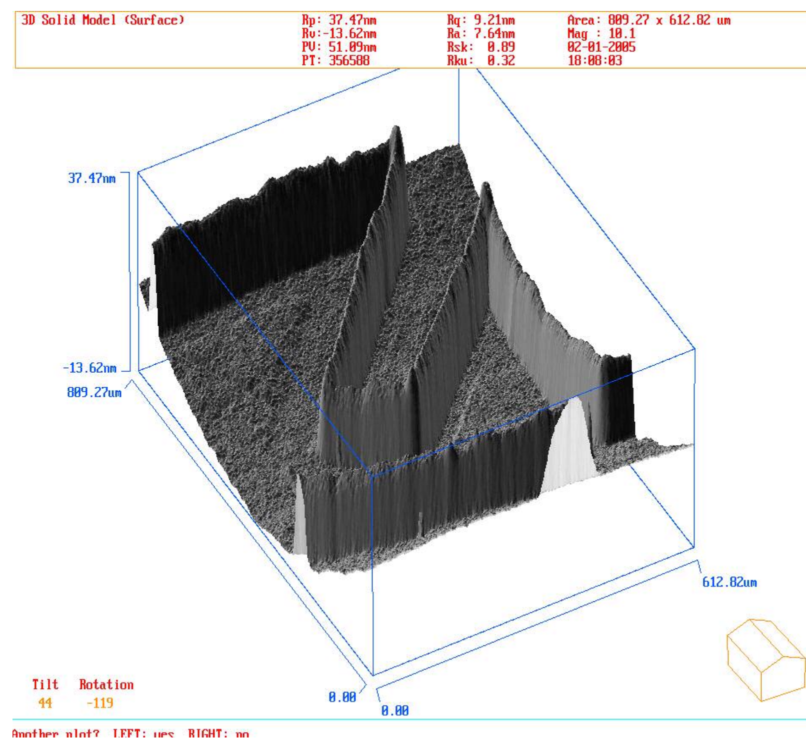

(b)

Figs.8.13 (a) Top view and (b) 3D surface map of borosilicate glass underwater at E = 37.6 μJ

Figs.8.15 (a) to (d) show photographs of laser machined geometries on borosilicate glass at a fluence of 2.81 J/cm^2. These geometries are commonly used in the microelectronic industry.

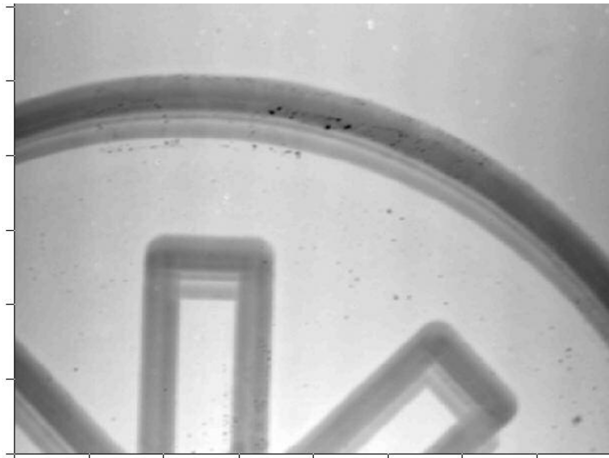

(a)

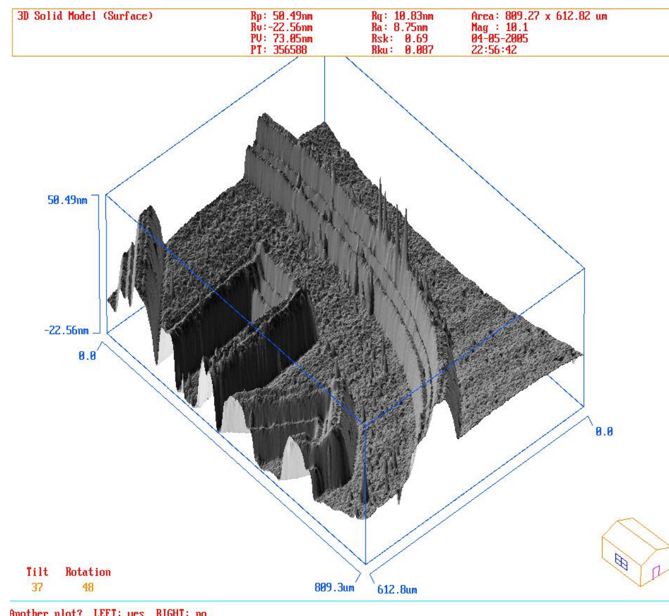

(b)

Fig.8.14 (a) Top view and (b) 3D surface map of micromachined borosilicate glass first dry and then under 50 % methanol + 50 % distilled water at E = 37.6 μJ

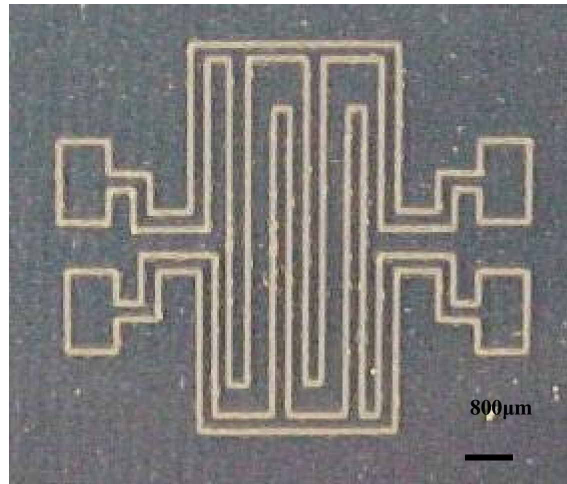

(a)

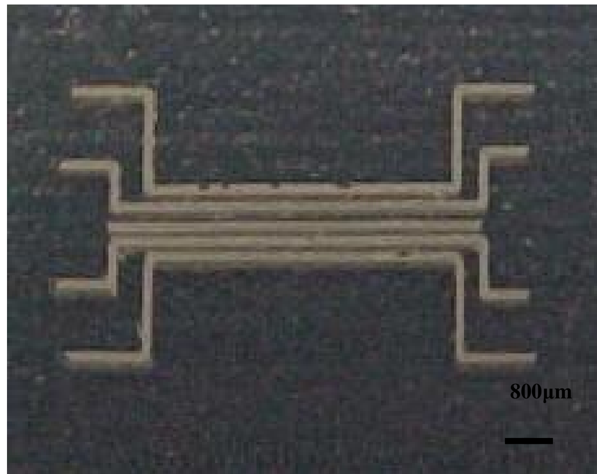

(b)

Figs.8.15 (a) Photographs of circuit similar to the one used in flat panel display and (b) Microfluidic channel micromachined on borosilicate

The circuit shown in Fig 8.15 (a) is widely used in flat panel display. Similarly Fig. 8.15 (b) is used as a microfluidic channel in the biomedical industry. Fig.8.15 (d) is an inductor circuit used in the electronic industry.

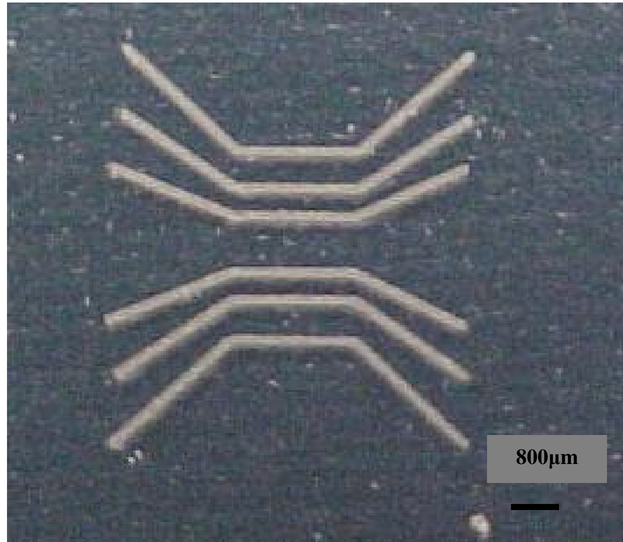

(c)

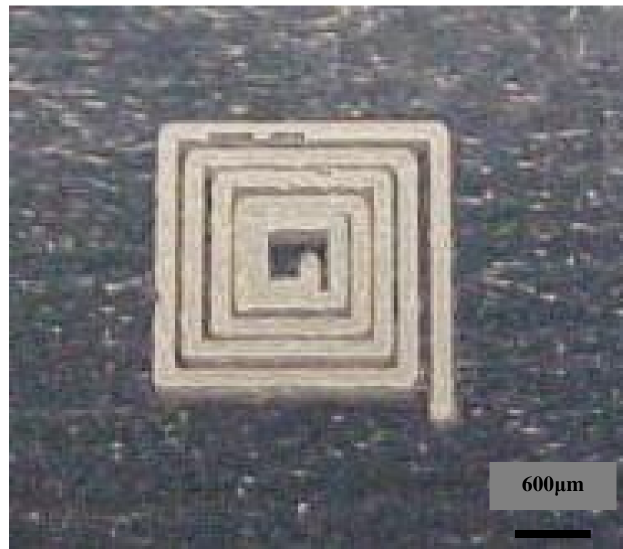

(d)

Fig.8.15 (c) Spider circuit micromachined on a borosilicate glass and (d) An inductor micromachined by excimer laser used in flat panel display

CHAPTER 9

LASER INDUCED BACKSIDE WET ETCHING (LIBWE) OF QUARTZ USING EXCIMER LASER

9.1 Introduction

Laser induced backside wet etching (LIBWE) is a novel one step method for machining transparent materials, such as quartz, fused silica, and sapphire. Wang *et al.* (2001) conducted laser ablation of polymethylmethacrylate (PMMA) films doped with aromatic organic compounds, such as pyrene and benzil. The polymer film, coated on the fused silica plate was irradiated with KrF excimer laser for 30 ns. One of the samples was irradiated from the opposite side due to an experimental mistake in the dark room. The authors found that the back surface of the fused silica plate was damaged along with the ablation of the polymer film. This accidental finding led to the origin of laser induced backside wet etching (LIBWE).

9.2 Experiment Set up for LIBWE

Schematic of the experimental setup used for quartz (thickness of 500 µm) etching is shown in Fig. 8.1. KrF laser (248 nm wavelength) was used as the laser source.

As shown in Fig. 8.1, the aqueous solution of toluene/ acetone is used in contact with one side of quartz plate, while irradiation is performed through the other side. Fig 9.2 shows the quartz transmission spectrum for different wavelengths.

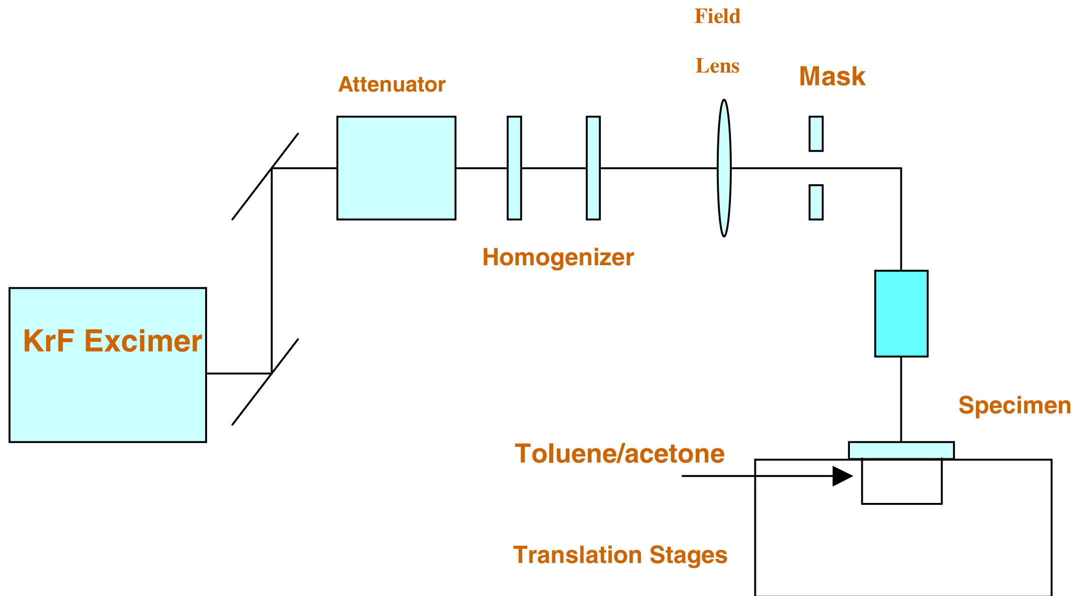

Fig.9.1 Experimental setup for backside etching of Quartz

Mechanism of etching:

The reason for using toluene as an etchant is because it absorbs most of the induced laser energy and finally induces ablation of the solution. Kawaguchi *et al*. (2002) studied the laser ablation of toluene solution under KrF excimer laser. They observed that laser ablation of toluene solution induces transient pressure of order of 10-100 MPa which strongly contributes to etching by LIBWE.

LIBWE originates from laser ablation of the solution rather laser ablation of quartz. The toluene/acetone solution absorbs the laser energy and reaches high temperatures. The superheated liquid heats the surface of quartz and evaporates and

forms bubbles. These bubbles create high pressure, which interacts with surface of melted quartz and hence results in the ablation/etching.

Table 9.1: Threshold fluence of quartz by light induced backside etching (LIBWE) and thermodynamic properties of quartz

	Quartz
Threshold fluence, J/cm^2	0.5
Softening point, K	1850
Thermal conductivity, W/m K	1.38
Heat capacity, J/g K	0.74
Hardness (Knoop), (kg/mm^2)	530
Threshold fluence for dry ablation-damage, J/cm^2	20*

*Ihlemann J., Wolf B., Simon P., Appl. Phys A, 54 (1992) 386.

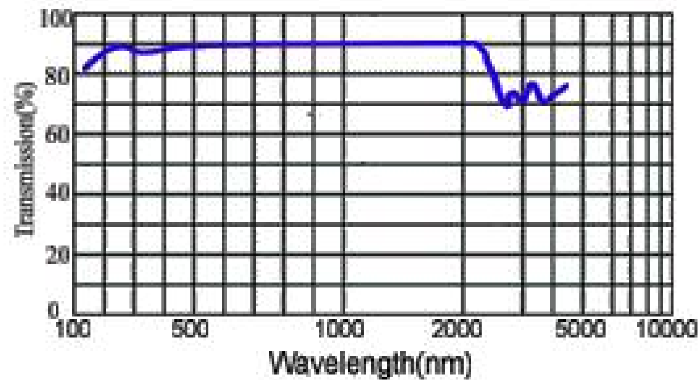

Fig.9.2 Quartz transmission spectrum

Toluene:

Toluene is a clear, colorless liquid with a distinctive smell. It is used in paints, paint thinners, fingernail polish, lacquers, adhesives, and rubber and in some printing and leather tanning processes.

The molecular formula is: C_7H_8 with a chemical structure

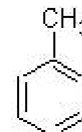

9.3 Results and Discussion:

In this study the absorbing liquid is a solution of toluene either in acetone, methyl alcohol or ethyl alcohol with different concentrations. The solutions used at room temperatures were replaced after each series of etching experiments. The experiments were carried at different pulse energies. Quartz is used as the substrate. The etched surfaces are subsequently examined using MicroXam laser interference microscope for surface mapping as well as to determine the ablation depth.

Table 9.2 Fluids used in laser ablation of quartz at E = 0.522 mJ

Substrate Material	Fluid	**Ablation depth in (nm)**
Quartz	Toluene: Methyl Alcohol 50: 50 70: 30	No Ablation No Ablation
Quartz	Toluene: Ethyl Alcohol 50:50 70:30	No ablation No ablation
Quartz	Toluene: Acetone :: 50:50	No ablation
Quartz	Toluene: Acetone:: 70:30	735 nm
Quartz	Toluene: Acetone:: 80:10	879 nm
Quartz	Toluene: Acetone:: 90:10	1025 nm
Quartz	Toluene: Acetone :: 85:15	1112 nm
Quartz	Toluene 100%	1140 nm

It can be seen from Table 9.2 that when toluene was mixed with different concentrations of methyl alcohol and ethyl alcohol, there was no ablation of quartz at E = 0.522 mJ. These results show that toluene/acetone solution is not completely consumed or decomposed by repeated laser irradiation. Also, there was no ablation when toluene and acetone are used at 50:50. But when the concentration of toluene was increased (and a decrease in the concentration of acetone) ablation was observed.

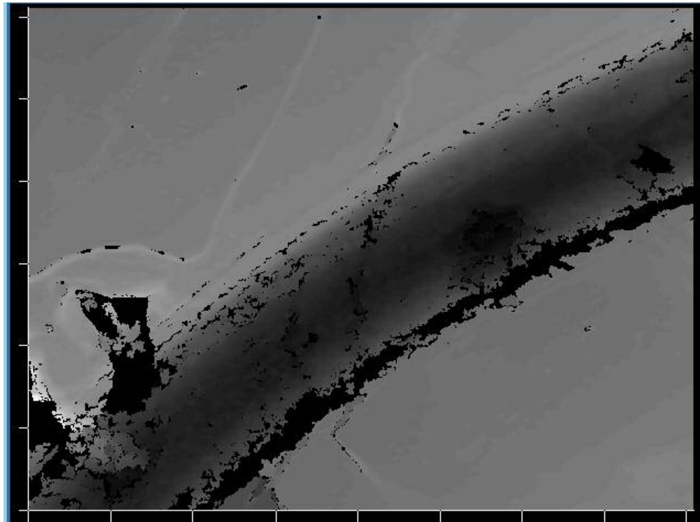

Fig.9.3 (a) Top view of quartz (100% Toluene)

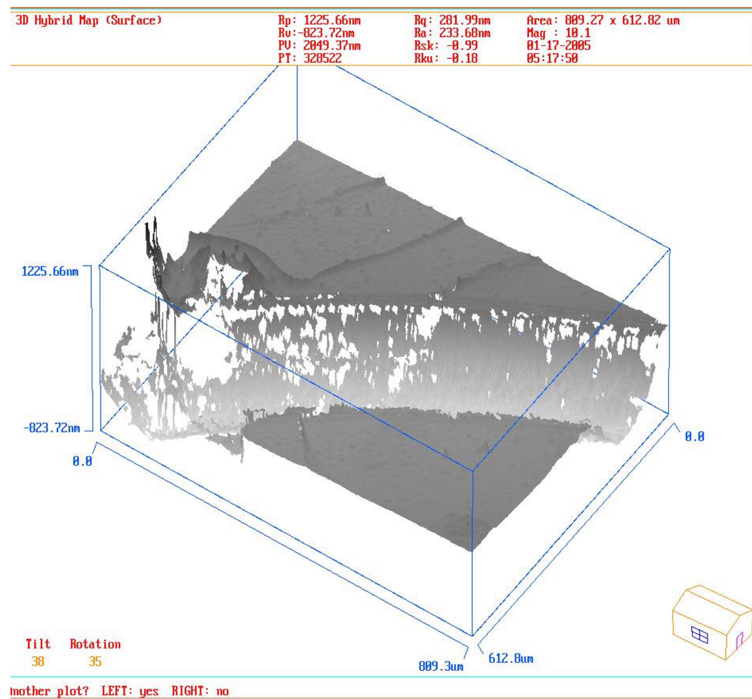

Fig.9.3 (b) 3D solid surface map of quartz (100% Toluene)

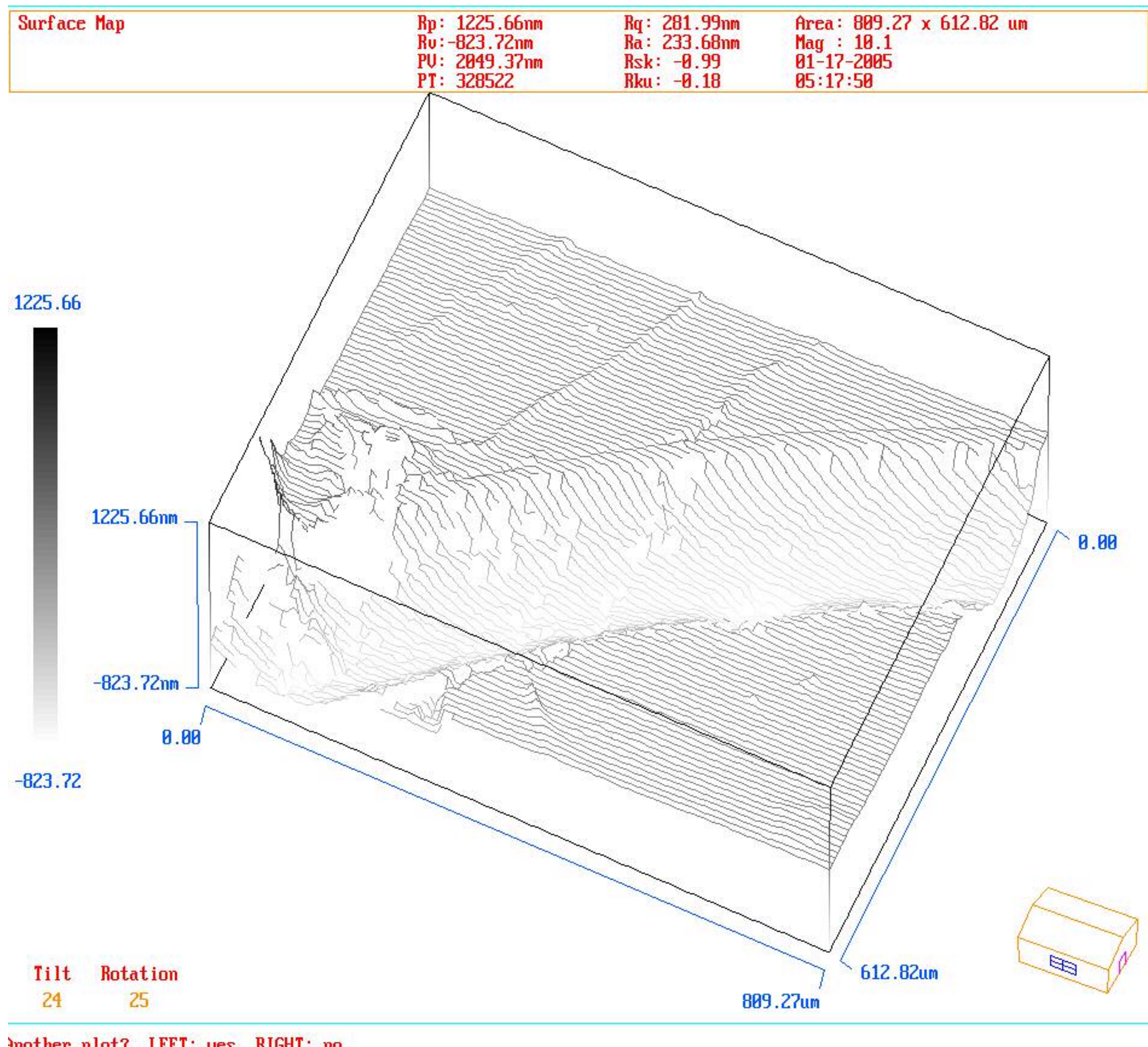

Fig.9.3(c) 3D wire map of quartz (100% Toluene)

From the Table 9.2, it can be seen that for concentration of toluene/ acetone :: 85:15, an ablation depth of 1.12 µm can be noted. It can be seen that with 100% toluene, the ablation depth was highest at this particular energy. Figs. 9.3 to 9.6 show backside wet etching of quartz with different concentrations of toluene/acetone at E = 0.522 mJ.

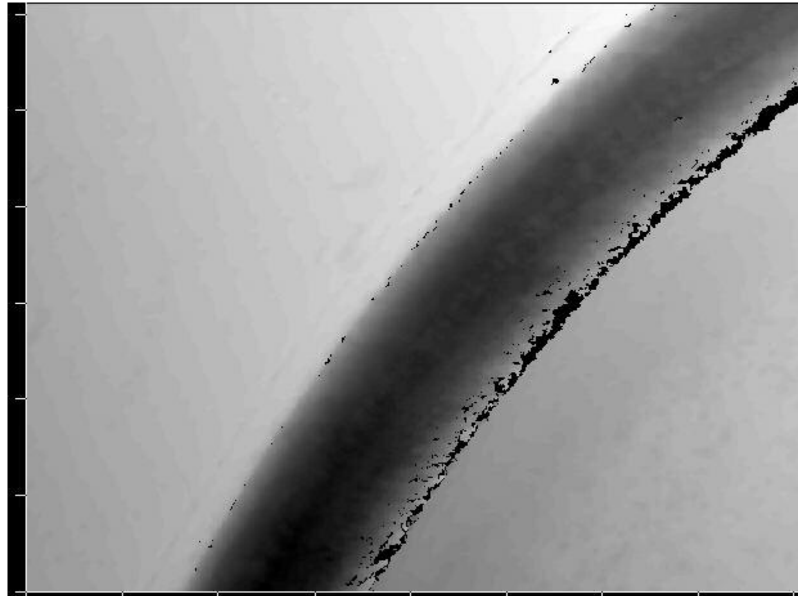

Fig.9.4 (a) Top view of quartz (toluene: acetone:: 90:10)

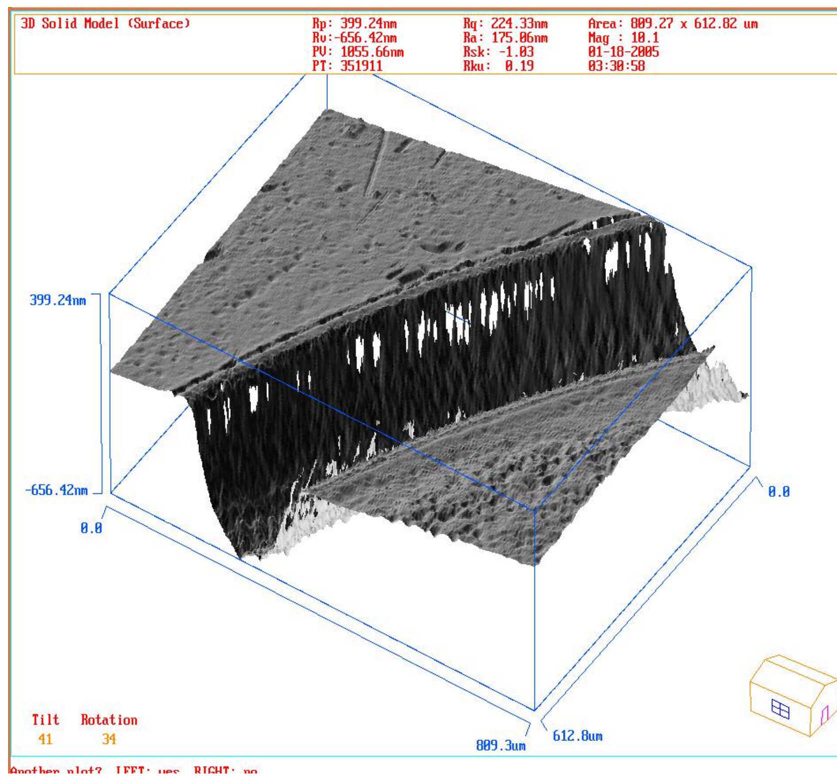

Fig.9.4 (b) 3D solid surface map of quartz (toluene: acetone:: 90:10)

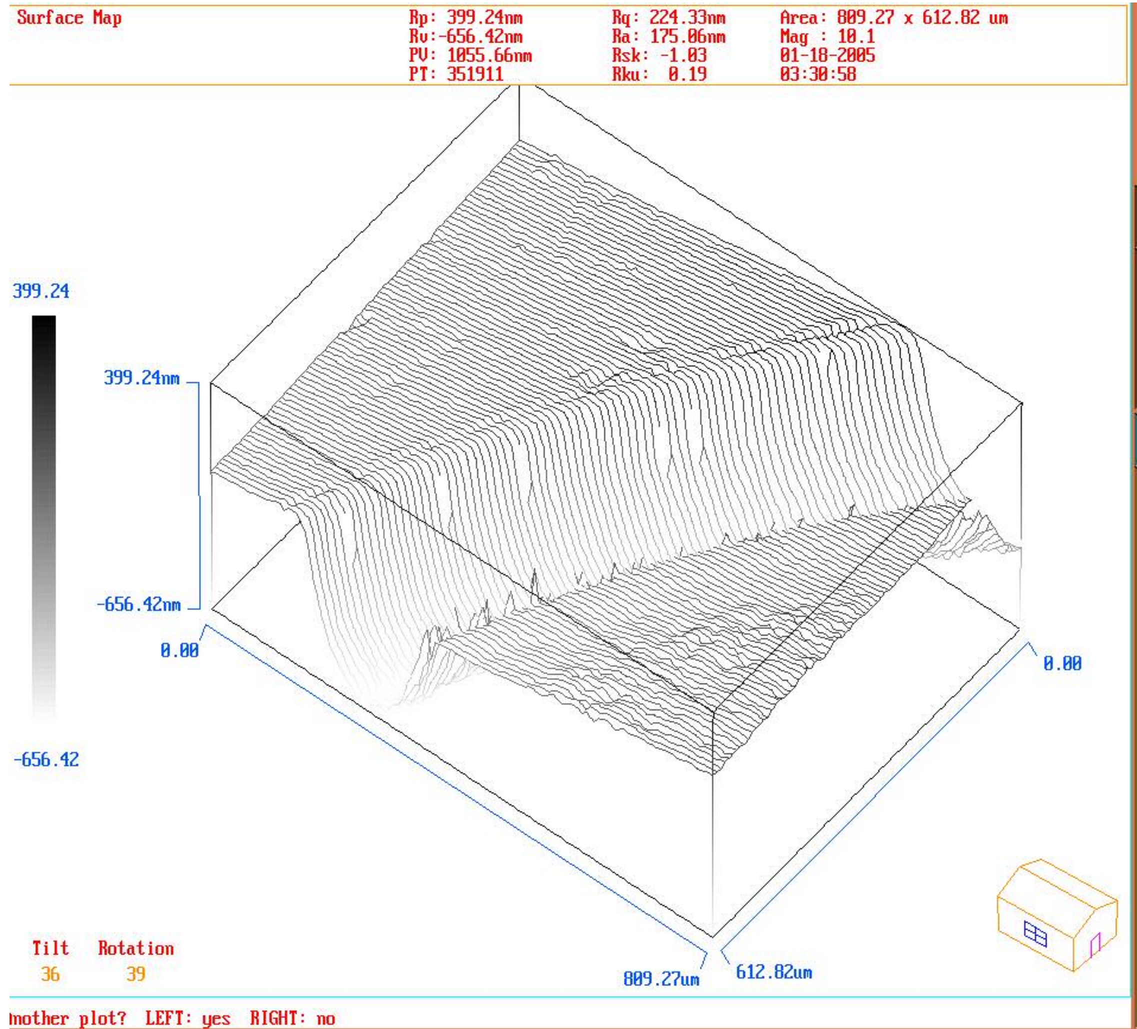

Fig.9.4(c) 3D wire map of quartz (toluene: acetone:: 90:10)

It can see that from Figs. 9.3 (a) to (c) there is over etching of the quartz surface with 100 % toluene. The possible explanation for the over etching is, that toluene absorbs most of the laser energy and as result induces pressure. This leads to vaporization of toluene and formation of bubbles. These bubbles create a pressure jump, which interacts with the surface of quartz and hence removes the material by mechanical force thereby resulting in overetching.

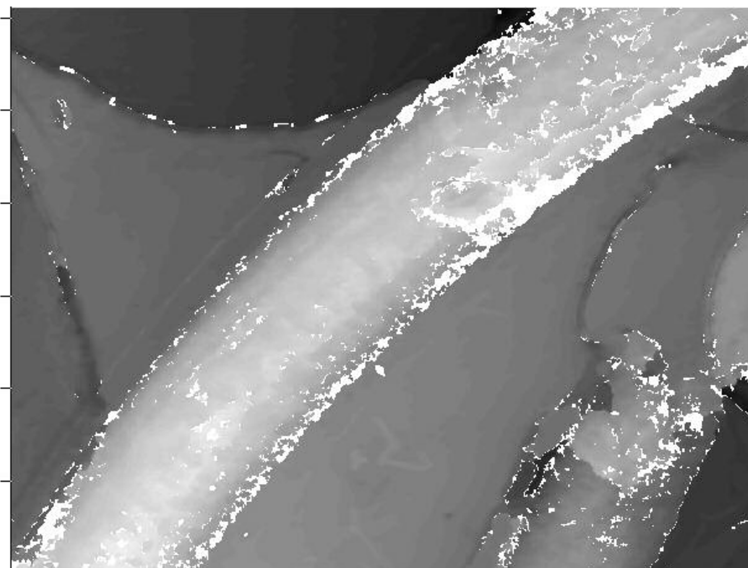

Fig.9.5 (a) Top view of quartz (toluene: acetone:: 70:30)

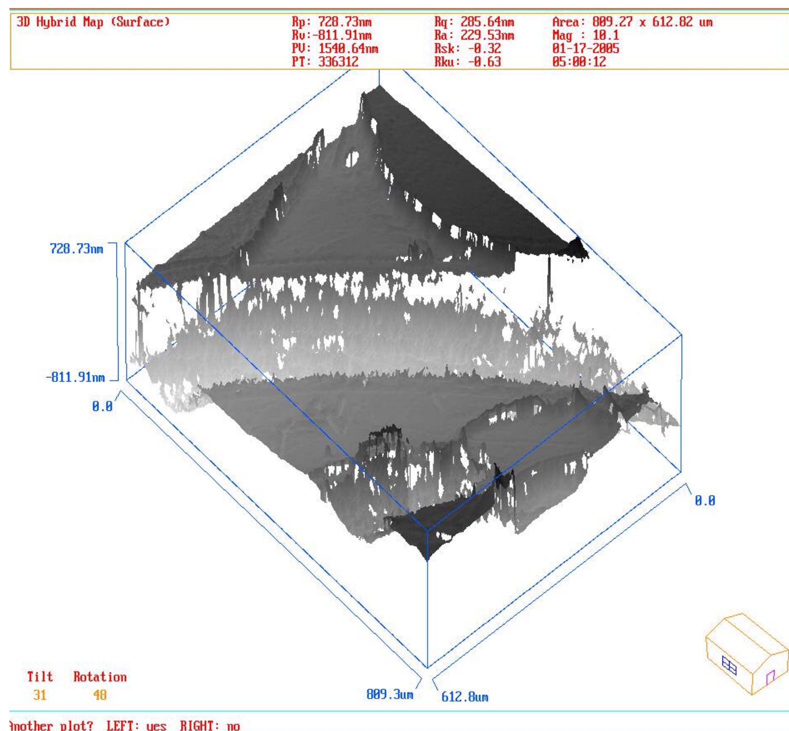

Fig.9.5 (b) 3D solid surface map of quartz (toluene: acetone:: 70:30)

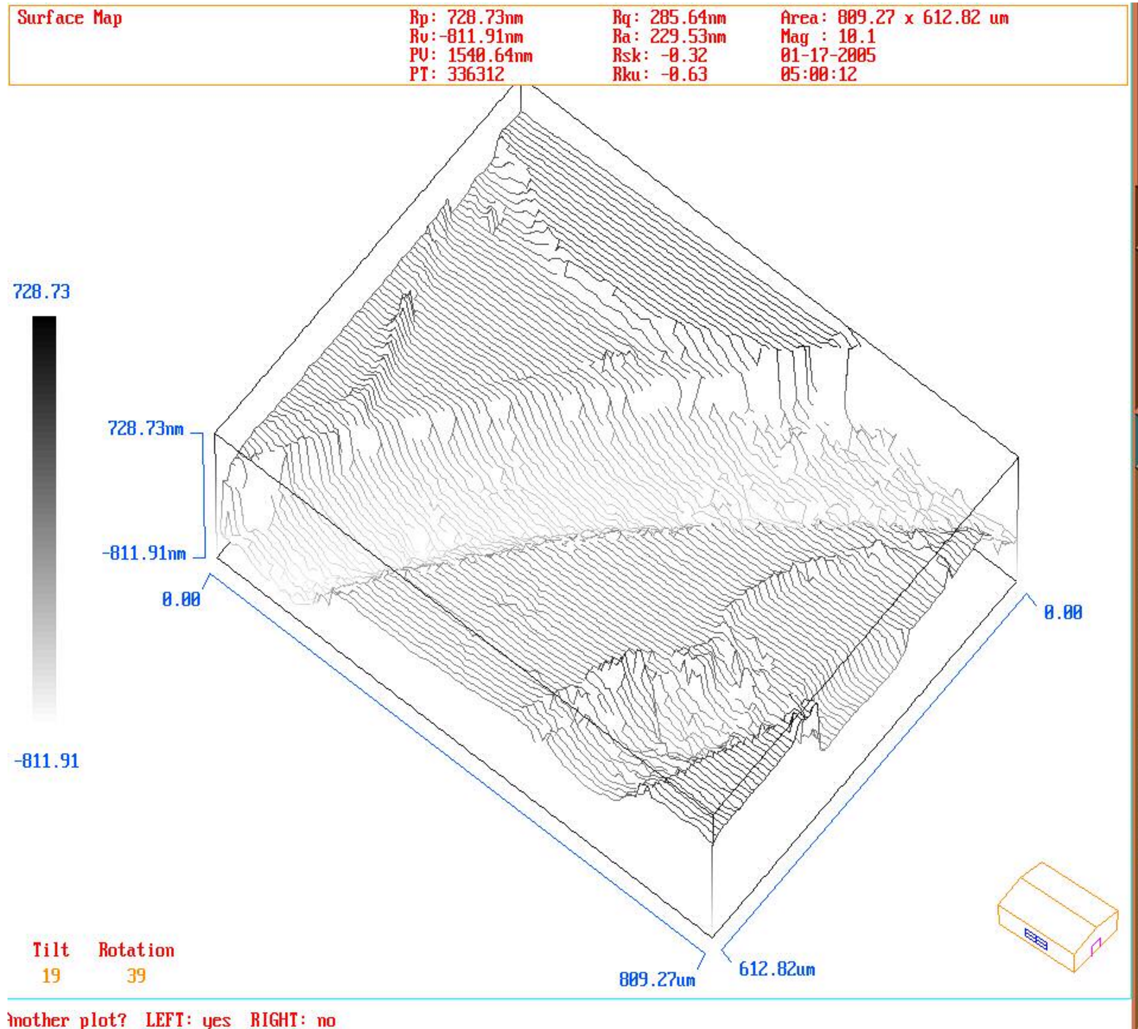

Fig.9.5 (c) 3D wire map of quartz (toluene: acetone:: 70:30)

Over-etching takes place when etching temperature is too high i.e. laser induced temperature of toluene solution. Another possible reason is that the concentration of the solution is very strong. It can see that from Figs. 9.4 (a) to (c) that there is uniform etching of the quartz surface. This can be due to high concentration of toluene/acetone mixture. Hence, additional experiments were conducted in this range to obtain the right concentration of toluene/acetone.

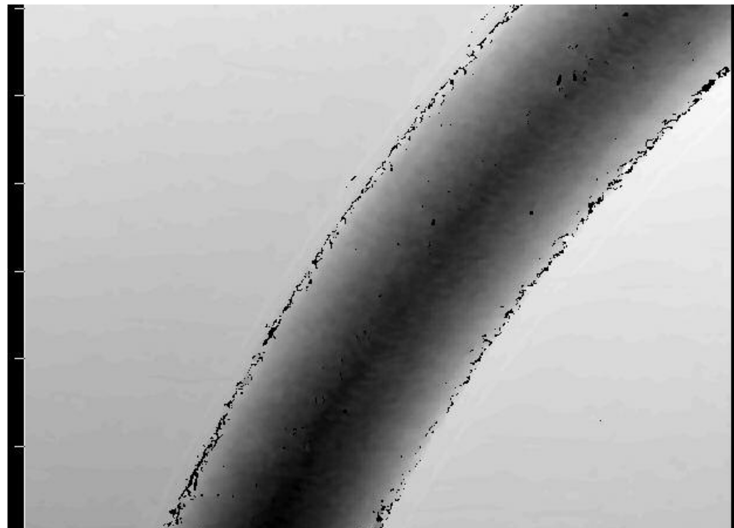

Fig.9.6 (a) Top view of etched surface of quartz (toluene: acetone:: 85:15)

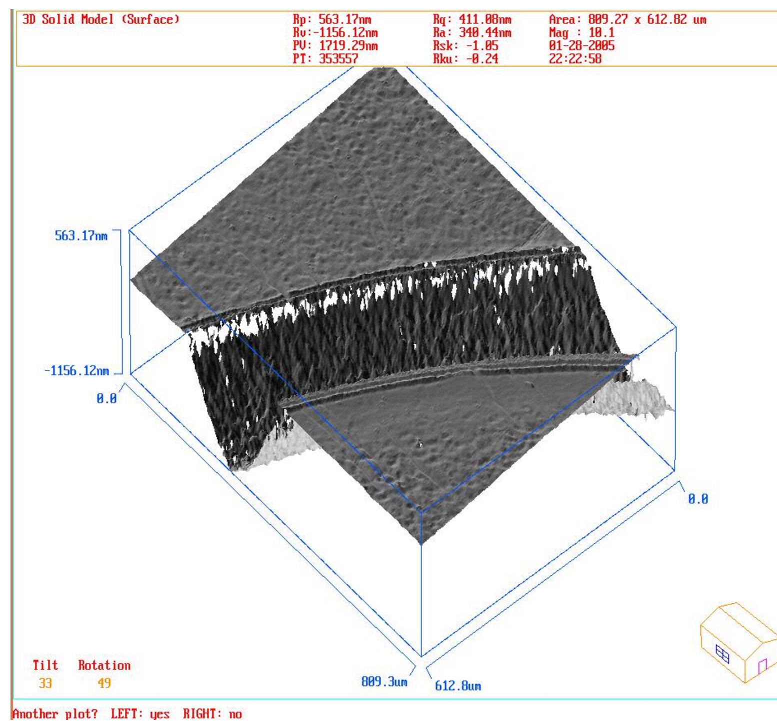

Fig.9.6 (b) 3D solid surface map of quartz (toluene: acetone:: 85:15)

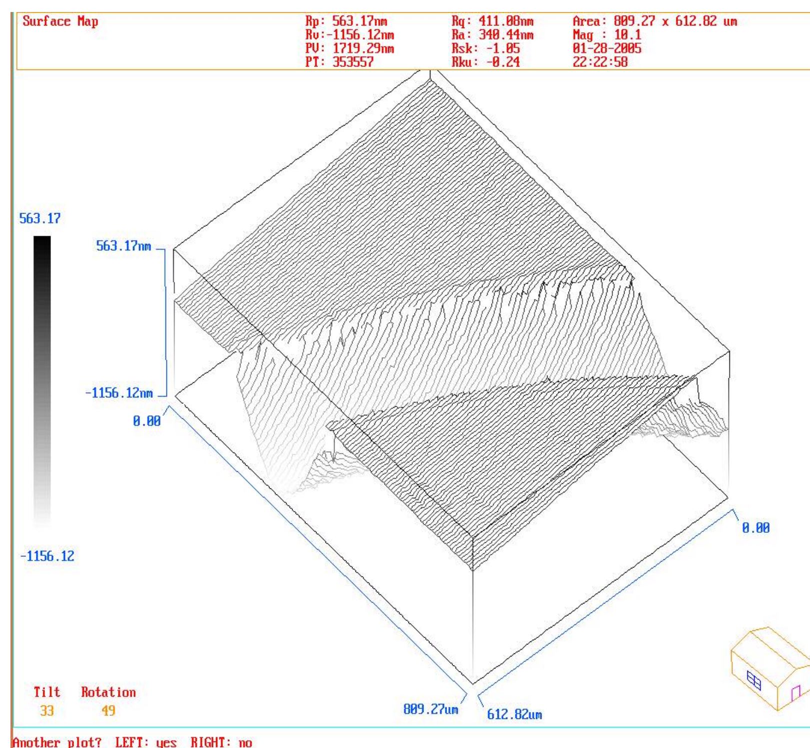

Fig.9.6 (c) 3 D wire map of quartz (toluene: acetone:: 85:15)

It can be seen from Figs. 9.5 (a) to (c) that as the concentration of toluene is decreased and the concentration of acetone is increased, the etching is not uniform and the surface is rough. Also, the etching rate was found to be less. From this we can see that for uniform etching the control of chemical composition is very critical. From Figs. 9.6 (a) to (c), we can see very uniform etching and the surface morphology is very smooth. Also, no debris was observed around the etched surface. The ablation depth was also found be 1.112 µm which is higher than other concentrations of toluene/acetone. Based on this observation the concentration of toluene/acetone was kept at 85:15, and

additional tests were conducted by changing the pulse energies and the surface morphology of etched quartz surface was studied.

Figs 9.7 to 9.13 show the etched surface of quartz with toluene/acetone 85:15 at different energies.

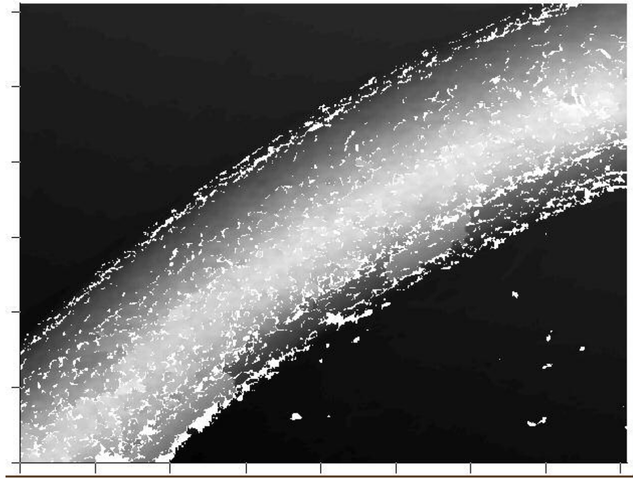

Fig.9.7 (a) Top view of the etched surface of quartz at E = 0.826 mJ

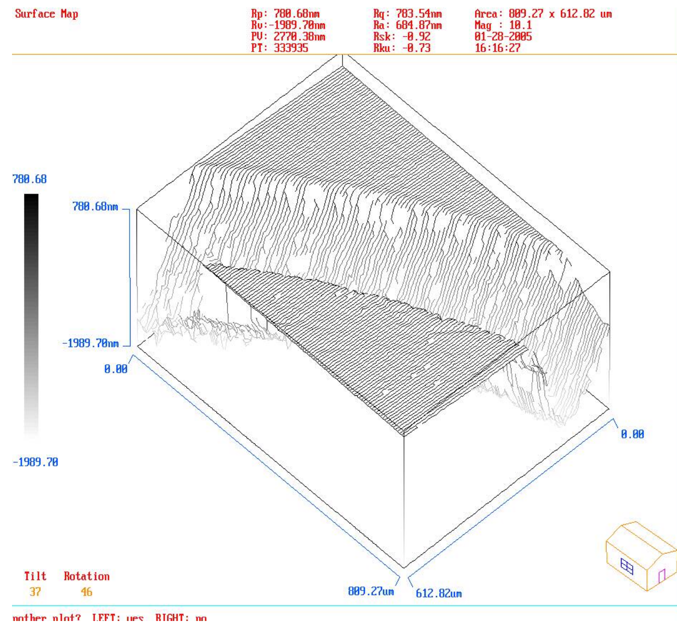

Fig.9.7 (b) 3D wire map of the etched surface of quartz at E = 0.826 mJ

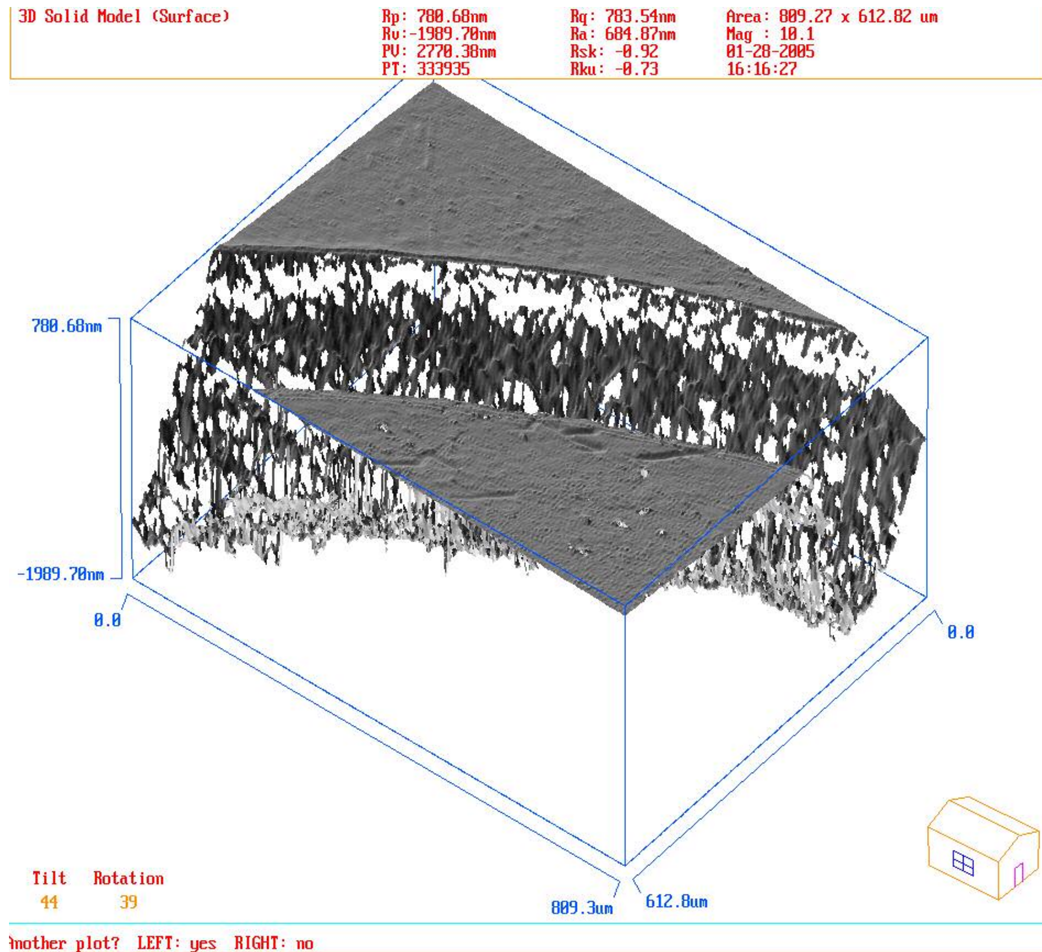

Fig.9.7(c) 3D solid surface map of quartz at E = 0.826 mJ

From Figs. 9.7(a) to (c), we can see that at high energy the surface is debris free. Also, laser etching of quartz is uniform but the etched area is rough. As a result of high energy, the laser induced temperature increases and leads to the vaporization of the solution of toluene/acetone and results in the formation of bubbles. The rapidly expanding or collapsing bubbles interact with the quartz substrate and remove the material by mechanical force thereby resulting in rough etched surface. This result indicates that etch rate and the etched surface quality depends on the laser fluence.

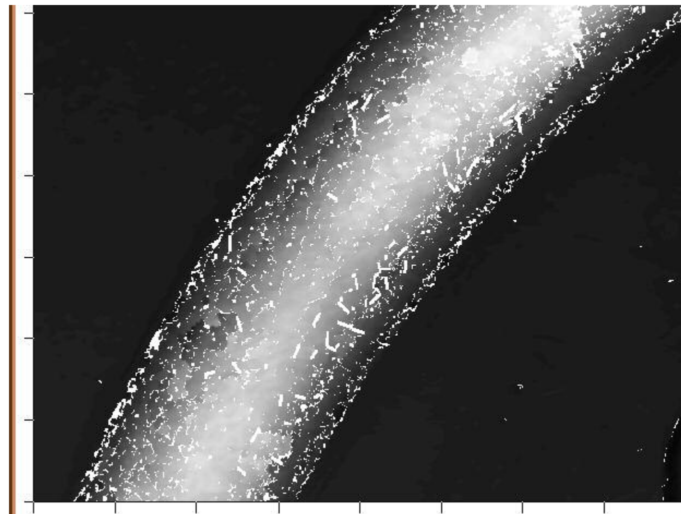

Fig.9.8 (a) Top view of the etched surface of quartz at E = 0.789 mJ

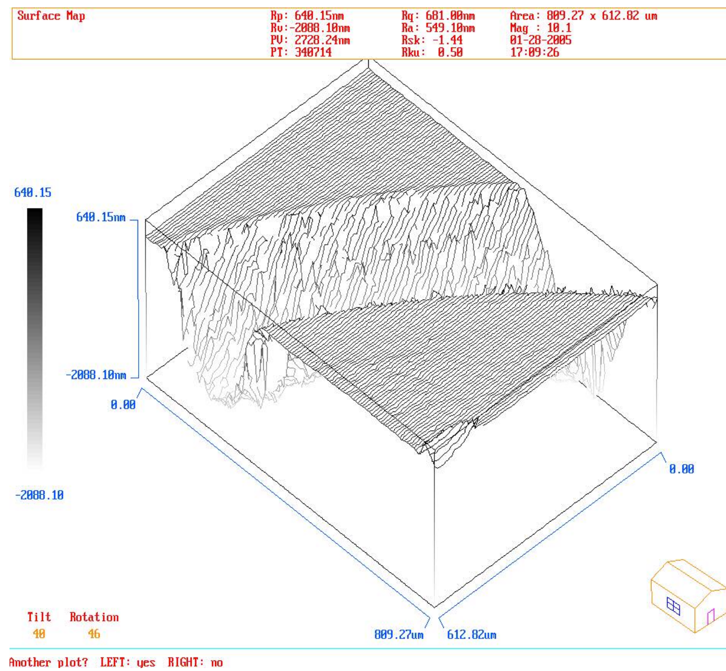

Fig.9.8 (b) 3D wire map of the etched surface of quartz at E = 0.789 mJ

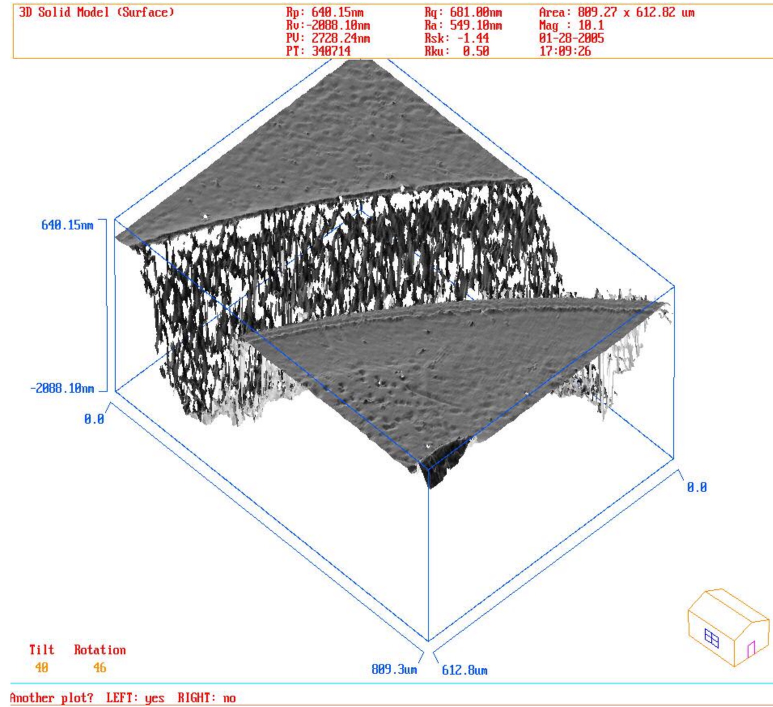

Fig.9.8 (c) 3D solid surface map of quartz at E = 0.789 mJ

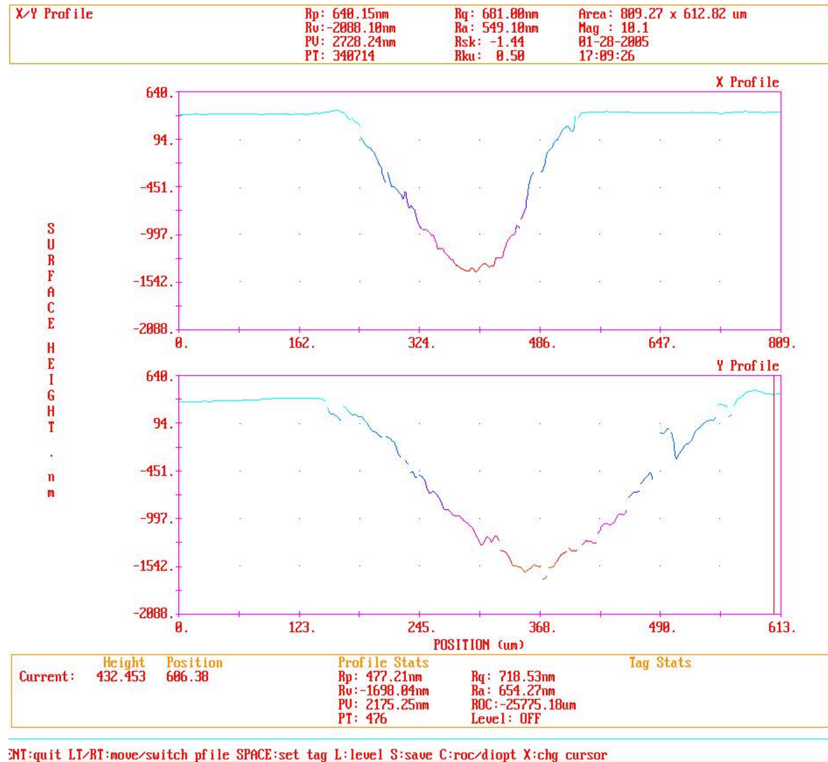

Fig.9.8 (d) X-Y profile of the etched surface of quartz at E = 0.789 mJ

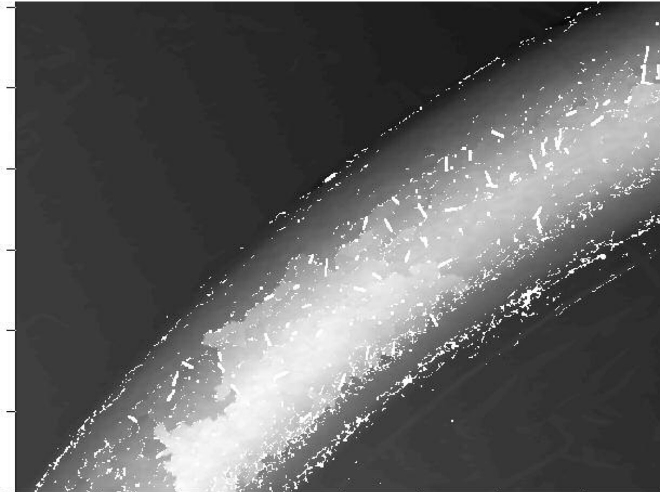

Fig.9.9 (a) Top view of the etched surface of quartz at E = 0.757 mJ

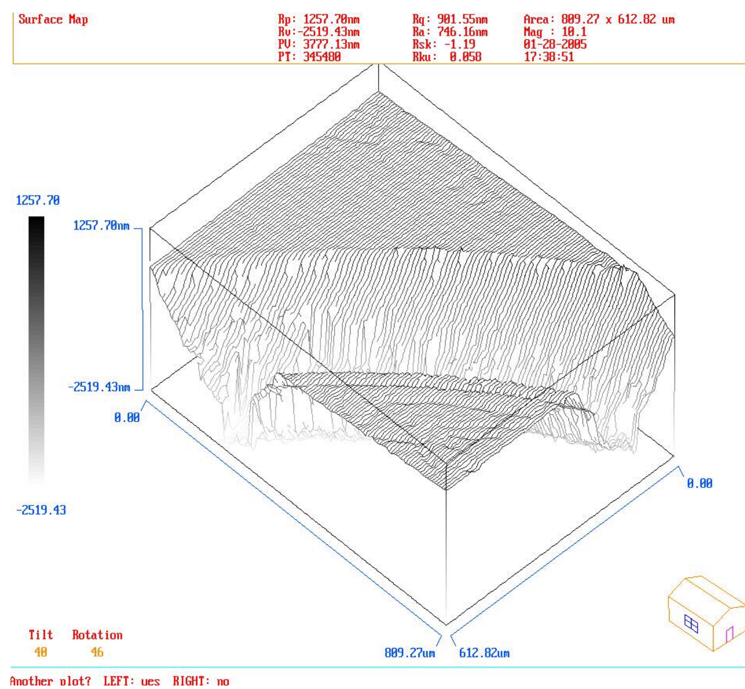

Fig.9.9 (b) 3D wire map of the etched surface of quartz at E = 0.757 mJ

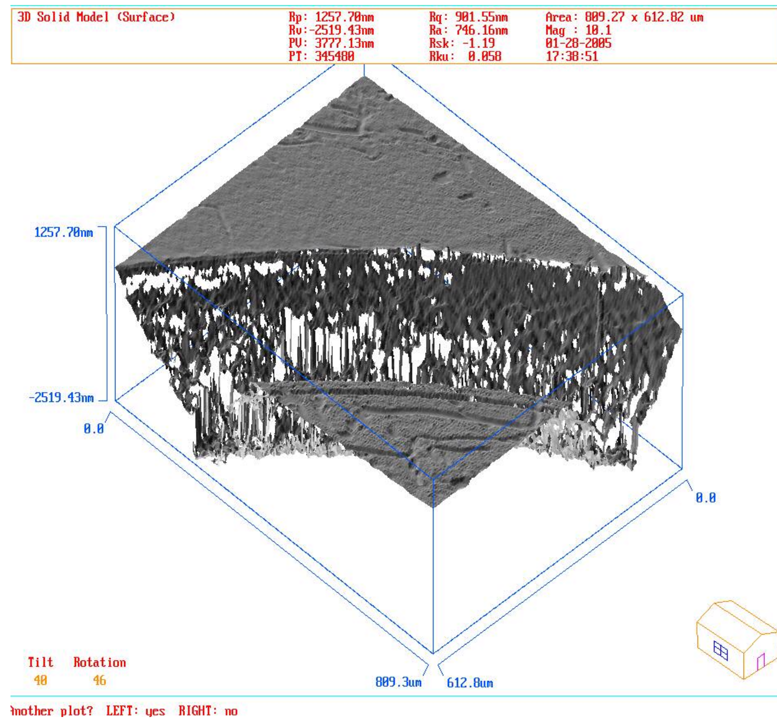

Fig.9.9(c) 3D solid surface map of quartz at E = 0.757 mJ)

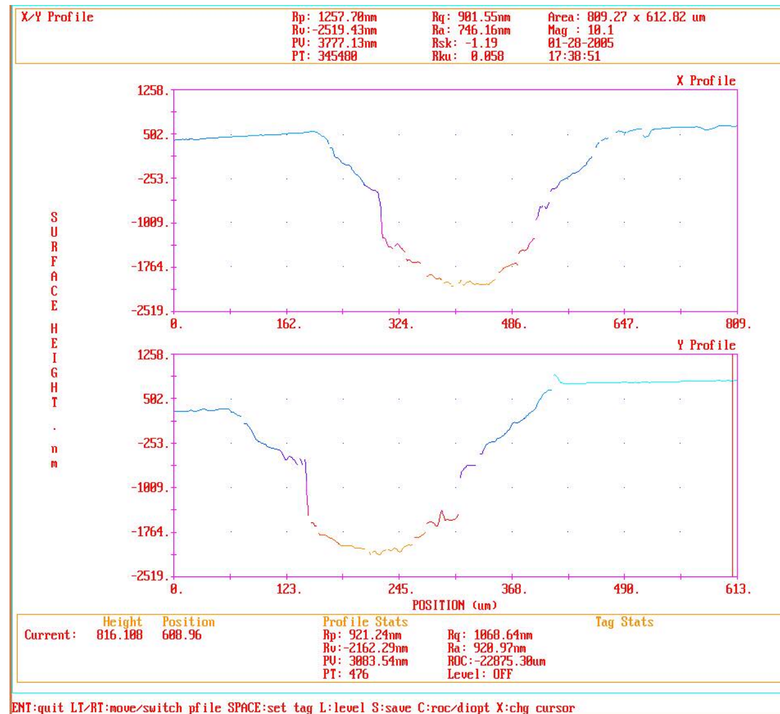

Fig.9.9 (d) X -Y profile of the etched surface of quartz at E = 0.757mJ

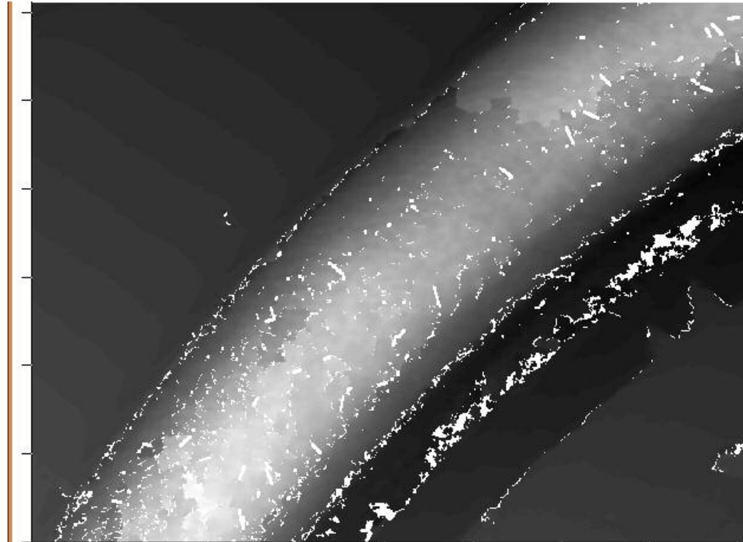

Fig.9.10 (a) Top view of the etched surface of quartz at E = 0.704 mJ

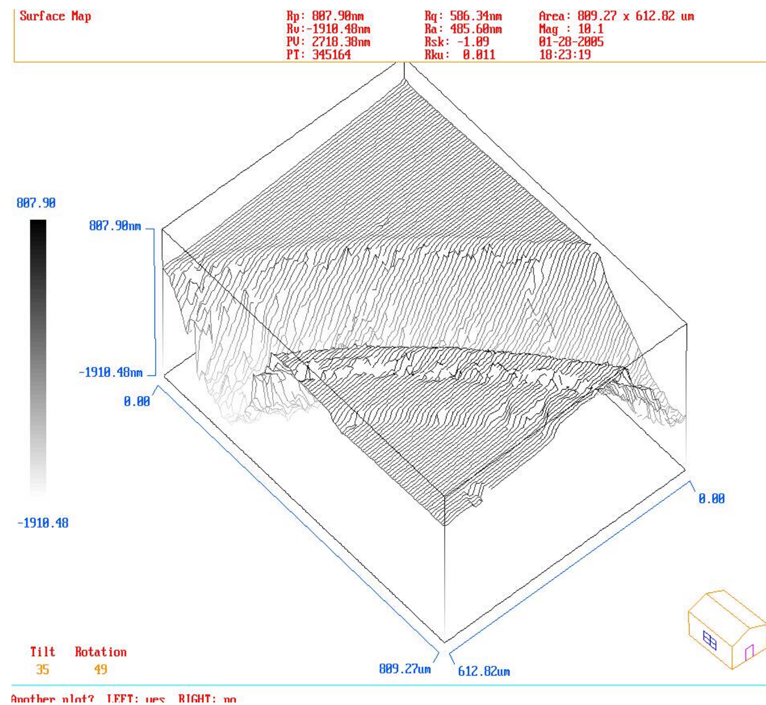

Fig.9.10 (b) 3D wire map of the etched surface of quartz at E = 0.704 mJ

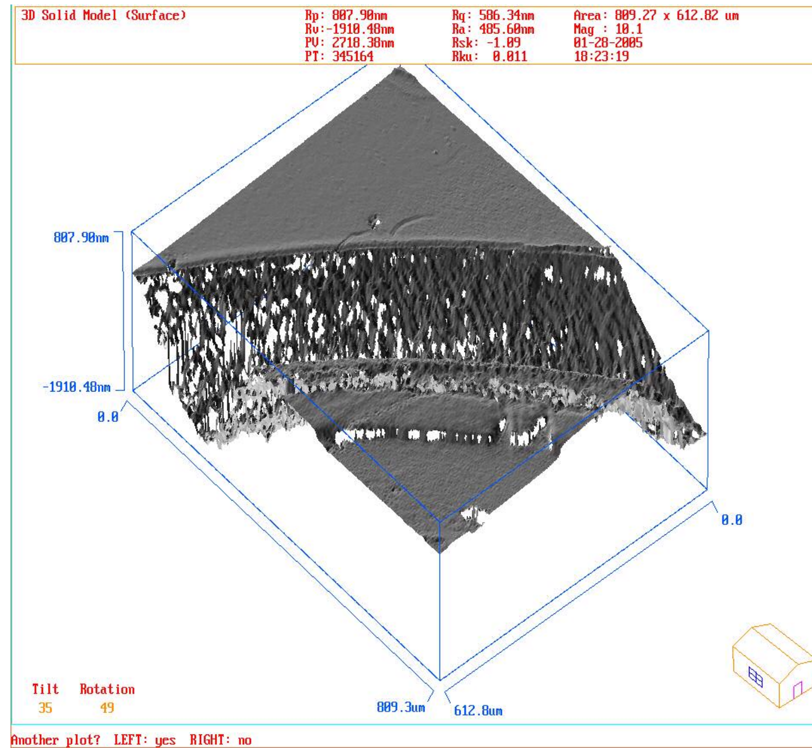

Fig.9.10(c) 3D solid surface map of quartz at E = 0.704 mJ

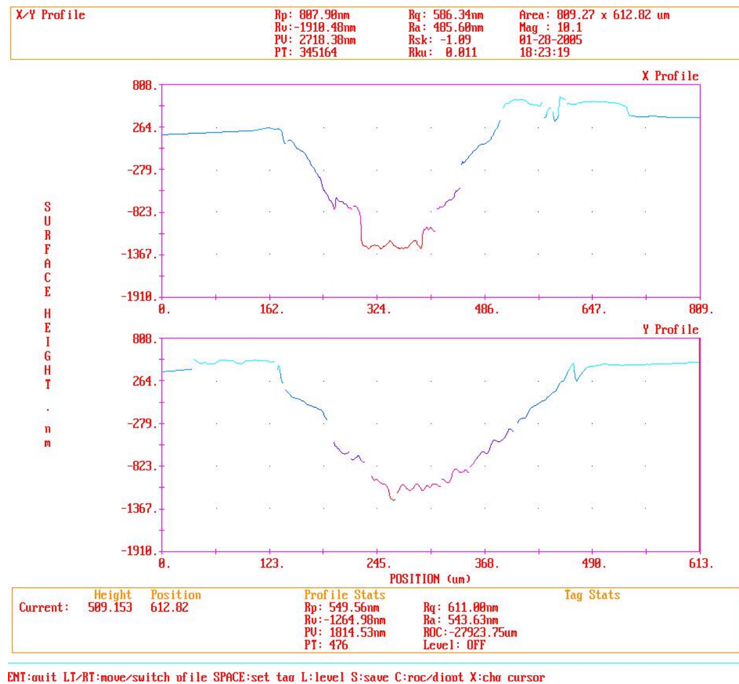

Fig.9.10 (d) X-Y profile of the etched surface of quartz at E = 0.704 mJ

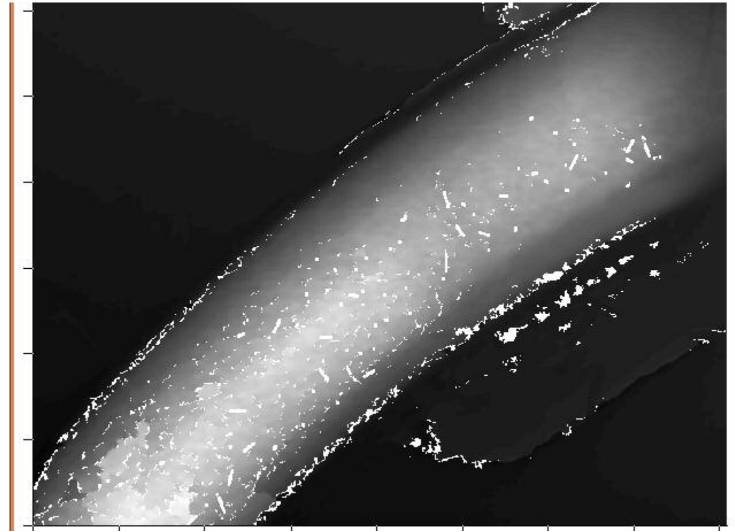

Fig.9.11 (a) Top view of the etched surface of quartz at E = 0.652 mJ

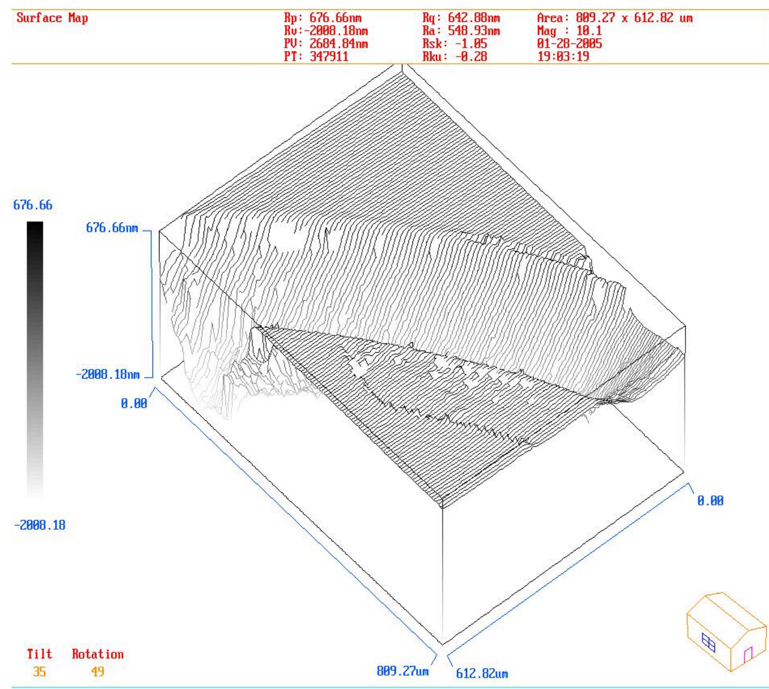

Fig.9.11 (b) 3D wire map of the etched of quartz at E = 0.652 mJ

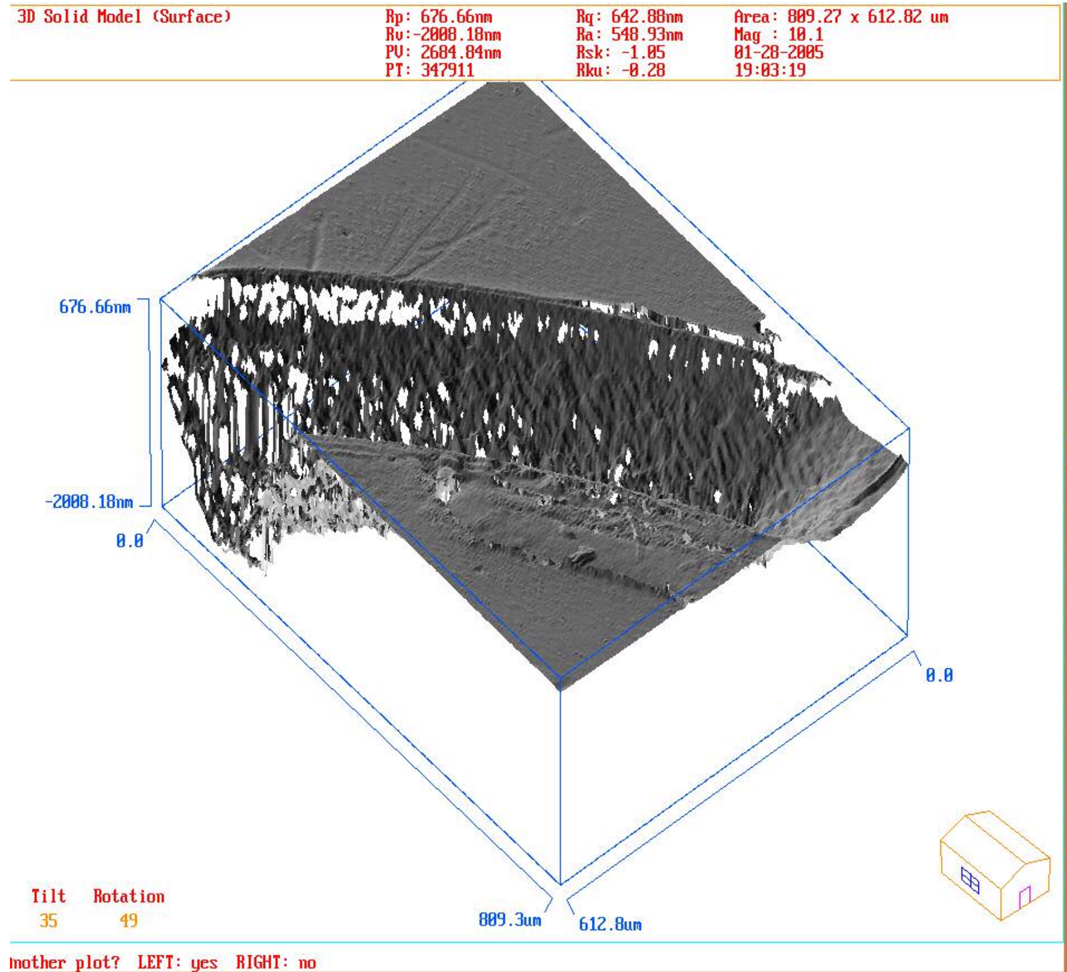

Fig.9.11 (c) 3D solid surface map of quartz at E = 0.652 mJ)

From Figs. 9.11 (a) and 9.12 (c), we can see that the etched surface is again rough and some part of the surrounding area is also etched. Thus, we can see that energy and concentration of organic solution have an affect on the etched surface. The X-Y profiles also show that surface is rough. From Figs. 9.13 (a) to (c), we can see that X-Y profile is smooth and also etching is uniform. Thus, from these experiments we can see that 85:15 of toluene/acetone concentration and an energy of E = 0.522 mJ results in debris free, uniform etching of quartz.

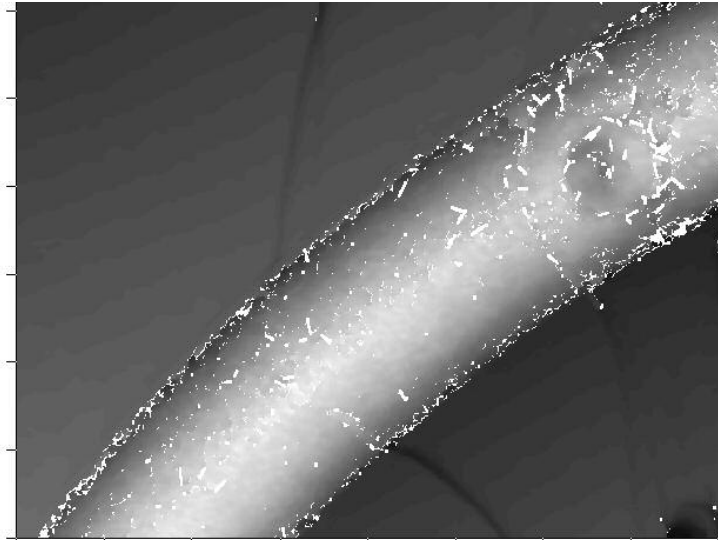

Fig.9.12 (a) Top view of the etched surface of quartz at E = 0.596 mJ

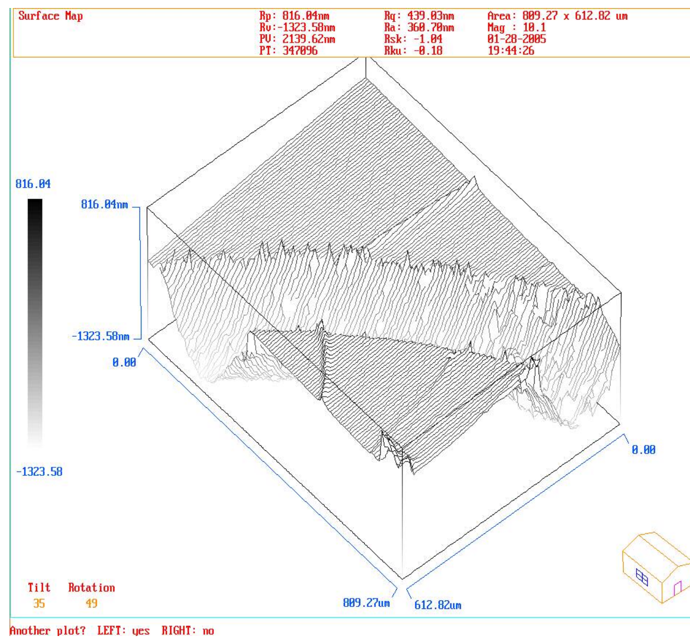

Fig.9.12 (b) 3D wire map of the etched surface of quartz at E = 0.596 mJ

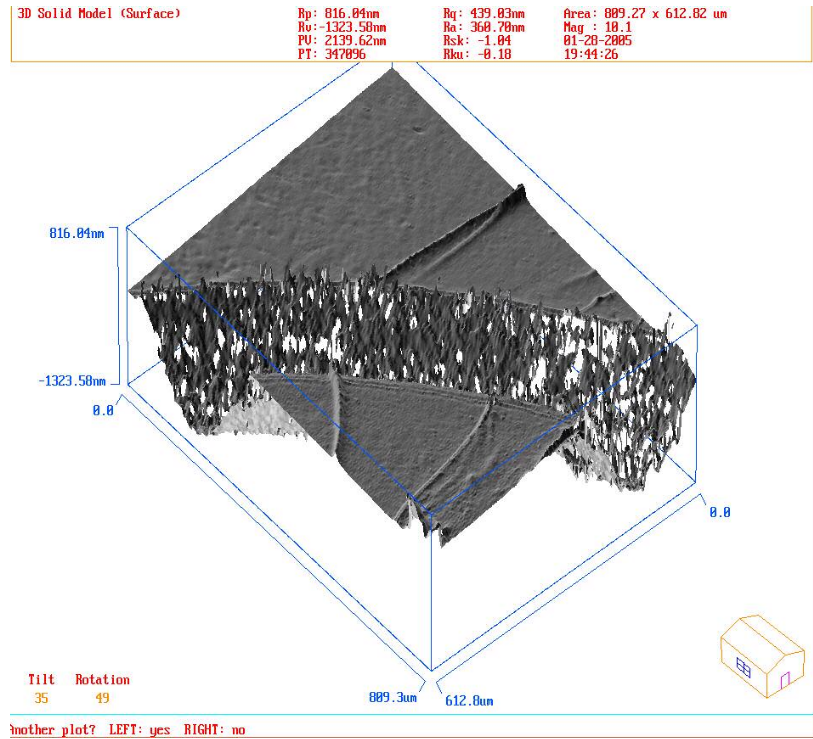

Fig.9.12 (c) 3D solid surface map of quartz at E = 0.596 mJ

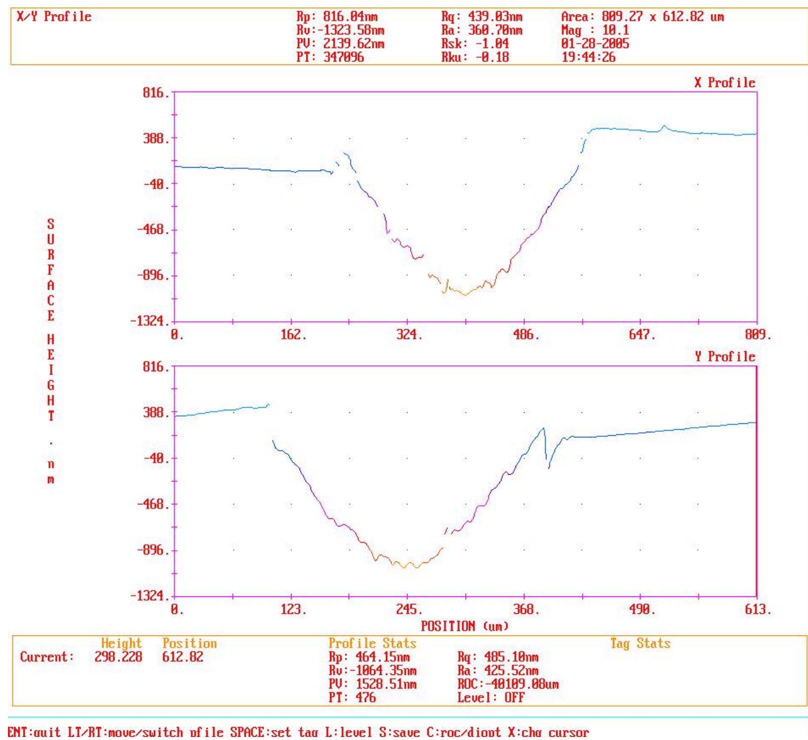

Fig.9.12 (d) X-Y profile of the etched surface of quartz at E = 0.596 mJ

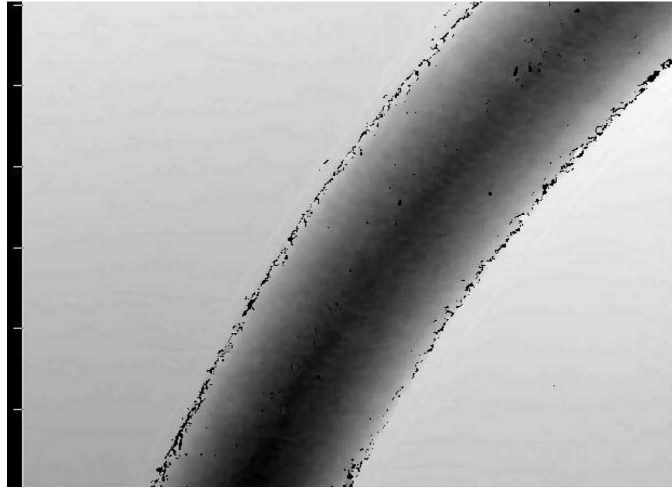

Fig.9.13 (a) Top view of the etched surface of quartz at E = 0.522 mJ

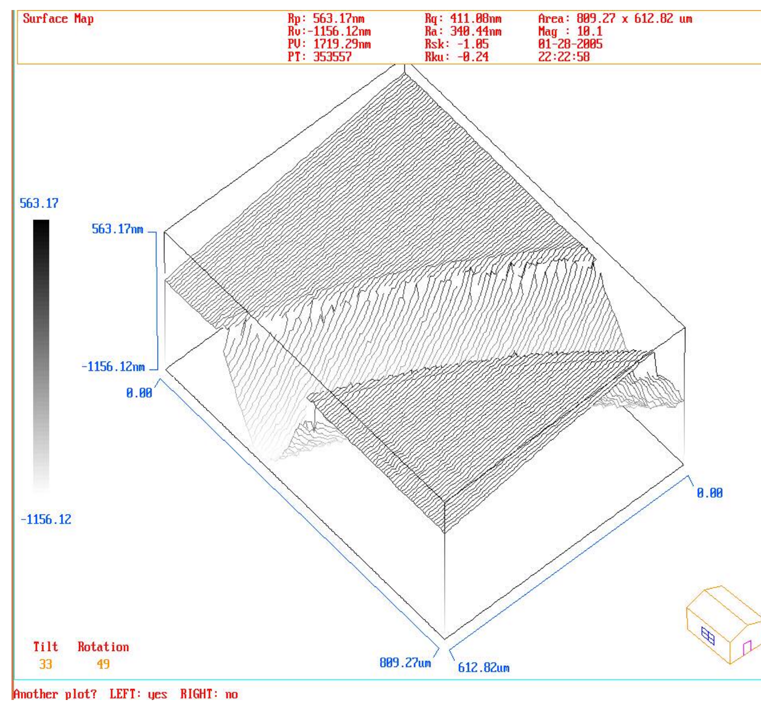

Fig.9.13 (b) 3D wire map of the etched surface of quartz at E = 0.522 mJ

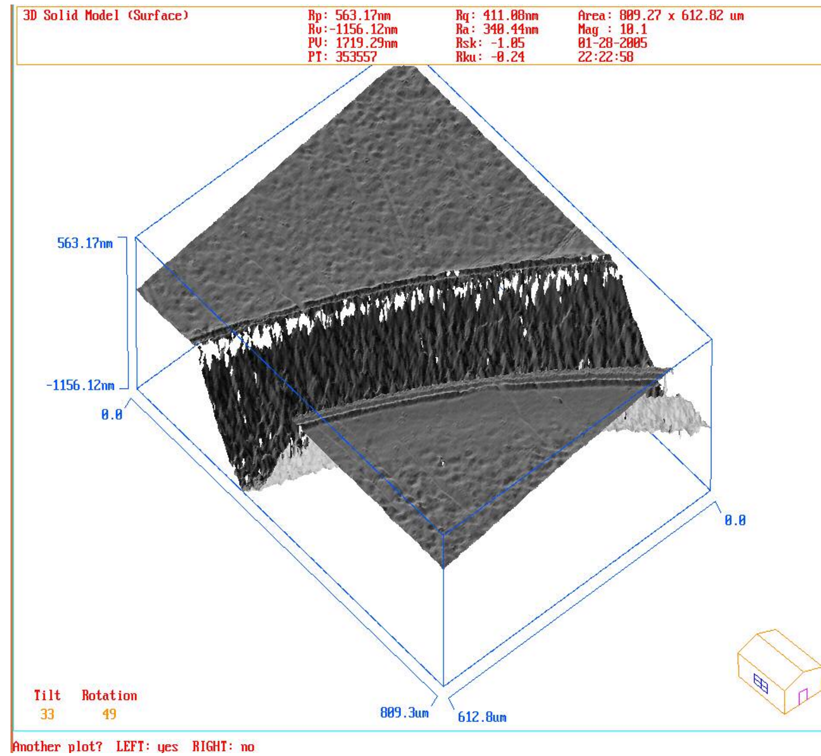

Fig.9.13 (c) 3D solid surface map of quartz at E = 0.522 mJ

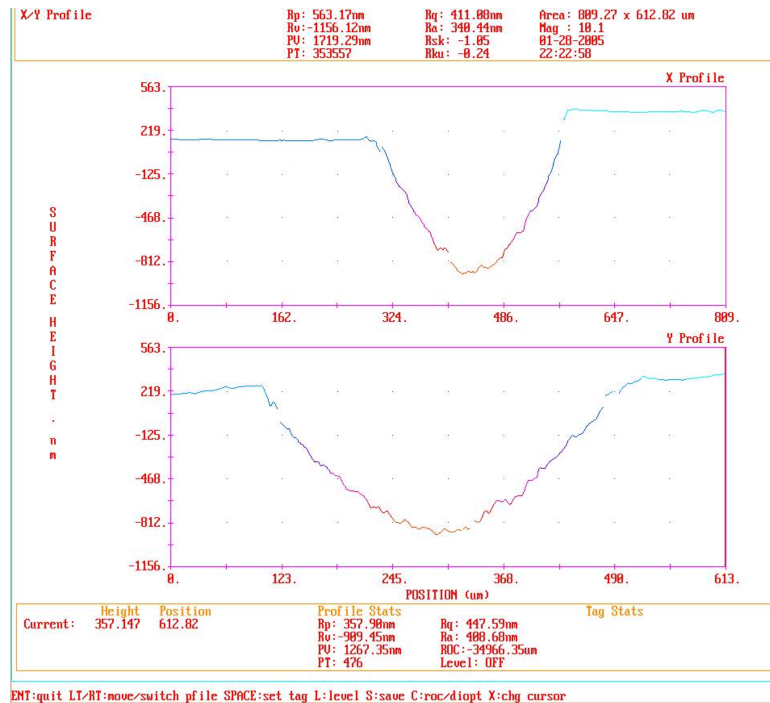

Fig.9.13 (d) X-Y profile of the etched surface of quartz at E = 0.522 mJ

Fig.9.14 shows the variation of ablation depth with fluence for quartz backside wet etching for toluene/acetone:: 85:15.

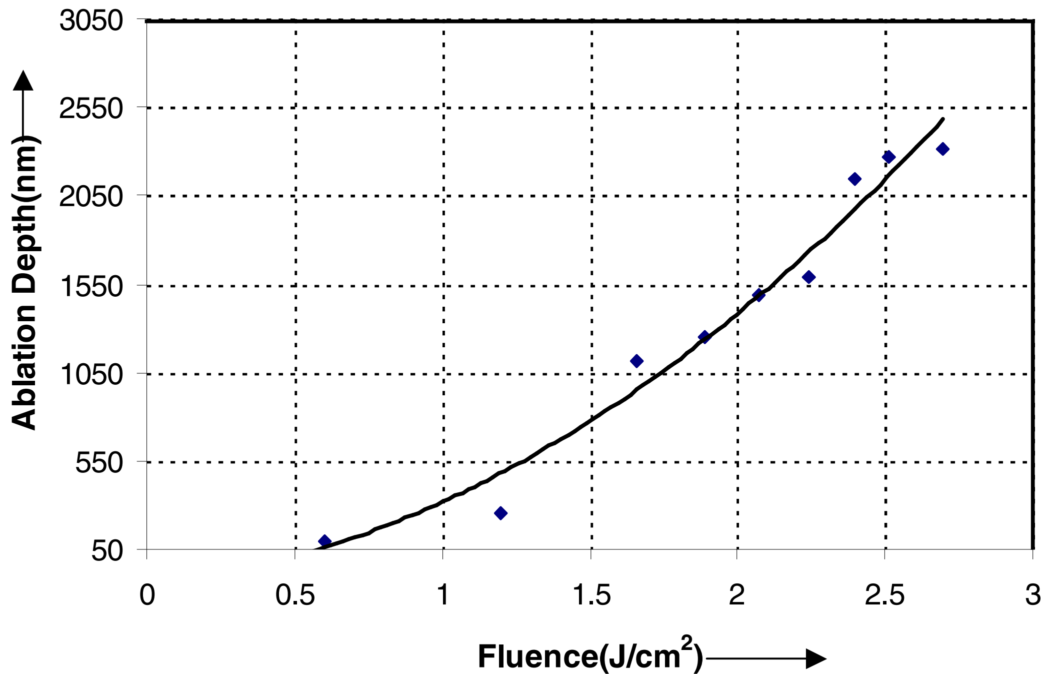

Fig.9.14 The variation of ablation depth with fluence

It can be seen that etching of quartz shows the same features as laser ablation, where threshold fluence exists below which no etching takes place. The threshold fluence for quartz was determined experimentally by measuring ablation depth at different fluences. The threshold fluence of quartz was found to be 0.604 J/cm^2, which is very close to value of 0.5 J/cm^2, reported by Ihlemann *et al.* (1992). As reported by Kopitkovas *et al.* (2003) these values are well below the damage threshold of quartz, which ranges from 10 to 20 J/cm^2. At a fluence of 0.39 J/cm^2, no ablation was observed. It can also be seen from Fig. 9.14 that the ablation depth increases slowly at low fluences than at high fluences. At high fluence, the ablation depth increases linearly with the

fluence. But from Figs. 9.6 to Fig. 9.11, we have seen that at high fluences the etched surface is rough. Hence, efficient etching depends upon the applied laser fluence as well as deposition of laser energy in toluene/acetone layer.

CHAPTER 10

CONCLUSIONS

The goal of this investigation is to study the effect of different laser processing parameters such as pulse energy, media, and micromachining different geometries. Following are the key features and results of this investigation:

1. Micromachining was conducted under methanol, water, dry, and acetone. Differences in the nature of ablation were observed with absence of thermal damage in the case of micromachining under fluids while thermal damage in the case of dry micromachining.
2. Water acts as a cooling media and carries away the debris generated during laser ablation.
3. At a low energy of 0.535 mJ and with a mask of 1000 μm built up of 12 nm was observed in the case of machining under 50% methanol + 50% distilled water and built-up of 4-6 nm was observed in the case of machining under salt water but the

surface was very rough. At this energy, ablation was observed for underwater and with wax on top with an ablation depth of more than 300 nm.

4. A mask of 300 µm was used and micromachining was performed at low energy in different media. For underwater, a built up of 18 nm was observed with a sharp profile of inverted "V". Results of tests under 50% methanol + 50% distilled water showed a built- up with an inverted "U" profile.
5. The sharp profile of the built-up obtained during low energy can be avoided by machining first dry and then under water.
6. Quartz backside etching was performed using toluene/acetone as liquid solution.
7. Concentrations of fluid were varied alongwith pulse energies. Good ablation depth as well as good surface finish with no cracks was observed at energy of 0.522 mJ and concentration of toluene/acetone of 85:15.
8. Several geometries used in MEMS applications such as microfluidic channels, display panel circuit, inductor circuits were fabricated on borosilicate glass using KrF excimer laser 248 nm. They are inductors, different circuits used in the electronic industry, and geometries that find applications in medical applications, such as microfluidic channels.

Future Work

In this investigation micromachining was conducted on borosilicate glass and quartz using a circular mask of diameter 1000 µm and 300 µm, respectively.

In future, different shapes of mask can be used. A mask with a smaller size can be used to machine complex geometries.

- Different materials, such as fused silica can be used for backside wet etching (BSWE) and to study the laser-material interactions.
- MD simulation of laser ablation can be performed and compared with the experimental results.
- Laser deposition on samples, such as glass can be performed using pulsed laser deposition followed by micromachining.

REFERENCES

Allcock, G., Dyer, P. E., Elliner, G., and H. V. Snelling, "Experimental Observations and Analysis of CO_2 Laser-Induced Microcracking of Glass" J. Appl. Phys. 78 (1995) 7295-7303.

Argument, M., Tsui, Y., Fedosejevs, R., Li, J., and P.Herman, "Drilling and Micromachining of Glasses with UV and VUV Laser Pulses," ICALEO (1999)

Balandin, Yu, V., Otte, D., and O. Bostanjoglo, "Thermocapillary Flow Excited by Focused Nanosecond Laser Pulses in Contaminated Thin Liquid Iron Films," J. Appl. Phys. 78 (1995) 2037-2044.

Berthe, L., Fabbro, R., Peyre, P., Tollier, L., and E. Bartnicki, "Shock Waves from a Water-Confined Laser-Generated Plasma," J. Appl. Phys. 82 (1997) 2826-2831.

Brannon, J. H., Lankard, J. R., Baise, A. I., Burns, F., and J. Kaufman, "Excimer Laser Etching of Polyimide," J. Appl. Phys. 58 (5) (1985) 2036-2043.

Bohme, R., Braun, A., and K. Zimmer, "Backside Etching of UV-Transparent Materials at the Interface to Liquids," App. Surf. Sci. 186 (2002) 276-281

Buerhop, C., Blumenthal, B., Weissmann, R., Lutz, N., and S. Biermann, "Glass Surface Treatment with Excimer and CO_2 Laser," Appl. Surf. Sci. 46 (1990) 430-434.

Buerhop, C., Weissmann, R., and N. Lutz, "Ablation of Silicate Glasses by Laser Irradiation: Modeling and Experimental Results," Appl. Surf. Sci. 54 (1992) 187-192.

Chen, Y. T., Ma, K. J., Tseng, A. A., and P. H. Chen, "Projection Ablation of Glass based Single and Arrayed Microstructures using Excimer Laser", Optics & Laser Technology (2004).

Choo, K. L, Ogawa, Y., Kanbargi, G., Raff, L. M., and R. Komanduri, "Micromachining of Silicon by Short Pulse Laser Ablation in Air and Under Water", Materials Science and Engineering A, Volume 372, Issues 1-2, 15 May 2004, Pages 145-162.

Choo, K.L, "Micromachining using an Excimer (248 nm) laser," MS thesis, School of Mechanical and Aerospace Engineering, Oklahoma State University, Stillwater, OK (2004).

Chryssolouris, G., "Laser Machining: Theory and Practice," Springer-Verlag, New York (1991).

Ding, X., Kawaguchi, Y., Sato, T., Narazaki, A., Kurosaki, R., and H. Niino, "Micron and Submicron- Sized Surface Patterning of Silica Glass by LIBWE Method," J. of Photochemistry and Photobiology A: Chemistry 166 (2004) 129-133.

Dupont A, Caminat P, Bournot P., "Enhancement of Material Ablation Using 248, 308, 532, 1064 nm Laser Pulse With a Water Film on the Treated Surface," J Appl Phys 78(3) (1995) 2022–8.

Dyer, P. E., Farley, R. J., Giedl, R., and D. M. Karnakis, "Excimer Laser Ablation of Polymers and Glasses For Grating Fabrication," Appl. Surface Sci. 96-98 (1996) 537-549.

Estler, R. C., and N. G. Nogar, "Mass Spectroscopic Identification of Wavelength Dependent UV Laser Photoablation Fragments From Polymethylmethacrylate," Appl. Phys. Lett. 49 (18) (1896) 1175-1177.

Fox, J. A., “Effect of Water and Paint Coating on Laser-Irradiated Target,” Appl. Phys. Lett. 24 (10) (1974) 461-464.

Garrison, B. J and R. Srinivasan, “Laser Ablation of Organic Polymers: Microscopic Models for Photochemical and Thermal Processes,” J. Appl. Phys. 57, (1985) 2909-2914.

Geiger, M., Roth, S., and W. Becker, “Microstructuring and Surface Modification by Excimer Laser Machining under Thin Liquid Films,” Proc. SPIE, 3407 (1998) 200-208.

Guthrie, R. I. L., and T. Iida, “Thermodynamic Properties of Liquid Metals,” Mater. Sci. Eng. A A178 (1994) 35-41.

Hecht, J., “Understanding laser,” Howard W. Sam & Company Hayden Books, California (1990).

Ho, J. R., Grigoropoulos, C.P., and J.A.C. Humphrey, “Computational Study of Heat Transfer and Gas dynamics in the Pulsed Laser Evaporation of Metals,” J. of Applied Physics 78(7)(1995) 4696-4709.

Ihlemann, J., “Excimer Laser Ablation of Fused Silica,” Appl. Surf. Sci. 54 (1992) 193-200.

Ihlemann, J., and B. W. Rottke, “Excimer Laser Micromachining of Inorganic Dielectrics,” Appl. Surf. Sci. 106 (1996) 282.

Jackson, S. R., Metheringham, W. J. and P. E. Dyer, “Excimer Laser Ablation of ND: YAG and Nd: Glass,” Appl. Surf. Sci. 86 (1995) 223-227.

Jeong, J. H. Grief, R. and R. E. Russo, “Shock Wave and Material Vapor Plume Propagation During Excimer Laser Ablation of Aluminum Samples,” J. Phys. D: Appl. Phys. 32 (1999) 2578-2585.

Kawaguchi, Y., Narazaki, A., Sato, T., Niino, H., Yabe, A., Langford, S.C. and J.T. Dickinson, “The Onset of Optical Breakdown in KrF-Laser-Irradiated Silica Glass Surfaces,” Appl. Surf. Sci. 197–198 (2002) 50–55.

Keiper, B., Exner, H., Loschner, U. and T. Kuntze, “Drilling of Glass by Excimer Laser Mask Projection Technique,” ICALEO M110 (1999) 1-7.

Kingery, W. D., “Surface Tension of Some Liquid Oxides and Their Temperature Coefficients,” J. Am. Ceram. Soc, 42 (1959) 6-10.

Kim, D., and C. P Grigoropoulos., “Phase Change Phenomenon and Acoustic Transient generation in Pulsed Laser Induced Ablation of Absorbing Liquids,” App. Surf. Sci. 127-129 (1998) 53-58.

Kim, D., Ye, M., and C. P. Grigoropoulous, “Pulsed Laser-induced Ablation of Absorbing Liquids and Acoustic-transient Generation,” App. Phys. A: Materials Science and Processing A 67(2) (1998) 169-181.

Konovalov, I. A. and P. R. Herman, “Ablation-Induced Stresses in Fused Silica by 157-nm F2-Laser Irradiation,” Mat. Res. Soc. Symp. 617 (2000) J3.3.1-J3.3.7.

Kopitkovas, G., Lippert, T., David, C., Wokaun, A., and J. Gobrecht, “Fabrication of Micro-optical Elements in Quartz by Laser Induced Backside Wet Etching,” Microelectronic Engg. 67-68 (2003) 438-444.

Kopitkovas, G., Lippert, T., David, C., Wokaun, A., and J. Gobrecht, "Surface Micromachining of UV Transparent Materials," Thin Solid Films 453-454 (2004) 31-35.

Kruger, J., Kautek, W., Lenzer, M., and S. Sartania, "Laser Micromachining of Barium Aluminum Borosilicate Glass with Pulse Durations between 20 fs and 3 ps," App. Surf. Sci. 127-129 (1996) 892-898.

Kruusing, A, "Underwater and Water Assisted Laser Processing: Part-1 General features, Stream Cleaning and Shock Processing," Optics and Lasers in Engineering 41 (2004) 307-327.

Kruusing, A, "Underwater and Water Assisted Laser Processing: Part 2 –Etching, Cutting and rarely used methods," Optics and Lasers in Engineering 41 (2004) 329-532.

Li, C., and S.Nikumb, "Optical Quality micromachining of Glass with Focused Laser-produced Metal Plasma Etching in the Atmosphere," Applied Optics 42 (2003) 2383-2387.

Navarrete, M., Muniz, M. V., Ponce, L., and T. Flores, "Photoacoustic Detection of Microcracks induced in BK7 Glass by Focused Laser Pulses," Optics and Lasers in Engg 40 (2003) 5-11.

Nikumb, S., Chen, Q., Li, C., Reshef, H., Zheng, H.Y., Qiu, H., and D. Low, "Precision Glass Machining, Drilling and Profile Cutting by Short Pulse Lasers," Thin Solid Films 477 (2005) 216-221.

Omori, N. and M. Inoue, "Excimer Laser Ablation of Inorganic Materials," Appl. Surf. Sci. 54 (1992) 232-236.

Park, H.K., Kim, D., Grigoropoulos, C.P., and A.C, "Pressure Generation and Measurement in Rapid Vaporization of Water on a Pulsed Laser Heated Surface," J. Appl. Physics 80 (7) (1996) 4072-4081.

Peyre, P., Fabbro, R., Merien, P. and H. P. Lieurade, "Laser Shock Processing of Aluminum Alloys. Application to High Cycle Fatigue Behavior," Mat. Sci Eng. A A210 (1996) 102-113.

Peyre, P., Berthe, L., Scherpereel, X., Fabbro, R., and E. Bartnicki, "Experimental Study of Laser-Driven Shock Waves in Stainless Steel," J. Appl. Phys. 84 (1998) 5985-5992.

Phillippe, B.C., William and Ali S., "Introduction to Micromachining Handbook," Version 2.2, Clark-MXR, Inc. (2001).

Sano, Y., Mukai, N., Okazaki, K., and M. Obata, "Residual Stress Improvement in Metal Surface by Underwater Laser Irradiation," Nuclear instruments and methods in Physical Research B 121 (1977) 432-436.

Schawlow, L., and Charles H. Townes, "Infrared and Optical masers," Physical Review 112 (1958) 1940.

Srinivasan, R., and V. Mayne-Banton, "Self-Developing Photoetchining of Poly (ethyleneterephthalate) Films by Far-Ultraviolet Excimer Laser Radiation," Appl. Phys. Letts. 41 (1982) 576-578.

Sokolowski-Tinten, K, Bialkowski, J., Cavalleri, A., and D. Von Der Linde, "Observation of A Transient Insulating Phase of Metals and Semiconductors during Short-Pulse Laser Ablation," Appl. Surf. Sci. 127–129 (1998) 755–760.

Theppakuttai, S., and S. Chen., “Nanoscale Surface Modification of Glass using a 1064 nm Pulsed Laser,” App. Phy. Lett. 83 (2003) 758-760.

Wang, J., Niino, H., and Akira Yabe, “Micromachining of Transparent Materials with Super-heated Liquid generated by Multiphotonic Absorption of Organic Molecule,” App. Surf. Sci 154-155 (2000) 571-576.

Wang, J., Niino, H., and A. Yabe, “Etching of Transparent Materials by Laser Ablation of An Organic Solution,” RIKEN Review 32 (2001) 43-46.

Yakar, A. B., and R. L. Byer, “Morphology of Femtosecond -Laser-ablated Borosilicate Glass Surfaces,” App. Physics Letters 83 (2003) 3030-3032.

Yen, M. H., and J. Y. Cheng, “Direct Writing and Debris Free Laser Micromachining on Glass by Photo Assisted Chemical Etching,” 7th Intl. Conference on Miniaturized chemical and Biochemical Analysis Systems (2003) 323- 326.

Zhang, W. and Y. L Yao, “Micro Scale Laser Shock Processing of Metallic Components,” J. Manufac. Sci. Eng., 124 (2002) 369-378.

Zhu, S., Lu, Y.F., Hong, M.J., and X.Y. Chen, “Laser Ablation of Solid Substrates in Water and Ambient Air,” J. of App. Physics 89(4) (2001) 2400-2403.

Zimmer, K., Braun, A., and R. Bohme, “Etching of Fused Silica and Glass with Excimer Laser at 351 nm,” App. Surf. Sci. 208-209 (2003) 199-204.

VITA

Ganesh P. Kanbargi

Candidate for the Degree of

Master of Science

Thesis: MICROMACHINING OF BOROSILICATE GLASS AND LASER INDUCED BACK SIDE WET ETCHING OF QUARTZ USING AN EXCIMER LASER (248 NM)

Major Field: Mechanical Engineering

Biographical:

Personal data: Born in Chikkamaglore, Karnataka, India, on July 15, 1975, the son of Pundalik and Pratibha Kanbargi.

Education: Received Bachelor of Engineering degree in Mechanical Engineering from Karnatak University Dharwar, India in August 1997.Completed the requirements for the Master of Science degree with a major in Mechanical and Aerospace Engineering at Oklahoma State University in July 2005.

Experience: Graduate Research Assistant in the School of Mechanical and Aerospace Engineering, Oklahoma State University, Stillwater, Oklahoma, Jan 2002 - present.

Name: Ganesh P. Kanbargi Date of Degree: July, 2005

Institution: Oklahoma State University Location: Stillwater, Oklahoma

Title of Study: MICROMACHINING OF BOROSILICATE GLASS AND LASER INDUCED BACKSIDE WET ETCHING OF QUARTZ USING AN EXCIMER LASER (248 NM)

Pages in Study: 110 Candidate for the Degree of Master of Science
Major Field: Mechanical Engineering

Scope and Methodology of Study:

Borosilicate glass, because of its optical transparency, electrical insulation, and thermal stability is widely used in the field of microelectronic industries. Microdevices composed of glass materials are in great demand in microelectormechanical system (MEMS) industry and sensor technology. But because of their inherent brittleness, they are difficult to machine by most conventional machining techniques. Further, UV transparent materials, such as quartz and sapphire are materials of importance in optical and optoelectronics because of their outstanding properties, such as transparency in a wide wavelength range and strong damage resistance for laser irradiation. However, laser micromachining of these dielectrics is restricted due to their high transparency. Laser induced backside wet etching (LIBWE) is a novel one step process for machining transparent materials, such as quartz, fused silica, and sapphire. Excimer lasers possess short pulse lengths, high average as well as peak powers. This lends excimer laser as an appropriate tool for micromachining applications. An Excimer laser (248 nm FWHM = 25 ns) is used in this investigation for micromachining of borosilicate glass and quartz.

Findings and Conclusions:

The machined surfaces were examined using optical and laser interference microscopes (MicroXam). The effect of process parameters, such as pulse fluence and different media on the resulting machining geometry is studied. Micromachining was conducted under methanol, water, dry, and acetone. Differences in the nature of ablation are observed with absence of thermal damage in the case of micromachining under fluids while presence of thermal damage in the case of dry micromachining. Quartz backside etching was performed using toluene/acetone as liquid solution. Concentrations of fluid were varied alongwith pulse energies. Good ablation depth as well as good surface finish with no cracks was observed at an energy of 0.522 mJ and concentration of toluene/acetone of 85:15. Several geometries used in MEMS applications were fabricated on borosilicate glass using KrF excimer laser (248 nm) wavelength. They are inductors, circuits used in the electronic industry and geometries that find applications in medical applications such as microfluidic channels

Advisor's Approval: **Dr. Ranga Komanduri**